The Development of Range Extender Generator By Evaluating The Eddy Current Losses and End Effect Using FE Method

MSc. Thesis Report

Author	**: Tofan Fadriansyah**
Student ID	**: 4039394**
Date	**: July 7th, 2011**
Supervisor	**: Dr. Henk Polinder**
Daily supervisor	**: Ir. Tim Strous**
Thesis Committee	**: Prof. Dr. J.A. Ferreira**
	Dr. Henk Polinder
	Dr. Domenico Lehaye
	Ing. D.J. Toeters

Abstract

Peec-Power B.V. is developing high power range extender for hybrid electric vehicles. The first generator designs for range extender have been built and tested in the laboratory. The prototype generators use a permanent magnets with a radial flux type. These prototypes use two kinds of fractional-slot concentrated winding. The slot pole combinations that were chosen are a multiple of 9 coils around 9 teeth with 8 magnet poles and a multiple of 3 coils around 3 teeth with 2 magnet poles. There are two types of permanent magnet constructions in the rotor, which are the Surface Mounted Permanent Magnet (SMPM) and Inset Permanent Magnet (IPM).

This thesis deals with further development of the range extender generator. Two topics will be further investigated by using 2D and 3D FEM model. The first topic is the investigation of eddy current losses in the permanent magnets and rotor back iron. The second topic is the investigation of the influence of the machine ends and end windings on the flux distribution and inductivity.

The rotor eddy current losses in the prototypes machine are calculated using analytic model, 2D FEM and 3D FEM model. The 3D FEM model is used to investigate the finite length effect in 2D FEM magnet loss calculations. This investigation needs to be done since the prototype generators have a short axial length. The lamination effect on the magnet loss also will be investigated in 3D FEM model. From this investigation, a correction factor to the 2D FEM magnet loss calculation is introduced.

3D FEM models are built to investigate the influence of the machine ends and end windings. With these models, the flux leakages, end inductances and the eddy current losses in the stator end are calculated.

Acknowledgement

I would like to thank to the Indonesian Ministry of Communications and Telecommunications (MCIT) for supporting me in my study in TU Delft for the past two years. I want to thank to my supervisor, Henk Polinder, and my daily supervisor, Tim Strous, who have spent a lot of their times to guide and discuss with me about my thesis works. I also want to thank Dirk Toeters, the director of the Peec-Power B.V. for providing me the opportunity to work in the development of their great idea of range extender for hybrid vehicles.

For my parents, my family and Ainil Syalvianty Abdullah, thank you for your support and your pray for my study.

I would like also to thank to my roommate, Giga, Dwi and Kemal for all of jokes and the friendships. Thank to all of my friends in Delft (Fadly and family, Helmi, marinda, Heidi, Desi, Ryan and family, Asyuda, mbak Santi, etc) for all of the brotherhood in the last two years in Delft. Thanks to Bhimo, Mirza, Dindin, Risang, etc for our special meeting in virtual life which can refresh my brain after it saturates due to the thesis. Thanks to the students of EPP group (Mohammad, Martin, Swagat, Long Lam, Ferdinant, Rick, Arne,etc) for the discussion and jokes in the room. I also want to thank to my colleagues in s`Gravendeel office for the last 9 months of working together.

List of Figures

List of Tables

Machine Geometry Symbols

d_1	[m]	stator teeth shoe top length
d_2	[m]	stator teeth shoe skew length
d_3	[m]	stator teeth length without shoe tooth
g	[m]	air gap length
l_m	[m]	magnet length
l_{stk}	[m]	machine axial length
r_{ri}	[m]	rotor inner radius
r_{rb}	[m]	rotor yoke outer radius
r_{ro}	[m]	rotor outer radius
r_{si}	[m]	stator inner radius
r_{sb}	[m]	stator yoke inner radius
r_{ro}	[m]	stator outer radius
w_t	[m]	teeth top width
w_{ti}	[m]	teeth inner width
w_{tb}	[m]	teeth outer width
w_s	[m]	slot top width
w_{si}	[m]	slot inner width
w_{sb}	[m]	slot outer width
w_{ry}	[m]	rotor yoke width
w_{sy}	[m]	stator yoke width
θ_m	[rad]	magnet angle
θ_p	[rad]	pole angle
θ_s	[rad]	slot angle
θ_{st}	[rad]	electric stator position angle
τ_p	[m]	pole pitch
τ_m	[m]	magnet pitch
τ_s	[m]	slot pitch

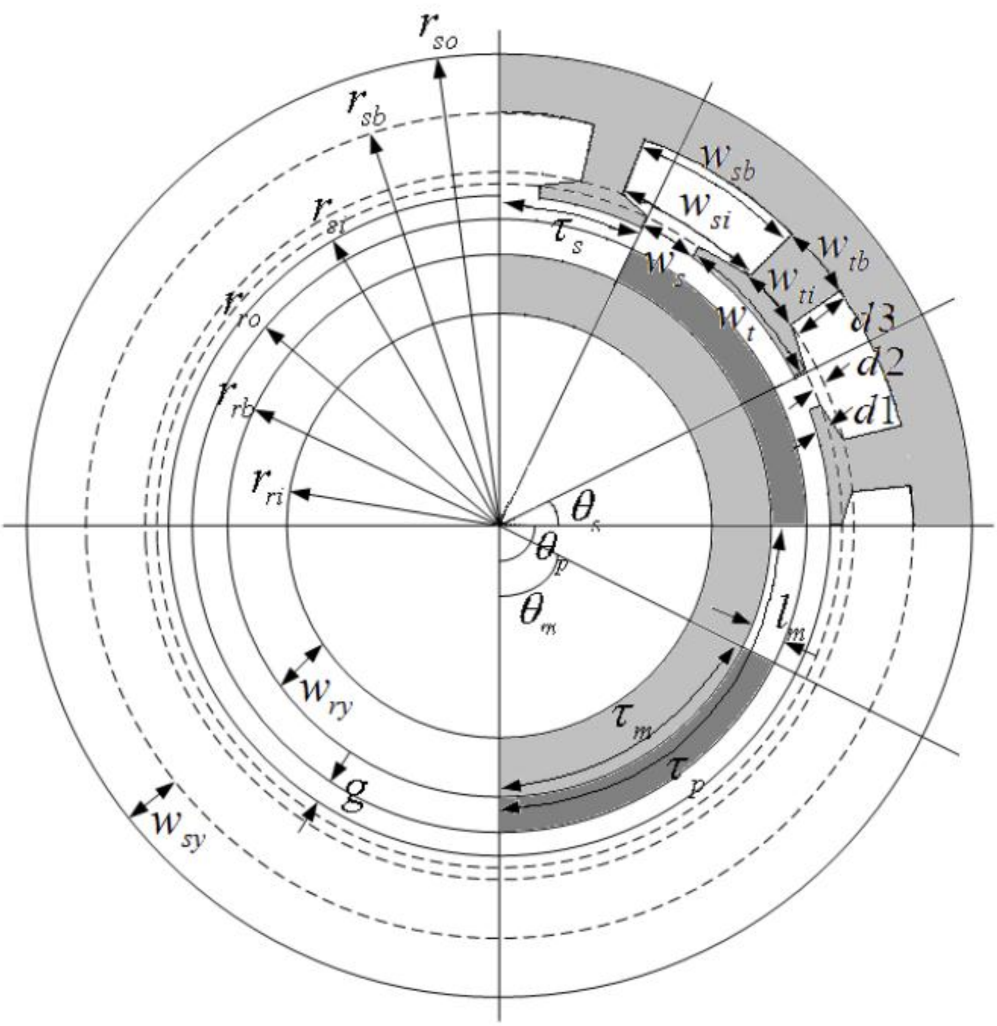

Table of Contents

1. Introduction

1.1 Background

The internal combustion engine (ICE) vehicle is one of the great human inventions for transportation. With this vehicle, the movement of people or goods is faster and therefore the productivity increases. It reduces the transportation time so that distance from one place to the other becomes smaller in terms of time. Because of its advantages, the number of ICE vehicle production increases. It finally increases the fuel consumptions. Figure 1 below shows the energy used for transportation in the OECD and non OECD country and its prediction in the future [Eia 10]. OECD is an organization which consists of 34 world`s most advanced countries and emerging country like Mexico, Chile and Turkey. The OECD promotes policies that will improve the economic and social well-being of people around the world [Oecd 11]. As can be seen from figure below, the OECD countries use half of the world`s transportation energy used in 2007. However, the prediction of transportation energy used is more dominant for non-OECD countries in 2035. It happens due to a high economic growth of emerging giants like China, India and Brazil which are not a member of OECD countries.

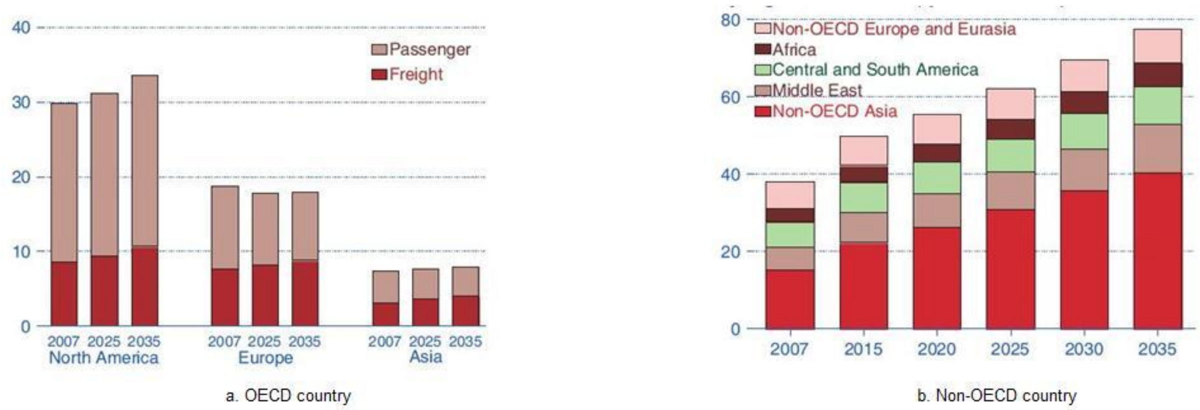

Fig. 1 World transportation energy used in the world (in quadrillion Btu)

The increases of oil needed for transportation reduces the oil reserve in the world. Since oil is a non renewable energy, it will deplete in the near future. Oil reserves will deplete in a couple of decades. Therefore the development of the electric vehicle (EV) to substitute internal combustion engine (ICE) vehicle is increasing. The needs of a substitution for ICE vehicles and the environmental concerns due to the exhaust gas from the ICE machine increase the interest in the development of electric vehicles.

Currently, electric vehicles suffer from several disadvantages over conventional vehicles. These disadvantages are:

- The limited driving range
- Large recharge times of electric batteries.
- High cost prices.
- The lack of a reliable infrastructure for electric vehicles.

To overcome the limitation above, a hybrid electric vehicle (HEV) is developed. HEV is a combination of electric and mechanical ICE drive train. The HEV is a transition technology while the fully electric vehicle technology is still in development. There are two kinds of HEV which are a parallel and a series HEV. A parallel HEV uses both the electric machine (EM) and ICE to drive the shaft while in series HEV only EM drives the shaft. In the latter cases, the ICE is coupled to a generator to generate electricity and charge battery storages. Peec-Power B.V. sees series HEV is the best technology for HEV and therefore they develop the High Power Range Extender (HPRE).

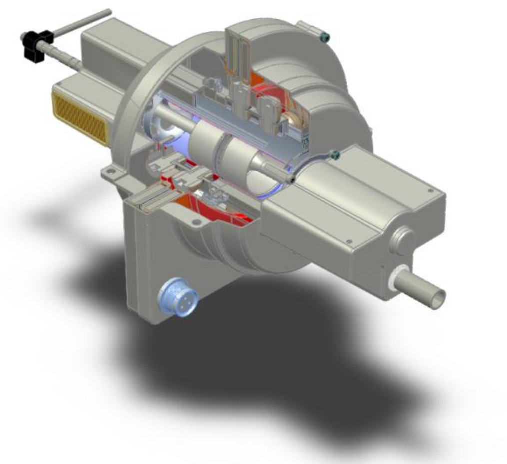

Fig. 2 High Power Range Extender

With Peec-Power Range Extender, the electric vehicles only needs the limited battery capacity to cover the shorter distances that are driven in 90% of the times. The range extender supplies the electric energy needed for a larger distance [PP10]. Therefore the drivers won`t lose their independency for driving range due to the expensive battery capacity.

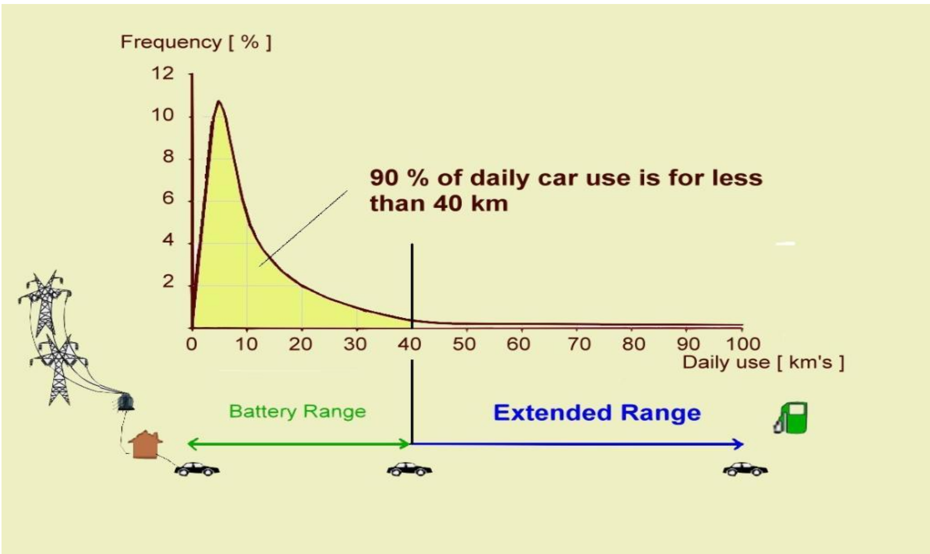

Fig. 3 Frequency of driving distance

The Peec-Power HPRE uses a generator which is coupled to an ICE with two pistons. The linear movement of the piston is transferred into a rotational movement to drive the generator. In this way, the energy from ICE is transferred into electric energy which is used to charge the batteries. The development of the Range Extender Generator based on the following criteria:

- Optimizing to cost criteria
- Optimizing to weight criteria
- Optimizing to efficiency criteria

The first prototype generators for range extender have been built and tested in the laboratory to measure the performance of the first design. The prototype generators use a permanent magnet machine with a radial flux type. These prototypes use two kinds of fractional-slot concentrated winding. The slot pole combinations that were chosen are a multiple of 9 coils around 9 teeth with 8 magnet poles and a multiple of 3 coils around 3 teeth with 2 magnet poles. There are two types of permanent magnet constructions in the rotor, which are the Surface Mounted Permanent Magnet (SMPM) and Inset Permanent Magnet (IPM). Furthermore, the IPM has three variations which correspond to different mechanical stresses in the rotor. The variations of IPM are made based on how the magnets are buried in the rotor steel. These variations give different mechanical stresses to the magnet due to centrifugal force when the rotor rotates.

After the first generator design was built, there will be further work in attempt to further optimize the generator design. Since the generator will be developed for the automotive industry, it should not be too expensive and heavy.

1.2 Problem definition

Designing an electrical machine can be done by using an analytical model, two-dimensional (2D) FEM model or three-dimensional (3D) FEM model. The analytical model has advantages due to its fast calculation time. The equations derived in analytic model are written in a program and run automatically for various parameter changes. In analytical modeling, some assumptions are used to make the model simpler and less complicated at the cost of less accurate results. On the other hand, a FEM model needs more time to be solved while the results are expected to be more accurate. Furthermore, a 3D model is much more time consuming and also needs a more powerful computer due to a vast equation matrix needed to be solved by the program.

Basically a 2D analytic model and 2D FEM model are the same in terms of the neglect of flux density flows in axial direction. It means the neglect of end region contribution to the machine performance. The use of reluctance network modeling as in [HAN 94] and [Str 10] made an assumption of a uniform flux distribution in certain regions of the machine. This assumption allows lumped calculation of reluctance in the machine. On the other hand, a 2D FEM model divides the machine model into small meshes and calculates numerically the flux density in each mesh so that a more accurate flux distribution could be expected in the machine. This difference leads to a different result between both methods depending on how accurate the analytic model is.

When an electric machine has a long axial length compared to the end windings length, the inductance due to end windings is small compared to the total inductance. Thus the 2D model is sufficient in designing the machine. For a machine with a small axial length, the end machine effects could be quite large and cannot be neglected.

In [Str 10], a 2D analytic model and its 2D FEM model were built for designing the prototype of the Range Extender Generator. An optimization routine was built by employing the analytic model and using the necessary parameter constraints for the intended machine. The existing prototypes of the Range Extender Generator were built from the results of the optimization routine.

The prototype generator has a quite small length in axial direction. The axial length of the machine is 5 cm while total diameter of the machine is around 16 cm. The end windings inductance could be quite significant in the total leakage reactance which can influence the performance of the machine. On the other hand, there will also be a leakage in the end called end leakage from the permanent magnets which doesn`t link with the stator coils. With these considerations, the end effects should be investigated to know how small the machine can be made in the axial direction.

The prototype generators use a concentrated windings permanent magnet design. According to [FIR 08], concentrated-windings has advantages compared to distributed-windings:

- It can be built automatically in the manufacture process. Thus more cost efficient compared to manual process in distributed windings.
- It has a lower copper loss. A machine with concentrated windings has a shorter end windings conductor. Therefore the resistive loss due to a current flow in the copper is lower.
- The generator can operate in fault tolerant condition for certain constraints. The coil of each phase is winded around a tooth so that it is separated physically and magnetically with another phase. Therefore a fault from one phase can have more limited influence to the other un-faulted phase.

Naturally, along with the advantages of the concentrated windings, there is also a disadvantage. A concentrated windings have more losses due to higher space harmonics components of the armature magnetic field in the air gap. In concentrated windings construction, the stator coils are wound around a tooth. The shape of air gap armature flux density produced in this construction is not sinusoidal. Therefore, the armature flux density has more space harmonics.

In the prototype range extender generator, a laminated construction is used for the rotor back iron and permanent magnet to significantly reduce the losses in the rotor due to a concentrated windings construction. With this construction, the eddy current in the rotor can be reduced but it also increases the overall cost of the machine. To cut the permanent magnets, it needs certain technology and additional work hours. This additional work increases the manufacturing cost of the laminated construction compared to a solid structure. Therefore, a solid construction should be investigated to find how much the loss in the rotor is so that a decision can be made whether a solid construction can be implemented or not.

The main objective of this thesis is to explore further development of range extender generator with the criteria explained above. With the backgrounds already described in previous paragraphs, the following topics will be investigated in this thesis:

- Investigate the eddy current losses in rotor back iron and magnets of the prototype generator for laminated or non laminated construction. The purpose is to reduce the manufacturing cost, especially from the permanent magnet lamination process.
- Investigate the influence of the machine ends and end windings on the flux distribution and inductivity in purpose to find how small a machine can be made in axial direction by using 3D FEM modeling.

To achieve the objective, an analytic, 2D and 3D FEM model will be built. By using these models, the following works will be done to answer the topics above:

- Calculate eddy current losses in rotor back iron and permanent magnet by using analytic model and 2D FEM model
- Calculate eddy current losses with 3D FEM model to explore the lamination effect on eddy current losses in the magnet.
- Calculate the end inductance
- Calculate the stator losses due to end windings in the end region
- Calculate various leakage flux due to end region

1.3 Thesis layout

In this section, a general layout of the thesis report will be presented. It explains about the objective of each chapter and provides a brief explanation of the method to accomplish the objectives.

Chapter one presents the thesis work in general. In this chapter, the background of the thesis is explained to give more information about the reason for this thesis work. After that, a problem definition is set to be more clear about the work that will be included in this thesis project. A thesis layout is presented to show the reader about the management of the thesis report.

In chapter two, an analytic calculation of eddy current losses is presented. The analytic calculation is used to give more insight about the electromagnetic behavior in the machine. This calculation also used as a second method to compared the result from FEM. A reluctance model is employed to calculate the flux distribution in the machine analytically.

Chapter three presents the FEM modeling. Finite element program is only a tool which help engineer to calculate the machine behavior numerically. The numerical calculation result is raw information which should be interpreted into more useful information about the machine. Therefore, the first thing to do is to understand about how the program works. In this chapter, the equations, modeling in FEM and general procedure of the program is presented, so that it provides a better understanding behind the numerical calculation process.

Chapter four presents 2D FEM modeling. It explains the 2D simulation setup for prototype generator and gives the results of the simulation.

Chapter five presents a 3D model of the prototype generator. The purpose of the 3D model is to evaluate the machine in the end region and the lamination effect on eddy current losses in the magnet. In this region, the flux density flows in three direction so that a 3D representation must be used. The system definition, equation used and the method to calculate the end inductance or end losses are presented here.

Chapter six presents the calculation results and analysis from the methods that are presented in chapter two until chapter five. Chapter seven presents the conclusion of the thesis and the future work that can be done.

2. Analytic calculation of eddy current losses in the rotor

Eddy currents in permanent magnet and rotor back iron are produced due to a changing flux density in time relative to the rotor. This changing flux density induces currents which flow in the material and produces heat due to resistive heating. This loss is called eddy current loss.

Eddy current loss can be calculated analytically and numerically. Numerical calculations are performed by using a Finite Element Method (FEM). In this thesis, numerical method will be carried out with a FEM program called Comsol Multiphysics v3.5a. FEM has advantage due to its accuracy but needs more time to be solved. On the other hand, analytic calculation uses more assumption which produces equation that predicts the machine behavior. Although the FEM modeling has a better accuracy, an analytic calculation gives a better insight into the machine. With this knowledge, we will have a good basis in interpreting the outcome of FEM simulation. In this thesis, the analytic calculation is used as a comparison to the result from FEM.

The derivation of the armature reaction flux density and how the eddy current losses calculated are discussed here. In the first part, an introduction of the prototype generator is presented to give more insight into the machine. After that, the reluctance network modeling and the method for calculation of eddy current losses in the rotor back iron and permanent magnets is presented.

2.1 Machine description

The prototype generators which are analyzed here are a fractional pitch concentrated windings machines with permanent magnets. The first machine has 36 teeth and 32 permanent magnet poles and the second machine has 48 teeth and 32 permanent magnet poles. The construction of the stator windings is a multiple of 9 coils around 9 teeth with 8 permanent magnet poles in the first machine and a multiple of 3 coils around 3 teeth with 2 permanent magnet poles. From here, the machine with a multiple of 9 coils around 9 teeth with 8 permanent magnet poles will be called a 9/8 slot-pole combination machine and the machine with a multiple of 3 coils around 3 teeth with 2 permanent magnet poles will be called 3/2 slot-pole combination machine. Figure 4 below shows the two machine combinations explained above.

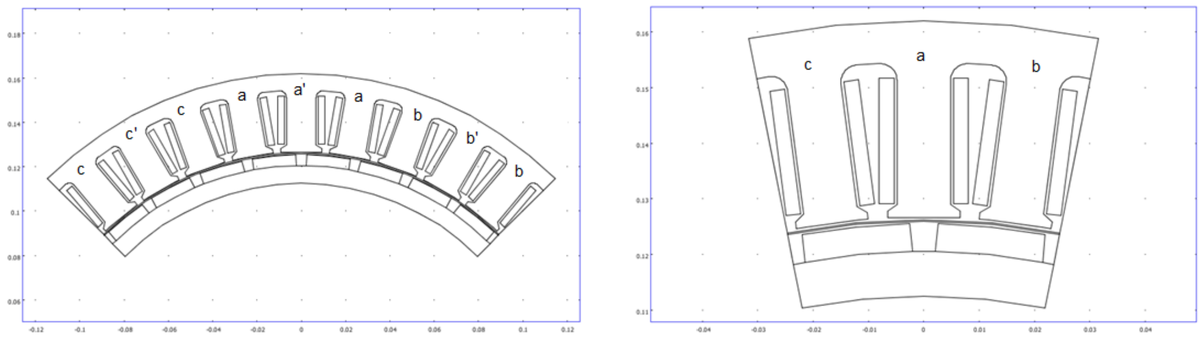

a. 9/8 Slot-pole combination machine b. 3/2 Slot-pole combination machine

Fig. 4 Machine construction for 98 and 32 combination

The prototype generators have 32 magnet poles with two kinds of permanent magnet constructions. The first one is a Surface Mounted Permanent Magnet (SMPM) and the second one is an Inset Permanent Magnet (IPM). Furthermore, the IPM have three construction variations constructions. These variations have different physical construction in how the magnet is buried in rotor steel. The mechanical stresses were calculated for each variation to see how the magnet is being stressed when the rotor rotates. These magnet constructions are depicted in figure 5 below.

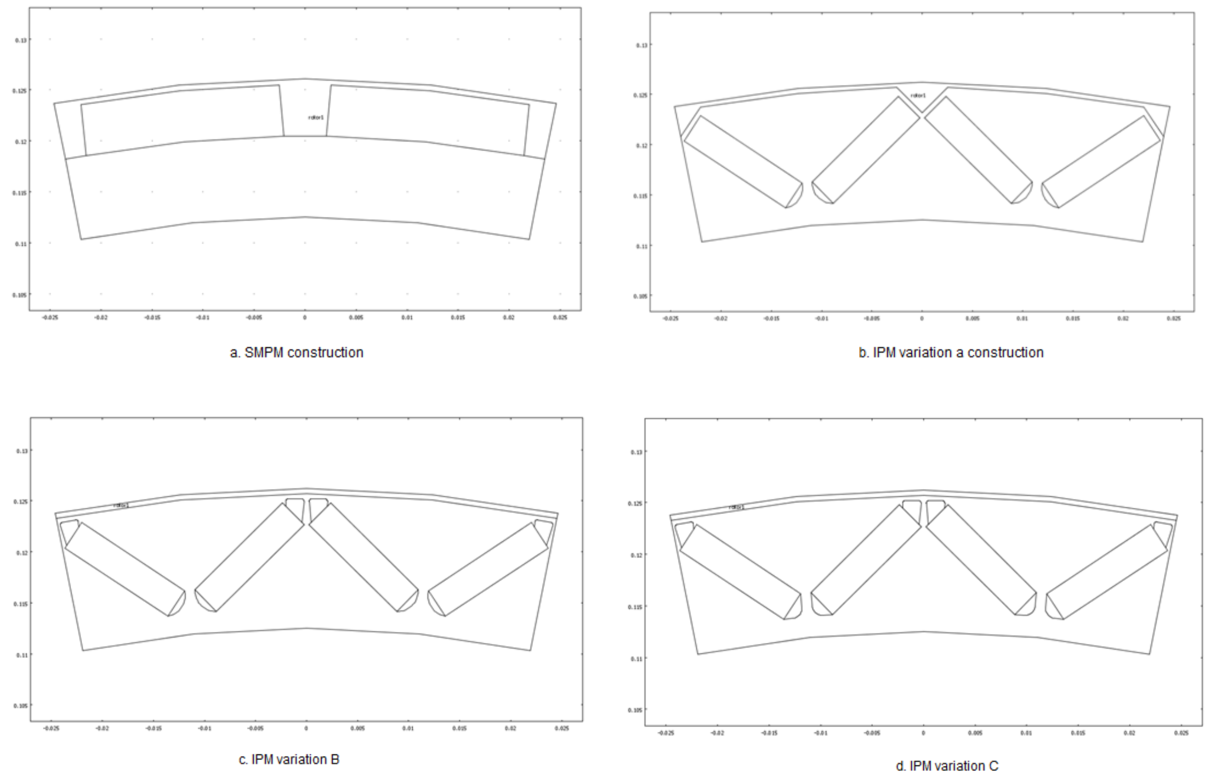

Fig. 5 Permanent magnet construction for 3/2 slot-pole combination machine

The IMPM variation B and IMPM variation C are different in the radius of the air pocket at the bottom of the magnet. IMPM variation C has a larger air pocket radius. A larger air pocket radius in the IPM variation C could create a narrower rotor back iron in this region. Thus this region saturate faster compared to the IPM variation B or variation A.

2.2 Armature reaction modeling

When the generator is loaded, the induced voltage creates a current flow in the stator windings. From Ampere`s law, a current carrying wire produces a flux density around it. It also happens in the stator windings of generator. According to Lenz`s law, for a resistive load, the direction of the current flow is such that it produces a flux density which opposes the change of magnetic field from the permanent magnets. The flux density which is produced by the stator windings interacts with the magnetic flux from the permanent magnets. This phenomena is called armature reaction.

For a concentrated windings machine, the armature reaction flux density can produce more losses in the rotor. Some of the armature reaction flux density flows through the permanent magnets and rotor back iron. Since the flux is not sinusoidally distributed, it has harmonics which can produce eddy currents when the flux has relative speed from the rotor rotation.

The armature flux density is first modeled by using the reluctance circuit. The following assumptions are used for this model.

- The current flow in the stator is purely sinusoidal.
- A balanced three phase system is assumed.
- The flux from the magnet is zero because it doesn`t contribute to the armature flux
- The air gap reluctance and permanent magnet reluctance don`t change as a function of position because the relative permeability of air and magnet is almost the same.

- The machine model is in normal operating conditions. In this condition, the flux density that flows in the machine is small so that the saturation effect is neglected
- The flux density crosses the air gap perpendicularly.

In the reluctance model, the machine is divided into a few parts and the reluctance of each part is calculated. After that, a reluctance network can be built and by employing an electric circuit law the flux distribution in the machine is obtained.

The model in this section is derived for one phase conducting current, in phase a. With this model, the flux distribution in the generator due to current in phase a can be determined. We can also calculate space harmonics in the air gap which will be used to calculate the eddy current losses in the rotor. The effect of the other phases in this model are assumed different for 9/8 slot-pole combination generator and 3/2 slot-pole combination. It will be discussed further in the next section.

When a current flows in the stator windings, it lags from the voltage waveform by angle φ[rad]. This happens because in nature, the stator windings have inductance and the increment of current delayed to charge the energy storage in the form of magnetic energy. In the calculation of eddy current losses in the rotor, this lag can be neglected because it doesn`t have any effect in the rate of change of flux density in the rotor part. So that the current waveform can be written in the following equations.

$$i_a(t) = \hat{I}_{ph} \cdot \sin(\omega_e \cdot t)$$

$$i_b(t) = \hat{I}_{ph} \cdot \sin\left(\omega_e \cdot t - \frac{2 \cdot \pi}{3}\right) \qquad (2.1)$$

$$i_c(t) = \hat{I}_{ph} \cdot \sin\left(\omega_e \cdot t - \frac{4 \cdot \pi}{3}\right)$$

Where $\hat{I}_{ph}$[A] is the amplitude of phase current, and ω_e [rad/s] is the electric rotational speed of the machine.

2.2.1 Armature reaction for a machine with a multiple 9 coils around 9 teeth with 8 poles machine

Figure 6 below shows the reluctance model for armature reaction from phase a of the 9/8 slot-pole combination machine in figure 4a.

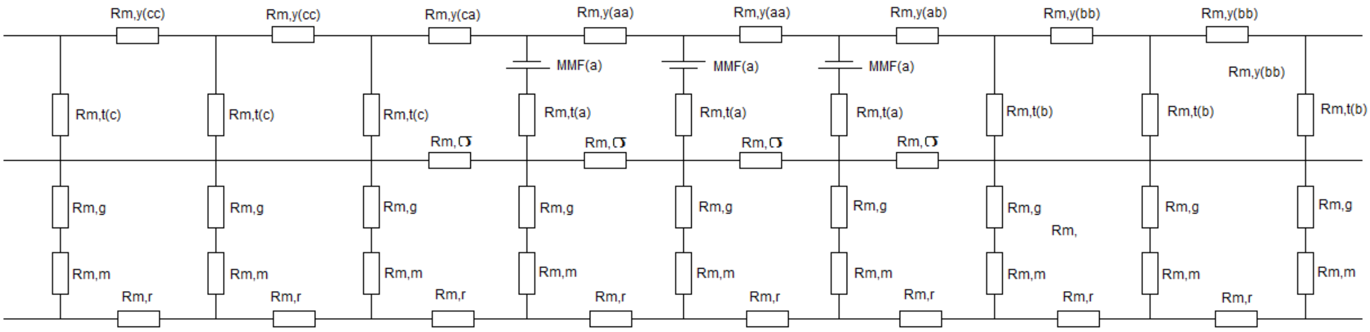

Fig. 6 Armature reaction reluctance model

Figure 6 above can be simplified into figure 7 below. With the assumption of a normal operation mode, the flux density flows in the stator iron and rotor back iron is assumed to be small so that the reluctance of the iron is negligible compared to the air gap reluctance.

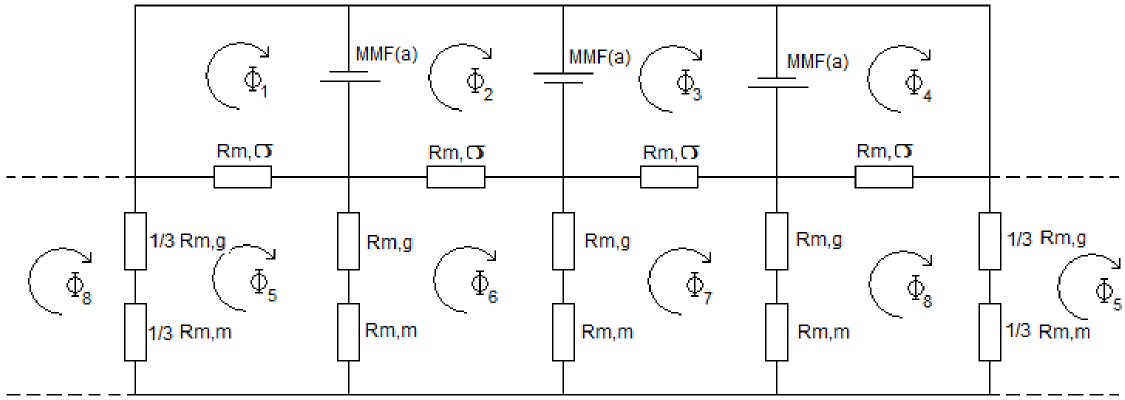

Fig. 7 Simplified armature reaction reluctance model

From the model in figure 7, 8 equations from 8 loops can be made according to Kirchoff`s law. The solution to this equation gives the flux distribution in the machine. First, the reluctance components in the figure above are derived.

The reluctance of each section of the machine can be calculated by using the following equation:

$$\mathbf{R} = \frac{\mathbf{l}}{\boldsymbol{\mu}\mathbf{A}} \qquad (2.2)$$

Where $R[A/Wb]$ is the reluctance of machine part, $l[m]$ is the distance travelled by the flux density, $\mu[H/m]$ is the permeability of the material, $A[m^2]$ is the cross section area perpendicular to the flux direction.

The flux density distribution in the air gap of the machine for one pole pitch is not homogenous. The flux from the magnet could create a fringing in the edge of the tooth tip in the air gap. The flux density in the edge of the magnet travels a longer distance compared to the flux in the middle. Therefore, the accuracy of the calculation result depends on how this fringing effect is modeled [Han 94].

To consider the flux fringing, an effective air gap $\boldsymbol{g_{eff}}[m]$ will be used throughout the air gap. This effective air gap is calculated by employing correction factor k_c.

$$\boldsymbol{g_{eff}} = \boldsymbol{g} \cdot \boldsymbol{k_c} \qquad (2.3)$$

The correction factor can be calculated from the calculation of permeance P_g which is divided into three parts in the air gap. Figure 8 below shows the permeances of the air gap.

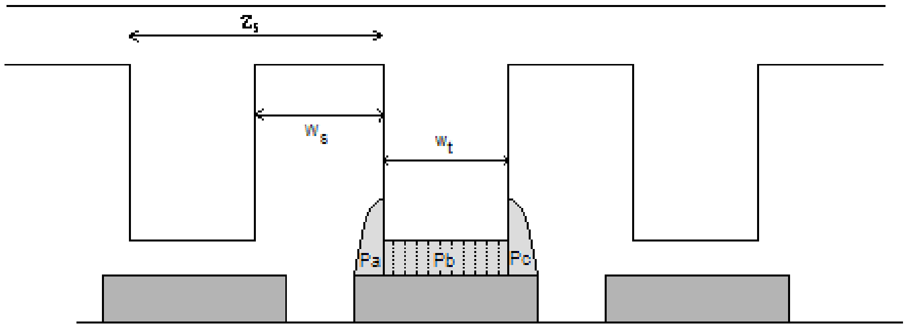

Fig. 8 Air gap flux density modeling

$$P_g = P_a + P_b + P_c = \mu_0 \cdot l_{stk} \cdot \left[\frac{w_t}{g} + \frac{4}{\pi}\log(1 + \pi \cdot \frac{w_s}{4g}\right] \quad (2.4)$$

Where $\boldsymbol{\mu_0}$ is the permeability of vacuum, $l_{stk}[m]$ is the axial length of the machine, $w_t[m]$ is the tooth width, $w_s[m]$ is the slot width and $g[m]$ is the air gap length. From [Han94], the solution above can be written in form of air gap length correction factor after some algebraic manipulation:

$$k_c = \left(1 - \frac{w_s}{\tau_s} + \frac{4g}{\pi\tau_s} \cdot \log(1 + \frac{\pi w_s}{4g})\right)^{-1} \quad (2.5)$$

Where $\boldsymbol{\tau_s}[m]$ is the slot pitch. The air gap reluctance is calculated by inserting the g_{eff} which calculated from equation 2.3 into equation 2.2.

$$R_{m.g} = \frac{g_{eff}}{\mu_0 \cdot \tau_s \cdot l_{stk}} \quad (2.6)$$

The reluctance through the permanent magnet can be calculated by using magnet thickness $\boldsymbol{l}_m[m]$ as the distance travelled by the flux density. The reluctance of the permanent magnet $\boldsymbol{R}_{m,m}[A/Wb]$ is calculated as follow:

$$R_{m.m} = \frac{l_m}{\mu_0 \cdot \mu_{rec} \cdot \tau_s \cdot l_{stk}} \quad (2.7)$$

The flux produced by the current in stator windings flows through the machine. Some of the flux crosses the air gap to the rotor and some of it does not. The flux which does not cross the air gap is regarded as a leakage flux. Figure 9 below shows the leakage which happens in the machine.

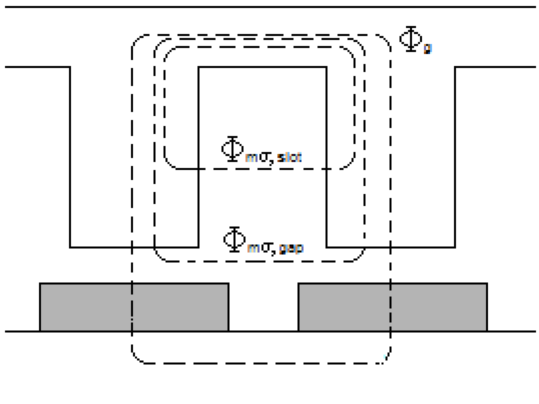

Fig. 9 Flux density contour in the machine

The flux in the machine can leak through various parts. It can leak through the slot, through the air gap or from the magnet. This leakage fluxes are part of the total inductance of the machine. The air gap leakage reluctance $R_{m\sigma,gap}$ [A/Wb] is calculated by the following equation [Gie 02].

$$R_{m\sigma,gap} = \frac{1}{\mu_0 \cdot l_{stk} \cdot \frac{5 \cdot (g/w_s)}{5 + 4 \cdot (g/w_s)}} \quad (2.8)$$

The slot leakage reluctance $\boldsymbol{R}_{m\sigma,slot}$ [A/Wb] is calculated by [Han 94]:

$$R_{m\sigma,slot} = \frac{1}{\mu_0 \cdot l_{stk} \cdot \left(\frac{d_3}{3 \cdot \frac{w_{sb} + w_{si}}{2}} + \frac{d_2}{\frac{w_s + w_{si}}{2}} + \frac{d_1}{w_s}\right)} \quad (2.9)$$

The leakage reluctance $\boldsymbol{R}_{m\sigma}$[A/Wb] is a total reluctance of the two reluctances above in parallel.

$$\boldsymbol{R}_{m\sigma} = \frac{\boldsymbol{R}_{m\sigma,gap} \cdot \boldsymbol{R}_{m\sigma,slot}}{\boldsymbol{R}_{m\sigma,gap} + \boldsymbol{R}_{m\sigma,slot}} \tag{2.10}$$

The magneto motive force MMF [A-t] of phase a windings is calculated below.

$$\overline{MMF}_a(t) = n_c \cdot i_a(t) \tag{2.11}$$

Eight sets of equation are produced by employing Kirchoff`s Voltage Law to each of the loops in figure 7. The flux distribution in the machine due to current in phase a can be calculated by using the following equation.

$$\overline{\Phi}_{\mathrm{a}}(t) = R^{-1} \cdot \overline{MMF}_a(t) \tag{2.12}$$

$$\begin{bmatrix} \phi_1(t) \\ \phi_2(t) \\ \phi_3(t) \\ \phi_4(t) \\ \phi_5(t) \\ \phi_6(t) \\ \phi_7(t) \\ \phi_8(t) \end{bmatrix} = \begin{bmatrix} \boldsymbol{R}_{m\sigma} & 0 & 0 & 0 & -\boldsymbol{R}_{m\sigma} & 0 & 0 & 0 \\ 0 & \boldsymbol{R}_{m\sigma} & 0 & 0 & 0 & -\boldsymbol{R}_{m\sigma} & 0 & 0 \\ 0 & 0 & \boldsymbol{R}_{m\sigma} & 0 & 0 & 0 & -\boldsymbol{R}_{m\sigma} & 0 \\ 0 & 0 & 0 & \boldsymbol{R}_{m\sigma} & 0 & 0 & 0 & -\boldsymbol{R}_{m\sigma} \\ -\boldsymbol{R}_{m\sigma} & 0 & 0 & 0 & \left(\frac{4}{3} \cdot (\boldsymbol{R}_{m,m} + \boldsymbol{R}_{m,g}) + \boldsymbol{R}_{m\sigma}\right) & -(\boldsymbol{R}_{m,m} + \boldsymbol{R}_{m,g}) & 0 & 0 \\ 0 & -\boldsymbol{R}_{m\sigma} & 0 & 0 & 0 & -(\boldsymbol{R}_{m,m} + \boldsymbol{R}_{m,g}) & (2 \cdot (\boldsymbol{R}_{m,m} + \boldsymbol{R}_{m,g}) + \boldsymbol{R}_{m\sigma}) & -(\boldsymbol{R}_{m,m} + \boldsymbol{R}_{m,g}) & 0 \\ 0 & 0 & -\boldsymbol{R}_{m\sigma} & 0 & 0 & -(\boldsymbol{R}_{m,m} + \boldsymbol{R}_{m,g}) & (2 \cdot (\boldsymbol{R}_{m,m} + \boldsymbol{R}_{m,g}) + \boldsymbol{R}_{m\sigma}) & -(\boldsymbol{R}_{m,m} + \boldsymbol{R}_{m,g}) \\ 0 & 0 & 0 & -\boldsymbol{R}_{m\sigma} & 0 & 0 & -(\boldsymbol{R}_{m,m} + \boldsymbol{R}_{m,g}) & \left(\frac{4}{3} \cdot (\boldsymbol{R}_{m,m} + \boldsymbol{R}_{m,g}) + \boldsymbol{R}_{m\sigma}\right) \end{bmatrix}^{-1} \cdot \begin{bmatrix} -n_c \cdot i_a(t) \\ 2 \cdot n_c \cdot i_a(t) \\ -2 \cdot n_c \cdot i_a(t) \\ n_c \cdot i_a(t) \\ 0 \\ 0 \\ 0 \\ 0 \end{bmatrix}$$

2.2.1.1 Armature reaction flux density distribution

Solving a set of equations in previous section gives the flux distribution in the machine. The fluxes that flow in the permanent magnet and rotor back iron will be used to calculate the eddy current losses in the permanent magnet and in back iron. The fluxes which flow in stator tooth, stator yoke, and rotor back iron are also provided in this section.

The effect of the other phases in this generator type is assumed to be small in the calculation of flux density in the middle stator tooth of phase a. With this assumption, the maximum flux density in the magnet is because the current flows in phase a only.

The armature reaction flux density which flows in the stator tooth is calculated below:

$$B_{ar,tooth}(t) = \frac{\phi_2(t) - \phi_3(t)}{w_t \cdot l_{stk} \cdot k_{stk}} \tag{2.13}$$

$$= \hat{B}_{ar,tooth} \cdot \sin(\omega_e t)$$

Where $\hat{B}_{ar,tooth}$ is the maximum armature reaction flux density which happens at a quarter of flux density wave length, $w_t[m]$ is the tooth width, $l_{stk}[m]$ is the axial length of the machine, and k_{stk} is lamination stacking factor.

$$\hat{B}_{ar,tooth} = B_{ar,tooth}\left(\frac{T_e}{4}\right) \tag{2.14}$$

The armature reaction flux density in the stator yoke is:

$$B_{ar,sy}(t) = \frac{\phi_2(t)}{w_{sy} \cdot l_{stk} \cdot k_{stk}} \tag{2.15}$$

$$= \hat{B}_{ar,sy} \cdot \sin(\omega_e t)$$

$$\hat{B}_{ar,sy} = B_{ar,sy}\left(\frac{T_e}{4}\right) \tag{2.16}$$

The armature reaction flux density in the rotor yoke is:

$$B_{ar,ry}(t) = \frac{\phi_7(t)}{w_{ry} \cdot l_{stk} \cdot k_{stk}} \tag{2.17}$$

$$= \hat{B}_{ar,ry} \cdot \sin(\omega_e t)$$

$$\hat{B}_{ar,ry} = B_{ar,ry}\left(\frac{T_e}{4}\right) \tag{2.18}$$

Where $w_{sy}[m]$ is the stator yoke width and $w_{ry}[m]$ is the rotor yoke width. The armature reaction flux density in air gap is equal to the armature reaction flux density in the permanent magnet in this calculation.

$$B_{ar,mag}(t) = \frac{\phi_6(t) - \phi_7(t)}{w_{ti} \cdot l_{stk} \cdot k_{stk}} \tag{2.19}$$

$$= \hat{B}_{ar,mag} \cdot \sin(\omega_e t)$$

$$\hat{B}_{ar,mag} = B_{ar,mag}\left(\frac{T_e}{4}\right) \tag{2.20}$$

2.2.1.2 Inductance calculation

The inductance of the stator windings determines the magnetic energy storage capacity. The magnetic flux is produced when a current flows through the stator windings. The inductance calculation is important for determining the performance of the machine. In this section, the inductance calculation is due to the current flows in the stator slots and doesn`t include the contribution of end turns of the windings.

The inductance calculation here is provided as comparison to the numerical inductance calculation in 2D FEM. Finally, the end leakage inductance from 3D FEM model is introduced in later chapter as the addition to the analytic calculation which will be validated with the inductance from measurement.

A self inductance L_{sa}[H] of phase a relates the current in phase a to the flux of phase a which links the phase a coils. A mutual inductance M_{ab}[H] relates the current in phase a with the flux of phase a which link the phase b coils.

$$L_{sa} = \frac{\lambda_{aa}(t)}{i_a(t)} \tag{2.21}$$

$$= \frac{n_c \cdot \phi_{aa}(t)}{i_a(t)}$$

$$M_{ab} = -\frac{\lambda_{ab}(t)}{i_a(t)} \tag{2.22}$$

The minus sign in the mutual inductance equation is because the flux density direction from current in phase a is in the opposite direction in the coils from phase b. For a balanced three phase system, the self inductance and mutual inductance in each phase is equal.

$L_s = L_{sa} = L_{sb} = L_{sc}$

$M_{ab} = M_{ac} = M_{ba} = M_{bc} = M_{ca} = M_{cb}$

The following equation shows a set of equations for the total flux linkage in each phase.

$$\begin{bmatrix}\lambda_a(t)\\ \lambda_b(t)\\ \lambda_c(t)\end{bmatrix} = \begin{bmatrix}L_s & M_{ab} & M_{ab}\\ M_{ab} & L_s & M_{ab}\\ M_{ab} & M_{ab} & L_s\end{bmatrix} \cdot \begin{bmatrix}i_a(t)\\ i_b(t)\\ i_c(t)\end{bmatrix} \tag{2.23}$$

$$\begin{bmatrix}\lambda_a(t)\\ \lambda_b(t)\\ \lambda_c(t)\end{bmatrix} = (L_s - M_{ab}) \cdot \begin{bmatrix}i_a(t)\\ i_b(t)\\ i_c(t)\end{bmatrix}$$

The self inductance can be divided into leakage inductance $L_{s\sigma}$ [H] and main inductance L_{sm} [H]. The leakage inductance is the inductance for flux that does not interact with the flux from the permanent magnet while the main inductance is the inductance for which the flux interacts with flux from permanent magnet.

$$L_s = L_{sm} + L_{s\sigma} \tag{2.24}$$

The leakage inductance can consists of the slot leakage, the air gap leakage, and also the end leakage. For the 2D analytic model in this section, the end leakage inductance is ignored. The end leakage inductance will be calculated numerically by using 3D FEM modeling in chapter 5.

$$L_{s\sigma} = L_{s\sigma(slot)} + L_{s\sigma(gap)} \tag{2.25}$$

With the flux calculated in equation 2.12 and from 2.21, 2.22 and 2.24, the inductances components are calculated as follow:

$$L_s = \frac{N_s}{3 \cdot N_{ph}} \cdot \frac{n_c \cdot (|\hat{\Phi}_1 - \hat{\Phi}_2| + |\hat{\Phi}_2 - \hat{\Phi}_3| + |\hat{\Phi}_3 - \hat{\Phi}_4|)}{\hat{I}_{ph}} \tag{2.26}$$

$$L_{sm} = \frac{N_s}{3 \cdot N_{ph}} \cdot \frac{n_c \cdot (|\hat{\Phi}_5 - \hat{\Phi}_6| + |\hat{\Phi}_6 - \hat{\Phi}_7| + |\hat{\Phi}_7 - \hat{\Phi}_8| + |\hat{\Phi}_8 - \hat{\Phi}_5|)}{\hat{I}_{ph}} \tag{2.27}$$

$$L_{s\sigma} = L_s - L_{sm} \tag{2.28}$$

$$M_{ab} = -\frac{N_s}{3 \cdot N_{ph}} \cdot \frac{n_c \cdot (|\hat{\Phi}_4|)}{\hat{I}_{ph}} \tag{2.29}$$

Where N_s is the number of slots, N_{ph} is the number of phases and n_c is the number of turns per coil.

2.2.2 Multitude 3 coils around 3 teeth with 2 poles

In this section, the reluctance network model is implemented for 3/2 slot-pole combination generator. The machine is divided into smaller parts in which the reluctance of each part will be calculated. These parts include the stator tooth, stator yoke, stator slot, air gap, permanent magnet, rotor back iron, and rotor back iron. The flux density in the stator iron and rotor back iron is assumed to be small so that the steel have a large relative permeability and a negligible reluctance compared to the reluctance in the air gap. The reluctance model in this section represents the reluctance model for one phase conducting, phase a. The reluctance network model from figure 2b is presented in figure 10 below.

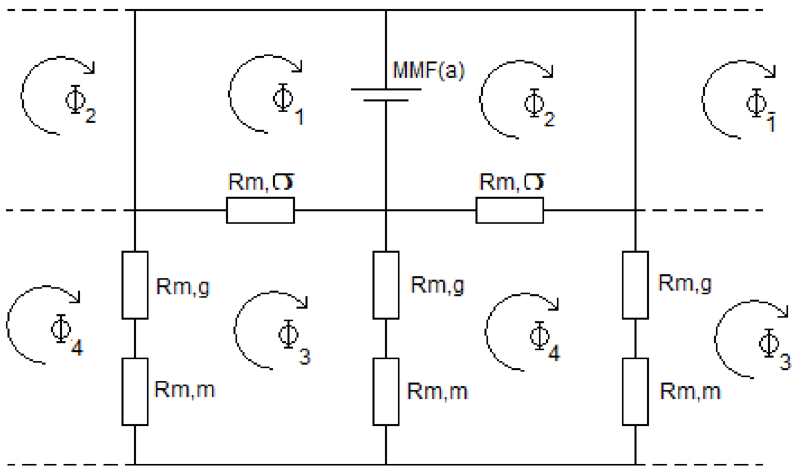

Fig. 10 Reluctance model for 3/2 slot-pole combination machine

The reluctance component in figure 10 above can be calculated by using equation 2.6, 2.7, 2.8, 2.9 and 2.10 from the previous section. After employing Kirchoff`s voltage law to the loops above, a set of 4 equations is obtained. The following equation is to solve the flux distribution in the machine.

$$\overline{\Phi}_a(t) = R^{-1} \cdot \overline{MMF_a}(t) \tag{2.30}$$

$$\begin{bmatrix}\phi_1(t)\\ \phi_2(t)\\ \phi_3(t)\\ \phi_4(t)\end{bmatrix} = \begin{bmatrix} \boldsymbol{R}_{m\sigma} & 0 & -\boldsymbol{R}_{m\sigma} & 0 \\ 0 & \boldsymbol{R}_{m\sigma} & 0 & -\boldsymbol{R}_{m\sigma} \\ -\boldsymbol{R}_{m\sigma} & 0 & (2\cdot\boldsymbol{R}_{mg}+\boldsymbol{R}_{m\sigma}) & -\boldsymbol{R}_{mg} \\ 0 & -\boldsymbol{R}_{m\sigma} & -\boldsymbol{R}_{mg} & (2\cdot\boldsymbol{R}_{mg}+\boldsymbol{R}_{m\sigma}) \end{bmatrix}^{-1} \cdot \begin{bmatrix} -n_c\cdot i_a(t) \\ n_c\cdot i_a(t) \\ 0 \\ 0 \end{bmatrix}$$

2.2.2.1 Armature reaction flux density distribution

By solving equation 2.30, the flux distribution in the machine can be obtained. The flux density distribution will be calculated from the flux density above. Additional note is that since only one phase conducting current, then the flux density distribution can be expected lower compared to when all phase windings conducting current. Since a balanced three-phase is assumed, the flux density in this model is 2/3 lower compared to when a balanced three phase current flows in the machine. Therefore, the flux density distribution calculation below will be corrected by a factor 3/2 to compensate the other phases.

The armature reaction flux density which flows in the stator tooth is calculated below:

$$B_{ar,tooth}(t) = \frac{3}{2}\cdot\frac{\phi_1(t)-\phi_2(t)}{w_{ti}\cdot l_{stk}\cdot k_{stk}} \tag{2.31}$$

$$= \hat{B}_{ar,tooth}\cdot\sin(\omega_e t)$$

Where $\hat{B}_{ar,tooth}$[T] is maximum armature reaction flux density which happens at a quarter of flux density wave length.

$$\hat{B}_{ar,tooth} = B_{ar,tooth}\left(\frac{T_e}{4}\right) \tag{2.32}$$

The armature reaction flux density in the stator yoke is:

$$B_{ar,sy}(t) = \frac{3}{2}\cdot\frac{\phi_1(t)}{w_{sy}\cdot l_{stk}\cdot k_{stk}} \tag{2.33}$$

$$= \hat{B}_{ar,sy} \cdot \sin(\omega_e t)$$

$$\hat{B}_{ar,sy} = B_{ar,sy}\left(\frac{T_e}{4}\right) \tag{2.34}$$

The armature reaction flux density in the rotor yoke is:

$$B_{ar,ry}(t) = \frac{\phi_3(t)}{w_{ry} \cdot l_{stk} \cdot k_{stk}} \tag{2.35}$$

$$= \hat{B}_{ar,ry} \cdot \sin(\omega_e t)$$

$$\hat{B}_{ar,ry} = B_{ar,ry}\left(\frac{T_e}{4}\right) \tag{2.36}$$

The armature reaction flux density in air gap is equal to the armature reaction flux density in the permanent magnet in this calculation.

$$B_{ar,mag}(t) = \frac{3}{2} \cdot \frac{\phi_6(t) - \phi_7(t)}{w_{ti} \cdot l_{stk} \cdot k_{stk}} \tag{2.37}$$

$$= \hat{B}_{ar,mag} \cdot \sin(\omega_e t)$$

$$\hat{B}_{ar,mag} = B_{ar,mag}\left(\frac{T_e}{4}\right) \tag{2.38}$$

2.2.2.2 Inductance calculation

The inductances calculation is calculated as in section 2.2.1.2 by using the result from 2.30.

$$L_s = \frac{N_s}{N_{ph}} \cdot \frac{n_c \cdot (|\hat{\phi}_1 - \hat{\phi}_2|)}{\hat{\imath}_{ph}} \tag{2.39}$$

$$L_{sm} = \frac{N_s}{N_{ph}} \cdot \frac{n_c \cdot (|\hat{\phi}_3 - \hat{\phi}_4|)}{\hat{\imath}_{ph}} \tag{2.40}$$

$$L_{s\sigma} = L_s - L_{sm} \tag{2.41}$$

$$M_{ab} = -\frac{N_s}{N_{ph}} \cdot \frac{n_c \cdot (|\hat{\phi}_q|)}{\hat{\imath}_{ph}} \tag{2.42}$$

2.3 Analytic calculation of eddy current losses in rotor back iron

Eddy current losses appear when there is a circulating current in a conductive material. This circulating current is induced due to a changing magnetic field is exposed to the material according to Faraday`s law. The direction of the induced current in such a way so that the flux density produced by the induced current opposes the flux changing in the material.

In a permanent magnet machine, the eddy current losses appear in the permanent magnets and in the rotor back iron. This loss can be harmful to the permanent magnet if the heat from the eddy current losses rises till the point where demagnetization of magnets happen. The problem of eddy current losses in the rotor is that there are difficulties in removing the heat from the losses to the cooling system in stator.

In the prototype generator, the permanent magnet and back iron are in laminated construction so that the losses in the rotor can be reduced significantly. This construction effectively reduced the eddy current in the rotor and also increases the production cost. Therefore, to investigate the possibility of using a solid rotor construction, the eddy current will be calculated. In this section, an analytic calculation is presented as a comparison to the numeric calculation by FEM. The FEM calculation is presented in chapter 4.

The eddy current losses calculation is presented in [Pol 06], [Pol 07] or in [Fir 09]. This method uses the following assumption:

- The flux density crosses the air gap perpendicularly
- The permeability of the stator iron is infinite
- The current flows in the stator windings are purely sinusoidal.

Since the prototype generator uses a concentrated windings construction, the flux density which is produced contains space harmonics which creates more losses in the rotor. Thus, the calculation of space harmonics of flux density is presented for the two types of machine combination, 9 teeth and 8 poles combination and 3 teeth and 2 poles combination. The flux density which is calculated in 2.2.1.1 and 2.2.2.1 will be presented as a Fourier series to obtain the harmonic flux density amplitude. After that, the eddy current losses in rotor back iron for laminated and solid construction is calculated. In 2.4, the eddy current losses calculation in permanent magnets is presented.

2.3.1 Stator windings space harmonics modeling

A non sinusoidal function can be written in its harmonics component in Fourier series. The following is a Fourier series of an arbitrary function g(v).

$$g(v) = a_0 + \sum_{k=1}^{\infty}(a_n \cdot \cos(nv) + b_n \cdot \sin(nv)) \qquad (2.43)$$

$$a_0 = \frac{1}{2\pi}\int_{-\pi}^{\pi} g(v) \cdot d(v)$$

$$a_n = \frac{1}{\pi}\int_{-\pi}^{\pi} g(v) \cdot \cos(nv) \cdot d(v)$$

$$b_n = \frac{1}{\pi}\int_{-\pi}^{\pi} g(v) \cdot \sin(nv) \cdot d(v)$$

Since the construction of the windings in the prototype generator is a concentrated windings, the flux density produced by the current in the stator has a non sinusoidal wave. Therefore, the armature flux density will be presented in Fourier`s series with fundamental wave length of λ_1[rad] and a function of stator position θ_{st}[rad]. The position of θ_{st}=0 is chosen in such a way so that the function is symmetrical. Thus the DC offset a_0 and sin function b_n in equation 2.43 become zero. The Fourier series of the armature flux density $B_{ar,a}$[T] is represented in the following equation:

$$B_{ar,a}(\theta_{st}) = \sum_{k=1}^{\infty} \hat{B}_{ar}(k) \cdot \cos\left(k \cdot \frac{2\pi \cdot \theta_{st}}{\lambda_1}\right) \qquad (2.44)$$

$$\hat{B}_{ar}(k) = \frac{2}{\lambda_1}\int_0^{\lambda_1} B_{ar,a}(\theta_{st}) \cdot \cos\left(k \cdot \frac{2\pi \cdot \theta_{st}}{\lambda_1}\right) \cdot d\theta_{st} \qquad (2.45)$$

The expression in 2.44 and 2.45 is for phase a. In a balanced three-phase system, the expression of space harmonics distribution is the same with phase a with a phase shifting in the equation. These expressions are changing in time since the current in each phase also a function of time. The expression of the flux density as a function of position and time is expressed below:

$$B_{ar,a}(\theta_{st}, t) = \sum_{k=1}^{\infty} \hat{B}_{ar}(k) \cdot \cos\left(k \cdot \frac{2\pi \cdot \theta_{st}}{\lambda_1}\right) \cdot \cos(\omega_e \cdot t) \qquad (2.46)$$

$$B_{ar,b}(\theta_{st}, t) = \sum_{k=1}^{\infty} \hat{B}_{ar}(k) \cdot \cos\left(k \cdot \frac{2\pi \cdot \theta_{st}}{\lambda_1} - \frac{2 \cdot \pi}{3}\right) \cdot \cos\left(\omega_e \cdot t - \frac{2 \cdot \pi}{3}\right)$$

$$B_{ar,c}(\theta_{st}, t) = \sum_{k=1}^{\infty} \hat{B}_{ar}(k) \cdot \cos\left(k \cdot \frac{2\pi \cdot \theta_{st}}{\lambda_1} - \frac{4 \cdot \pi}{3}\right) \cdot \cos\left(\omega_e \cdot t - \frac{4 \cdot \pi}{3}\right)$$

The total armature reaction flux density of the machine is the summation of the armature flux density each phases in 2.46

$$B_{ar}(\theta_{st}, t) = \sum_{k=1}^{\infty} B_{ar,a}(\theta_{st}, t) + B_{ar,b}(\theta_{st}, t) + B_{ar,c}(\theta_{st}, t) \quad (2.47)$$

Where:

$$B_{ar}(\theta_{st}, t) = \frac{3}{2} \cdot \hat{B}_{ar}(k) \cdot \cos\left(k \cdot \frac{2\pi\theta_{st}}{\lambda_1} - \omega_e \cdot t\right) \qquad \text{for k= 1,4,7,...} \quad (2.48)$$

$$B_{ar}(\theta_{st}, t) = \frac{3}{2} \cdot \hat{B}_{ar}(k) \cdot \cos\left(k \cdot \frac{2\pi\theta_{st}}{\lambda_1} + \omega_e \cdot t\right) \qquad \text{for k= 2,5,8,...}$$

$$B_{ar}(\theta_{st}, t) = 0 \qquad \text{for k= 3,6,9,...}$$

The space harmonics flux density distribution derived above is a function of stator position. The changing of flux density relative to the stator is the frequency of the current in the windings, which is ω_e[rad/s]. To calculate the eddy current losses in the rotor, the relative speed of the armature flux density to the rotor position will be determined. The relative speed of the flux density to the rotor position is showed in the following equation [Str 10]:

$$\omega_{r(k)} = \left(\frac{p_\lambda}{k} - 1\right) \cdot \omega_e \quad \text{for k= 1, 4, 7,...} \quad (2.49)$$

$$= -\left(\frac{p_\lambda}{k} + 1\right) \cdot \omega_e \qquad \text{for k=2, 5, 8,...}$$

p_λ is the number of pole pairs that fit for one wave length λ_1.

2.3.1.1 Multitude 9 coils around 9 teeth with 8 poles

The armature flux density of phase a is calculated in 2.19 for the fractional pitch 9 coils and 8 poles machine. The space flux density distribution when the current in phase a reach its maximum and the position of θ_{st}=0 is shown in the figure 11 below

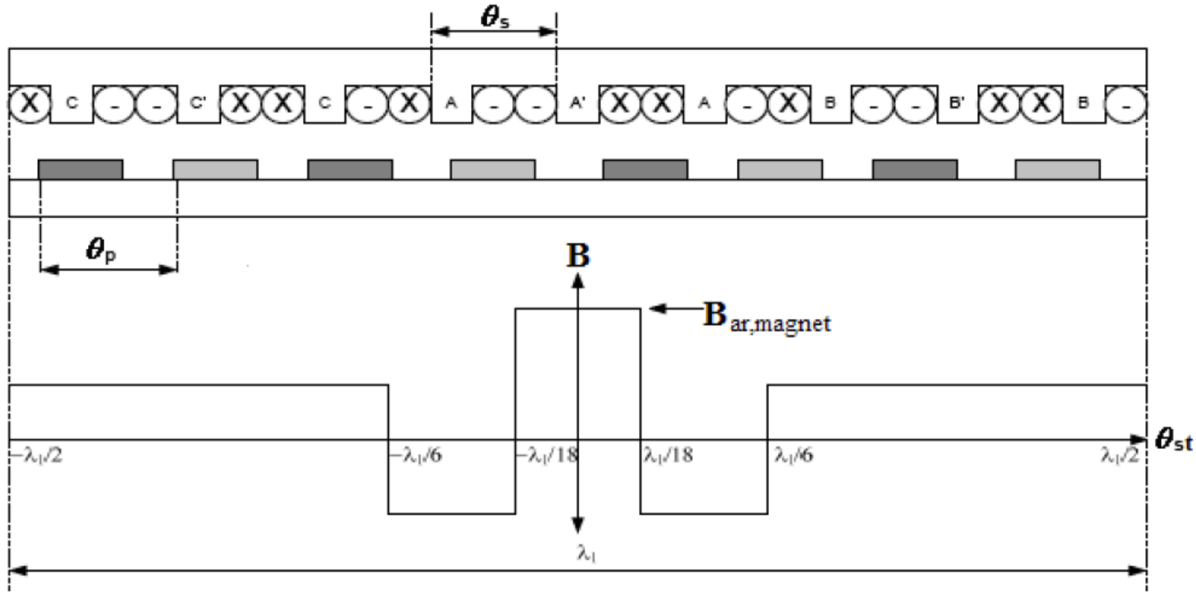

Fig. 11 Armature flux density space distribution

In this machine construction, the fundamental wave length of flux density λ_1 is equal to the number of slots multiplied by the number of pole pairs.

$$\lambda_1 = 9 \cdot \theta_s \cdot p$$

$= 8\pi$

While the number of pole pairs:

$p_\lambda = 4$

The armature reaction flux density space distribution of phase a is expressed in the following equation:

$$B_{ar,a} = \hat{B}_{ar,mag} \quad \text{for} \quad -\frac{\lambda_1}{18} < \theta_{st} < \frac{\lambda_1}{18} \tag{2.50}$$

$$= -\frac{8}{10} \cdot \hat{B}_{ar,mag} \quad \text{for} \quad -\frac{\lambda_1}{6} < \theta_{st} < -\frac{\lambda_1}{18}$$

$$\frac{\lambda_1}{18} < \theta_{st} < -\frac{\lambda_1}{6}$$

$$= \frac{1}{10} \cdot \hat{B}_{ar,mag} \quad \text{for} \quad -\frac{\lambda_1}{2} < \theta_{st} < -\frac{\lambda_1}{6}$$

$$\frac{\lambda_1}{6} < \theta_{st} < \frac{\lambda_1}{2}$$

From 2.47, the space harmonics flux density is calculated as follow:

$$\hat{B}_{ar}(k) = \frac{9}{5 \cdot k \cdot \pi} \cdot \hat{B}_{ar,mag} \cdot \left(2 \cdot \sin\left(\frac{k \cdot \pi}{9}\right) - \sin\left(\frac{k \cdot \pi}{3}\right)\right) \tag{2.51}$$

2.3.2 Armature reaction for a machine with a multiple 3 coils around 3 teeth with 2 poles machine

The armature reaction flux density in the magnet for the machine with 3 coils and 2 magnet poles is calculated from 2.37. This equation is a calculation of flux density when the current in phase b and phase c conducting a current. To calculate the flux density only due to current in phase a while the other phase current is zero, equation 2.37 will be multiplied by 2/3. The following is the armature flux density at $\theta_{st} = 0$ radian.

$$B_{ar,a}(0) = \frac{2}{3} \cdot \hat{B}_{ar,mag}$$

Figure 12 below shows the armature flux density space distribution for machine with 3 teeth and 2 magnet poles

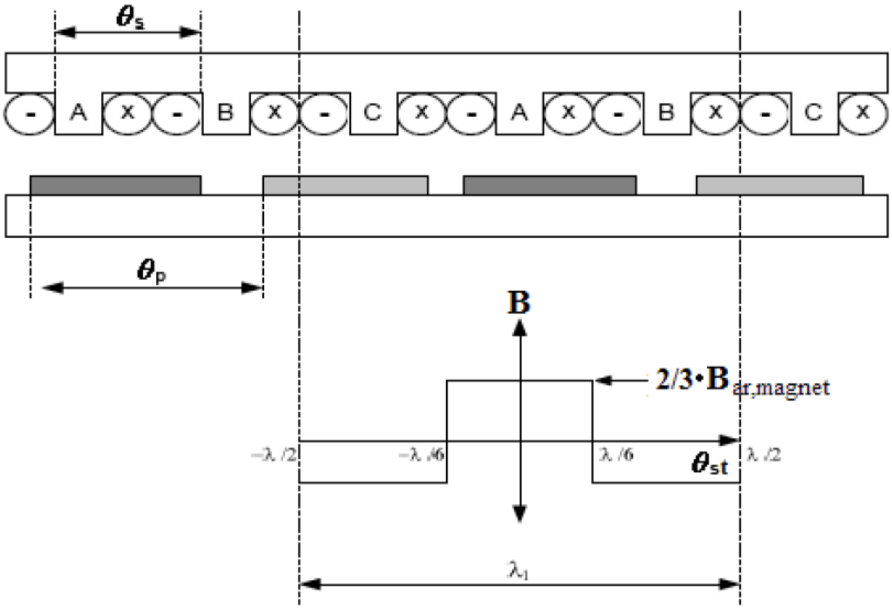

Fig. 12 Armature flux density space distribution

The fundamental wave length of flux density λ_1 is as follow:

$$\lambda_1 = 3 \cdot \theta_s \cdot p$$
$$= 2\pi$$

While the number of pole pairs:

$$p_\lambda = 1$$

The armature reaction flux density space distribution of phase a is expressed in the following equation:

$$B_{ar,a} = \frac{2}{3} \cdot \hat{B}_{ar,mag} \quad \text{for} \quad -\frac{\lambda_1}{6} < \theta_{st} < \frac{\lambda_1}{6} \tag{2.52}$$

$$= -\frac{1}{3} \cdot \hat{B}_{ar,mag} \quad \text{for} \quad -\frac{\lambda_1}{2} < \theta_{st} < -\frac{\lambda_1}{6}$$

$$\frac{\lambda_1}{6} < \theta_{st} < \frac{\lambda_1}{2}$$

The amplitude of space harmonics is calculated from equation 2.47:

$$\hat{B}_{ar}(k) = \frac{2}{k \cdot \pi} \cdot \hat{B}_{ar,mag} \cdot \sin\left(\frac{k \cdot \pi}{3}\right) \tag{2.53}$$

2.3.3 Analytic calculation of eddy current calculation in rotor back iron

The eddy current losses in rotor back iron will be calculated for a laminated construction and a solid construction. The laminated construction is already calculated in [Str 10] and also presented in [Pol 98]. The eddy current for a laminated rotor back iron is calculated in the following equation:

$$P_{loss,back\ iron} = 2 \cdot p_{Fe,Spec} \cdot \left(\frac{\omega_r}{2\pi 500}\right)^{1.5} \cdot \left(m_{s,ry} \cdot \left(\frac{B_{ar,ry}}{1.3}\right)^2\right) \tag{2.54}$$

Where $p_{Fe,Spec}$ [W/kg] is the specific loss of the laminated back iron

The eddy current losses in solid back iron construction is calculated in the following equation as in [Fir 08], [Pol 06] and [Pol 07]. The eddy current loss in 2.55 below is the losses per square meter of surface are.

$$P_A = \sum_{k=1}^{\infty} \frac{\hat{B}_{ar}(k)^2 v(k)^2 \delta(k)}{4\rho_{Fe}} \quad (2.55)$$

The translational relative speed v [m/s] is calculated from relative rotational speed in 2.49 as follow:

$$v_r = \frac{\tau_p}{\pi} \cdot \omega_r \quad (2.56)$$

With the skin depth is given by:

$$\delta = \sqrt{\frac{2\rho_{Fe}}{\mu_0 \mu_{rFe} \omega_r}} \quad (2.57)$$

Where $\rho_{Fe}[\Omega \cdot m]$ is back iron resistivity, μ_0 is the permeability of vacuum, μ_{rFe} is the relative permeability of rotor back iron and $\omega_r[rad \cdot s^{-1}]$.

2.4 Analytic calculation of eddy current losses in permanent magnet

In this section, the eddy current losses in permanent magnet will be derived. The losses derivation is based on the Faraday`s law. The following equation shows the Faraday`s law in integral form.

$$\oint_c \bar{E} \cdot dl = -\frac{d}{dt} \iint_s \bar{B} \cdot dA \quad (2.58)$$

This equation says that an electric field will appear in a closed contour C when there is a changing flux density crosses a surface area enclosed by the contour C. This electric field finally creates a current flow in the contour and due to the presence of resistance in the magnet, it create a resistive heating in it. The equation of eddy current losses in permanent magnet is derived from equation 2.58 with the following set of assumptions [Pol 98]:

- The flux density in the magnet is purely sinusoidal as a function of time
- The flux density in the magnet has only radial direction which crosses perpendicularly to the magnet plane
- The flux density is homogenous throughout the magnet width τ_m.
- The effect of eddy current on the magnetic field is negligible.
- The magnet length in z direction is assumed much longer compared to the magnet width. In this way, the resistance in the axial length is more dominant compared to in width direction. Therefore, the end effect is neglected. In this way, the field strength $\bar{E}$[Vm^{-1}] is assumed only appear in z direction. Considering the end effect would increases the resistance and reduces the eddy current losses. Neglecting the end effect means an overestimated approximation of the magnet loss.

From the first assumption, the following is the magnetic flux density in the magnet as a function of time:

$$B(t) = \hat{B} \cdot \sin(\omega_r \cdot t) \quad (2.59)$$

Figure 13 below shows the magnet figures.

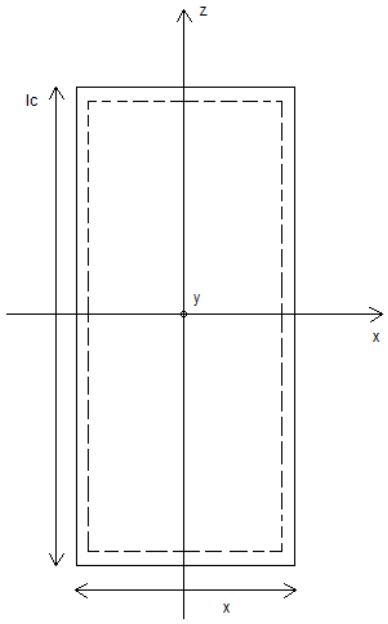

Fig. 13 Magnet representation

With these assumptions, the contour for electric field in equation 2.58 only appears in z direction.

$$\begin{aligned} -l_c \cdot E_z(x) + l_c \cdot E_z(-x) &= -l_c \cdot \frac{d}{dt}\int_{-x}^{x} \bar{B}(t) \cdot dA \\ &= -2 \cdot l_c \cdot x \cdot \frac{d\bar{B}(t)}{dt} \\ &= -2 \cdot l_c \cdot x \cdot \omega_r \cdot \hat{B} \cdot \cos(\omega_r \cdot t) \end{aligned} \tag{2.60}$$

The position of the x=0 so that it will be in the middle of the magnet. Thus the electric field will be an odd function:

$$-E_z(x) = E_z(-x)$$

The electric field can be expressed with the current density with the same direction of electric field J_z[A.m^{-2}] and the magnet resistivity ρ_m[Ωm].

$$E_z(x) = \rho_m \cdot J_z(x) \tag{2.61}$$

With 2.61 and electric field expression, equation 2.60 can be written:

$$J_z(x) = \frac{1}{\rho_m} \cdot x \cdot \omega_r \cdot \hat{B} \cdot \cos(\omega_r \cdot t) \tag{2.62}$$

By using equation 2.62, a specific magnet loss (magnet loss per unit volume) $p_{m,spec}$[W/m^3] as a function of width and time is expressed below:

$$\begin{aligned} p_{m,spec}(x,t) &= \rho_m \cdot {J_z}^2(x) \\ &= \rho_m \cdot \left(\frac{1}{\rho_m} \cdot x \cdot \omega_r \cdot \hat{B} \cdot \cos(\omega_r \cdot t)\right)^2 \end{aligned} \tag{2.63}$$

The average specific magnet losses for one period of time can be calculated by integration of equation 2.63 divided by its period of time:

$$p_{m,spec}(x) = \frac{1}{2 \cdot \rho_m} \cdot \left(x \cdot \omega_r \cdot \hat{B}\right)^2 \qquad (2.64)$$

The average specific magnet losses for one unit length can be calculated by integration of equation 2.64 divided by its unit length:

$$p_{m,spec} = \frac{1}{24 \cdot \rho_m} \cdot \left(x \cdot \omega_r \cdot \hat{B}\right)^2 \qquad (2.65)$$

Equation 2.65 shows that the specific magnet loss is proportional to the square of magnet width x[m], the relative speed of magnetic flux to the rotor ω_r[rad/s] and the amplitude of magnetic flux $\hat{B}$[T]. Therefore, the eddy current losses for a solid and laminated magnet, the width x is substitute by solid magnet length τ_m[m] and lamination length l_m[m].

$$p_{m,spec} = \frac{1}{24 \cdot \rho_m} \cdot \left(\tau_m \cdot \omega_r \cdot \hat{B}\right)^2 \qquad (2.66)$$

$$p_{ml,spec} = \frac{1}{24 \cdot \rho_m} \cdot \left(l_m \cdot \omega_r \cdot \hat{B}\right)^2$$

Since the flux density for concentrated windings consist many space harmonics as calculated in section 2.3.1.1 and 2.3.1.2, the losses calculation for all of the harmonics becomes:

$$p_{m,spec} = \sum_{k=1}^{\infty} \left(\frac{1}{24 \cdot \rho_m} \cdot \left(\tau_m \cdot \omega_{r,(k)} \cdot \hat{\boldsymbol{B}}_{ar,(k)}\right)^2\right) \qquad (2.67)$$

$$p_{ml,spec} = \sum_{k=1}^{\infty} \left(\frac{1}{24 \cdot \rho_m} \cdot \left(l_m \cdot \omega_{r,(k)} \cdot \hat{\boldsymbol{B}}_{ar,(k)}\right)^2\right)$$

By using the magnet volume V_m[m^3] and equation 2.67, the magnet losses for solid and laminated construction is calculated as follow:

$$P_{loss,m} = V_m \cdot p_{m,spec} \qquad (2.68)$$

$$P_{loss,ml} = V_m \cdot p_{ml,spec}$$

The analytic model to calculate the eddy current losses in permanent magnets and rotor back iron have been shown in this chapter. The calculation results in this chapter will be presented in chapter six as a comparison with 2D FEM or 3D FEM model. Together with these two FEM model, some of it will be compared with the measurement result of prototype machines from the laboratory.

3. Finite element method modeling

This chapter describes about the numerical calculation method of the machine performance by using Finite Element Method (FEM). The advantage of using Fem is that it can deal with complex models. The drawback is that it needs more time to solve the problem depends on the model complexity. The machine model is divided into small meshes and then the electromagnetic quantities are solved for each of the meshes.

The FEM method in this thesis is COMSOL v3.5a. The program is used to assist the student in predicting the machine design. The result that is obtained from the program is a raw result which must be interpreted by the student. The process in the program basically uses the electromagnetic problem described by well known Maxwell` equations. Therefore, the understanding of the equations and also how the model be solved by the program is an important aspect when dealing with the FEM modeling.

In the first part, the Maxwell`s equations that is used in the program will be provided. After that setting some parameter in the model is provided. In the last part, the general-procedure is explained.

3.1 Maxwell equations in FEM

The electromagnetic field behavior can be explained by the Maxwell`s equations. These equations show the relationship between the electromagnetic quantities: electric field intensity E [Vm^{-1}], the electric flux density D[Cm^{-2}], the magnetic field intensity H[Am^{-1}], the magnetic flux density B(T), the current density J(Am^{-2}), and the electric charge density ρ[Cm^{-3}]. These relations can be expressed in differential or integral form. The differential form of Maxwell equations will be presented here because this form is used by the FEM to be solved. The following set of equations shows the Maxwell equations:

$$\nabla \times \vec{H} = \vec{J} + \frac{\partial \vec{D}}{\partial t} \tag{3.1}$$

$$\nabla \times \vec{E} = -\frac{\partial \vec{B}}{\partial t} \tag{3.2}$$

$$\nabla \cdot \vec{D} = \rho \tag{3.3}$$

$$\nabla \cdot \vec{B} = 0 \tag{3.4}$$

Equation 3.1 is called Maxwell-Ampere`s law and 3.2 is Faraday`s law. The equation 3.3 and 3.4 are called Gauss`s law in electric and in magnetic field respectively. The other fundamental equation is continuity equation as follow:

$$\nabla \cdot \vec{\mathrm{J}} = -\frac{\partial \rho}{\partial t} \tag{3.5}$$

The following are the generalized constitutive relations that describe the macroscopic properties of the medium. These equations are well suited for modeling non linear material:

$$\vec{\mathrm{D}} = \varepsilon_0 \varepsilon_r \vec{E} + \vec{D}_r \tag{3.6}$$

$$\vec{\mathrm{B}} = \mu_0 \mu_r (\vec{H} + \vec{B}_r) \tag{3.7}$$

$$\vec{J} = \sigma \vec{E} + \vec{J}^e \tag{3.8}$$

Here ε_0 [Fm^{-1}] is the permittivity vacuum, ε_r is the relative permittivity of material, μ_0[Hm^{-1}] is the permeability of vacuum, μ_r is the relative permeability of the material, $\sigma[\Omega^{-1} m^{-1}]$ is the electric conductivity and J^e is external current density. D_r is the remanent displacement which is the displacement when no electric field is present. B_r is the remanent magnetic flux density which is the magnetic flux density when no magnetic field is present.

3.2 Potentials

Electric fields can be calculated from the Coulomb`s law as in [Fey 64] by calculating the integral of static electric charge in space. In this reference, an electric scalar potential is introduced to simplify the equation. When we get the electric potential, the electric field can be calculated by differentiate it. The electric field in magnetostatic condition is calculated as follow:

$$\vec{\mathrm{E}} = -\nabla \mathrm{V} \tag{3.9}$$

As have been done in electric field, a magnetic vector potential A is introduced. From the differential calculus we know that the divergence of a curl is zero. Therefore, the flux density B[T] in equation 3.4 can be expressed by the curl of vector field. This vector field defines the flux density as follow:

$$\vec{\mathrm{B}} = \nabla \times \vec{A} \tag{3.10}$$

By inserting 3.10 into 3.2 we get:

$$\nabla \times \left(\vec{E} + \frac{\partial \vec{A}}{\partial t}\right) = 0 \tag{3.11}$$

In 3.11, we can suggest that the term in the bracket is a gradient of scalar field because a curl of gradient of a scalar field is zero. From 3.2, 3.9 and 3.11, the electric field when there is a changing magnetic field can be expressed as follow:

$$\vec{\mathrm{E}} = -\nabla \mathrm{V} - \frac{\partial \vec{A}}{\partial t} \tag{3.12}$$

Equation 3.10 and 3.12 do not define the magnetic and electric fields uniquely because the there will be others magnetic vector potential A’ and electric scalar potential V’ which give the same result. The addition of a constant C in V or a gradient in A will give the same result since a derivative of a constant and a curl of a gradient is zero. This variable transformation is called gauge transformation. Helmholtz`s theorem says that to have a vector field is uniquely defined, both the divergence $\nabla \cdot A$ and the curl $\nabla \times A$ are given. When there is no current appear, the curl of magnetic field in 3.1 is zero, therefore, a scalar magnetic potential is introduced as follow:

$$\vec{\mathrm{B}} = -\nabla \mathrm{V}_{\mathrm{m}} \tag{3.13}$$

3.3 Boundary condition

Electrical machines contain various materials with different characteristics. The material for stator and back iron steel is a material with high relative permeability while the permanent magnet has a low relative permeability which closes to the air permeability. On the other hand, a highly conductive material like in the stator coils and also the aluminum has a low relative permeability.

The different material characteristics influence the flux density in the machine. The flux density distribution or the flux intensity can change from one material to the adjacent material. Therefore, a definition of how the electromagnetic quantities relate each other in the boundary of two materials must be defined. These definitions are specified in the boundary condition. At interfaces between two materials, the boundary conditions are expressed as follow:

$$n_2 \times \left(\vec{E}_1 - \vec{E}_2\right) = 0 \tag{3.14}$$

$$n_2 \cdot (\vec{D}_1 - \vec{D}_2) = \rho_s \tag{3.15}$$

$$n_2 \times (\vec{H}_1 - \vec{H}_2) = \vec{J}_s \tag{3.16}$$

$$n_2 \cdot (\vec{B}_1 - \vec{B}_2) = 0 \tag{3.17}$$

Where n_2 is the normal unit vector outward from medium 2, $\rho_s[Cm^{-2}]$ is surface charge density and $J_s[Am^{-2}]$ is surface current density. For current density condition on interface between material:

$$n_2 \times (\vec{J}_1 - \vec{J}_2) = \frac{\partial \rho_s}{\partial t} \tag{3.18}$$

3.3.1 Periodic boundary condition

When a machine`s magnetic behavior repeats after some distance in rotational direction, it is useful to model of a fraction of full machine model. By this symmetry, the 9/8 slot-pole combination machine is only drawn for one fourth and one sixteenth for 3/2 slot-pole combination machine. With this modeling, the model to be solved is smaller and more time efficient in computation times.

To build the model, a periodic boundary condition is implemented to determine the magnetic behavior between two model parts. There are two types periodic boundary condition:

- Continuity: when the electromagnet quantity continue from source to destination.
- Anti periodicity: when the electromagnet quantity changing sign from source to destination.

For the 2D model in this thesis, the magnetic vector potential in boundary condition is continuity. The following shows the condition for continuity periodic boundary condition:

$$\mathrm{A_{dst}} = \mathrm{A_{src}} \tag{3.19}$$

3.4 Permanent magnet modeling

Permanent magnet modeling is used to give the magnetization direction for the flux density from the permanent magnet. The magnets are modeled according to the Maxwell`s constitutive relation in 3.7. The remanent flux density B_r[T] determines the magnetic field direction. Since the magnet position in the rotor is changing in its position, B_r will change as a function of position. Figure 14 below shows the principle of Comsol program assigns the magnetization to the permanent magnet

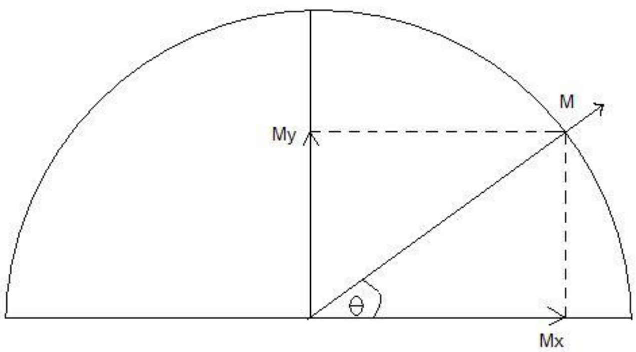

Fig. 14 Magnetization of permanent magnet

Where M is the magnetization direction, M_x is magnetization in x axis direction and M_y is magnetization in y axis direction. The magnetization M is calculated with the following equation:

$$\overline{\mathrm{M}} = M_x + M_y \tag{3.20}$$

$$M_x = \bar{M} \cdot \cos\theta \tag{3.21}$$

$$M_y = \bar{M} \cdot \sin\theta \tag{3.22}$$

3.4.1 Surface mounted permanent magnet

The SMPM machine has a radial magnetization of permanent magnet in the x-y reference frame. The remanent flux B_r[T] determines the direction of the magnetic field. In this model, the remanent flux is for the operating temperature of 120° Celsius. For radial outward magnetization of the magnet, Br becomes:

$$\begin{bmatrix} B_{r,x} \\ B_{r,y} \end{bmatrix} = \begin{bmatrix} B_{r,120} \cdot \frac{X}{\sqrt{X^2+Y^2}} \\ B_{r,120} \cdot \frac{Y}{\sqrt{X^2+Y^2}} \end{bmatrix} \tag{3.23}$$

For radial inward magnetization of the magnet, Br[T] becomes:

$$\begin{bmatrix} B_{r,x} \\ B_{r,y} \end{bmatrix} = \begin{bmatrix} -B_{r,120} \cdot \frac{X}{\sqrt{X^2+Y^2}} \\ -B_{r,120} \cdot \frac{Y}{\sqrt{X^2+Y^2}} \end{bmatrix} \tag{3.24}$$

3.4.2 Inset mounted permanent magnet

The permanent magnet position in the IPM rotor is rotated 45 degree from the radial direction. Therefore, the magnetization direction of the IPM rotor model is adjusted 45 degree. The equation in 3.25 and 3.26 becomes:

$$M_x = M \cdot \cos\left(\theta + \frac{\pi}{4}\right) \tag{3.25}$$

$$M_y = M \cdot \sin\left(\theta + \frac{\pi}{4}\right) \tag{3.26}$$

Since there are two magnets in one pole pitch, then there will be four magnetization equations for one pole pair. As in section 3.4.1, the magnetization direction is determined by the remanent flux density B_r. Figure 15 below shows four magnetizations of one pole pair.

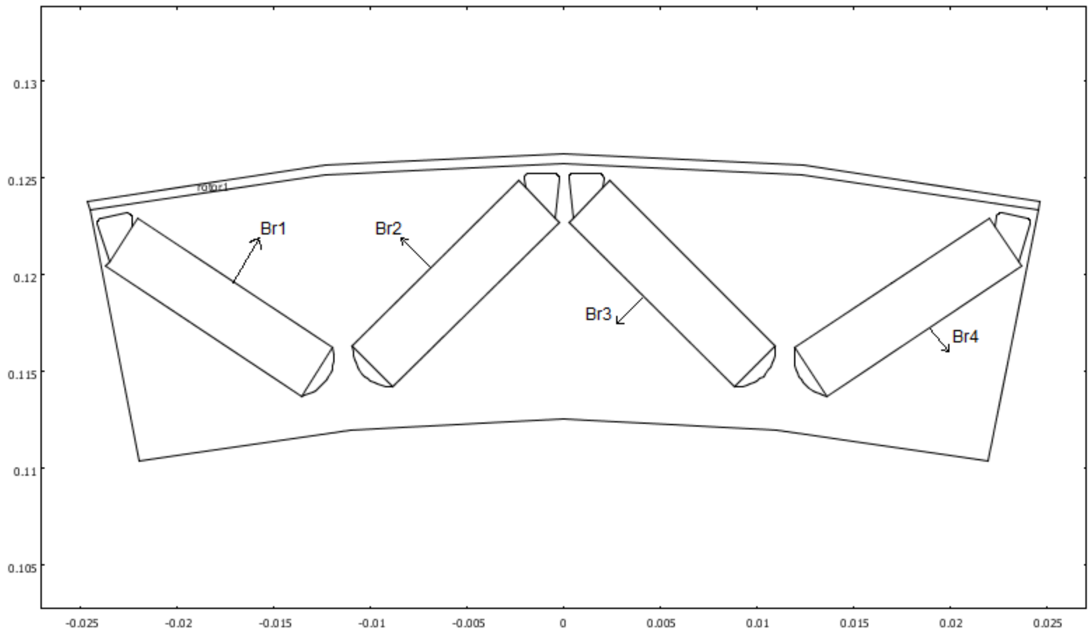

Fig. 15 Magnetization of IPM

After employing trigonometry identity to equation 3.25 and 3.36, the following four set of equations are acquired

$$\begin{bmatrix} B_{r,x1} \\ B_{r,y1} \end{bmatrix} = \begin{bmatrix} B_{r,120} \cdot \left(\frac{X}{\sqrt{X^2+Y^2}} \cdot \cos\left(\frac{\pi}{4}\right) + \frac{Y}{\sqrt{X^2+Y^2}} \cdot \sin\left(\frac{\pi}{4}\right) \right) \\ B_{r,120} \cdot \left(\frac{Y}{\sqrt{X^2+Y^2}} \cdot \cos\left(\frac{\pi}{4}\right) - \frac{X}{\sqrt{X^2+Y^2}} \cdot \sin\left(\frac{\pi}{4}\right) \right) \end{bmatrix} \tag{3.27}$$

$$\begin{bmatrix} B_{r,x2} \\ B_{r,y2} \end{bmatrix} = \begin{bmatrix} B_{r,120} \cdot \left(\frac{X}{\sqrt{X^2+Y^2}} \cdot \cos\left(\frac{\pi}{4}\right) - \frac{Y}{\sqrt{X^2+Y^2}} \cdot \sin\left(\frac{\pi}{4}\right) \right) \\ B_{r,120} \cdot \left(\frac{Y}{\sqrt{X^2+Y^2}} \cdot \cos\left(\frac{\pi}{4}\right) + \frac{X}{\sqrt{X^2+Y^2}} \cdot \sin\left(\frac{\pi}{4}\right) \right) \end{bmatrix} \tag{3.28}$$

$$\begin{bmatrix} B_{r,x3} \\ B_{r,y3} \end{bmatrix} = \begin{bmatrix} -B_{r,120} \cdot \left(\frac{X}{\sqrt{X^2+Y^2}} \cdot \cos\left(\frac{\pi}{4}\right) + \frac{Y}{\sqrt{X^2+Y^2}} \cdot \sin\left(\frac{\pi}{4}\right) \right) \\ -B_{r,120} \cdot \left(\frac{Y}{\sqrt{X^2+Y^2}} \cdot \cos\left(\frac{\pi}{4}\right) - \frac{X}{\sqrt{X^2+Y^2}} \cdot \sin\left(\frac{\pi}{4}\right) \right) \end{bmatrix} \tag{3.29}$$

$$\begin{bmatrix} B_{r,x4} \\ B_{r,y4} \end{bmatrix} = \begin{bmatrix} -B_{r,120} \cdot \left(\frac{X}{\sqrt{X^2+Y^2}} \cdot \cos\left(\frac{\pi}{4}\right) - \frac{Y}{\sqrt{X^2+Y^2}} \cdot \sin\left(\frac{\pi}{4}\right) \right) \\ -B_{r,120} \cdot \left(\frac{Y}{\sqrt{X^2+Y^2}} \cdot \cos\left(\frac{\pi}{4}\right) + \frac{X}{\sqrt{X^2+Y^2}} \cdot \sin\left(\frac{\pi}{4}\right) \right) \end{bmatrix} \tag{3.30}$$

3.5 Moving mesh

A rotor rotation can be simulated in the Comsol by assigning a displacement in rotor sub domain as a function of time t[s]. The rotor displacement depends on the rotational speed n_m[rpm] of the machine. The displacement of the rotor sub domain is calculated by the following equation:

$$\begin{bmatrix} \frac{dx}{dt} \\ \frac{dy}{dt} \end{bmatrix} = \begin{bmatrix} \cos\left(2 \cdot \pi \cdot \frac{n_m}{60} \cdot t\right) \cdot x - \sin\left(2 \cdot \pi \cdot \frac{n_m}{60} \cdot t\right) \cdot y - x \\ \sin\left(2 \cdot \pi \cdot \frac{n_m}{60} \cdot t\right) \cdot x + \cos\left(2 \cdot \pi \cdot \frac{n_m}{60} \cdot t\right) \cdot y - y \end{bmatrix} \tag{3.31}$$

3.6 General procedure

In this section, a general procedure to make a FEM modeling in Comsol v3.5a is presented.

Application modes selection

Comsol has variation of application modes. These application modes are the specification of the equations and also variables that are going to be solved. The equations will be different from one application mode to the other and they consist of Maxwell equations which have been already described in previous section with adjustment depending on the model to be solved. The application mode of the FEM-model in the following chapter is described first to give the information what equation involved in the model.

Geometry modeling:

After choosing the application mode, the model drawing is made in Comsol. The drawing could be done by using Comsol GUI and/or by using Matlab incorporation. The other method is by importing from another graphical drawing program in dxf format. The drawing of the model could be full machine or only part of it due to its symmetry condition. The use of symmetry can saved time consumption when solving the model.

Sub-domain description:

Sub-domain is the part of FEM model which represent the real machine. The material characteristic of each sub-domain or the current injection are defined in this section.

Boundary condition:

The boundary conditions between different sub-domains in the machine are described according to boundary condition which already described in section 3.3. There are additional boundary conditions for specific condition such as a relative movement of one sub-domain to the others. Another specific boundary is the periodic boundary when a model with symmetry is applied.

Mesh generation:

After setting the material physical description and the boundary condition are specified, the FEM model is divided into small meshes. The mesh generation can be done automatically by initialize the mesh or by specific setting for more accurate result in some part. The meshing quality corresponds to the simulation result accuracy. But with a higher accuracy the computing time increases.

Problem solution:

The electromagnetic which is described in the application mode is solved in each mesh. Various solvers can be used to be solved for the FEM model. Different solver uses different method when solving the problem.

4. 2D Modeling of prototype generator

In this chapter, a 2D FEM model of prototype generator by using Comsol Multiphysics 3.5a is presented. This model has two purposes which are as a method to validate the analytic model in chapter two and to calculate for a more complex model. The machine with the IPM rotor has a more complex configuration. Therefore, a FEM model is chosen to calculate the eddy current losses numerically.

Due to the symmetry, the machine model will be built only one fourth for 98-combination machine and one sixteenth for 32-combination machines. This method has advantage that it creates a smaller model to be solved.

In the first section, the application modes that are used will be presented. It shows about the Maxwell equations behind the model. After that the simulation setup is presented. In the last part, the results of the simulation are given.

4.1 System definition

The 2D model which has already been built lies in the x-y axis. The two models for SMPM and two combinations machine are shown in figure 2. When the machine is loaded, a current flows in the stator coils and this current produces a magnetic flux density which we called armature reaction flux density. In modeling this armature reaction, an external current density is injected perpendicularly to the modeling plane. Hence the magnetic flux density presents only in the modeling plane. For this purpose, a perpendicular induction current application mode will be used. On the other hand, a rotor rotation simulation also needed. For these two purposes, a special *Rotating Machinery* application mode is used. This application mode consists of *Perpendicular Induction Currents* to give the possibility for current injection and *Moving Mesh* for the possibility of rotor rotation simulation.

Two simulations will be done which are a static simulation and a transient time dependant simulation. The first simulation is used for initial condition of the second one. Since the simulation is static, the time dependant terms in equation 3.1 and 3.2 are zero. By injecting external current density J^e in the stator windings sub domain and setting the conductivity of the coil to zero we can simulate a current flow in the stator windings. From equations 3.1, 3.7, 3.8 and 3.10, the Maxwell`s-Ampere`s law become:

$$\nabla \times \left(\mu_0{}^{-1}\mu_r{}^{-1}\nabla \times \vec{\mathrm{A}} - \vec{\mathrm{B}}_{\mathrm{r}}\right) = \vec{J}^e \tag{4.1}$$

4.2 Simulation setup

There are eight 2D FEM models that have been built. The models can be divided into SMPM machine model and the IPM machine model. In each machine model, two types machine combination are built which are 98-combination and 32-combination. In addition, each of machine types for IPM, there are three variation types of magnet construction. These variations have different physical construction how the magnet is buried in rotor steel. The mechanical stresses were calculated for each variation to see how the magnet is being stressed.

The simulation procedure of each machine is explained in section 3.6. After the application mode definition in section 4.1 is chosen, the machine models were built by using both Comsol graphical user interface and also with Matlab. Table 1 below gives the machine specification and the material used in the model. Due to confidentiality, the information about machine geometry is shown in the confidential appendices. In addition, the stator and rotor back iron steel characteristic is shown in the appendix 1.

Parameter	Description	Value
P_{rat}	Rated power	35000 [W]
n_m	Mechanical rotational speed	3000 [rpm]
$\hat{I}_{ph}$	Amplitude phase current	65 [A]
ρ_{fe}	Back iron resistivity	$2 \cdot 10^{-7}\ [\Omega \cdot m]$
ρ_m	Magnet resistivity	$1.3 \cdot 10^{-6}\ [\Omega \cdot m]$
$B_{r,SMPM}$	Remanent flux density for SMPM	1.1 [T]
$B_{r,IMPM}$	Remanent flux density for IPM	1.2 [T]
$\mu_{r,m}$	Relative permeability of magnet	1.05

Table 1. Model Parameter

There are three different boundary conditions used in these models:

- Magnetic insulation boundary: This boundary is applied in the outer stator back iron and inner rotor back iron. In reality, the material on top of this layer has a much lower relative permeability compared to rotor or stator steel back iron. Therefore it is assumed there will be no flux density crosses this boundary. In Comsol, the magnetic vector potential in z direction is set to zero, A_z=0 so that there is no flux crossing this boundary.
- Continuity boundary: In this boundary, the tangential component of the magnetic flux is expressed by $n \times \left(\vec{H}_1 - \vec{H}_2\right) = 0$.
- Periodic boundary condition: The periodic boundary condition between two sections of the machine model is set to continuity which means that magnetic vector potential source is equal to magnetic potential destination as in equation 3.23.

The next step is to create meshes in the model. Meshing process is important because it correspond to the accuracy of the simulation result. As explained before, there are two kinds of simulations involved, first for no-load induced voltage and for eddy current losses calculation. For these purposes, the meshing in the air gap was made finer because in this area the exchange of energy happens. In the other part, the mesh in the rotor back iron also made finer because the eddy current losses is concentrated in a small layer on top of the rotor due to the skin effect. The skin effect in the magnet is rather longer compared to the magnet length. Therefore the meshes in the magnet boundary were made finer as well.

The meshing in periodic boundary needs more attention. This boundary condition connect one section of the model to the other and define how the electromagnet behavior in this boundary. Or we can say how the electromagnetic behavior between the boundaries in left of the model to the right of the model. Therefore, the boundary setting in this section should have an identical mesh. It can be done by meshing one periodic boundary and copy the mesh to the other periodic boundary. The quality of the mesh in this section also depends on its position. In the air gap or in the rotor back iron is important so that in the boundary in this section should be finer. Figure 16 below shows an example of the meshing for SMPM with 9/8 slot-pole combination machine.

The simulation is carried out twice. First, a static simulation is done to get a result for time t=0[s]. After that a transient time dependant to simulate the rotation is done for one electric period T=0.00125[s] with 50 time steps for no load simulation and 1.5-2 times electrical period for eddy current simulation to overcome the overshoot. The simulation was done by using direct solver with accuracy of $1x10^{-6}$ for magnetic vector potential A_z.

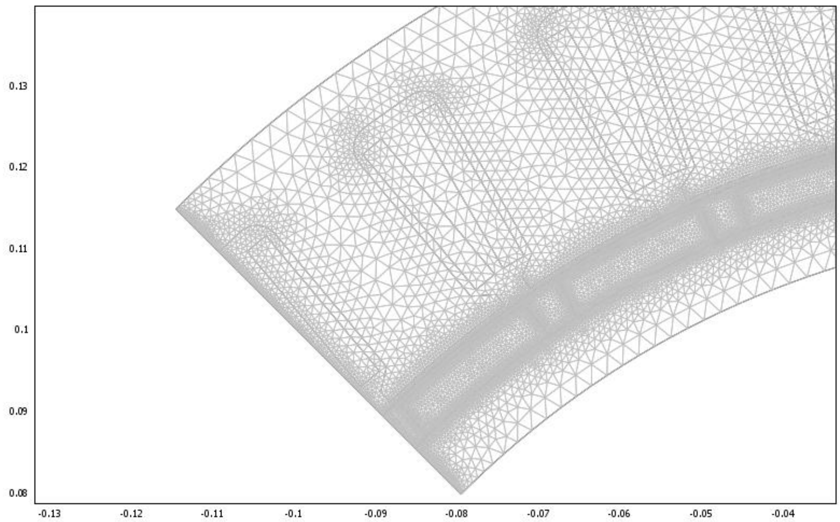

Fig. 16 Meshing result for SMPM of 9/8 slot-pole combination machine

4.3 Simulation result

This section shows the two simulations that already conducted: no load induced voltage and eddy current losses calculation. The first part of simulation shows the result of prediction of no load induced voltage of the machine. This result will be compared to the measurement of the prototype generator in the laboratory. The second simulation is for eddy current calculation. All of eddy current calculation in this model is only for solid construction

4.3.1 No load induced voltage

The no load induced voltage simulation was done by setting the current in conductor to zero and rotating the machine for one electrical period. The induced voltage in the coil V_c[V] is calculated from the Faraday`s law by integrating the electric field $\bar{E}[V/m]$ over the stator windings. But since a 2D model doesn`t see the end connection, an approximation to neglect the voltage due to end windings is done. The voltage is calculated by taking the average electric field in z component E_z over its sub domain surface area and multiplies it by the stack length l_{stk} of the machine and the number of conductor for each phase. To accommodate the other section model, the total voltage equation is multiplied by the number of sector symmetry n_{symm}. In this model, the n_{symm} is equal to 4 for 9/8 slot-pole combination and 16 to 3/2 slot-pole combination machine

$$V_c = n_{symm} \cdot n_c \cdot \frac{l_{stk}}{A_{draw}} \cdot \int E_z \cdot dA_{draw} \qquad (4.2)$$

Figure 17 and 18 below show the induced voltage, phase to neutral, for four kind machines. The figure shows the comparison of induced voltage between SMPM and the IPM construction for each machine combination. As can be seen, the IPM machine induced less voltage compared to SMPM machine. It means that less flux density crosses the air gap to the stator windings.

Table 2 below shows the induced voltage amplitude for each of the model.

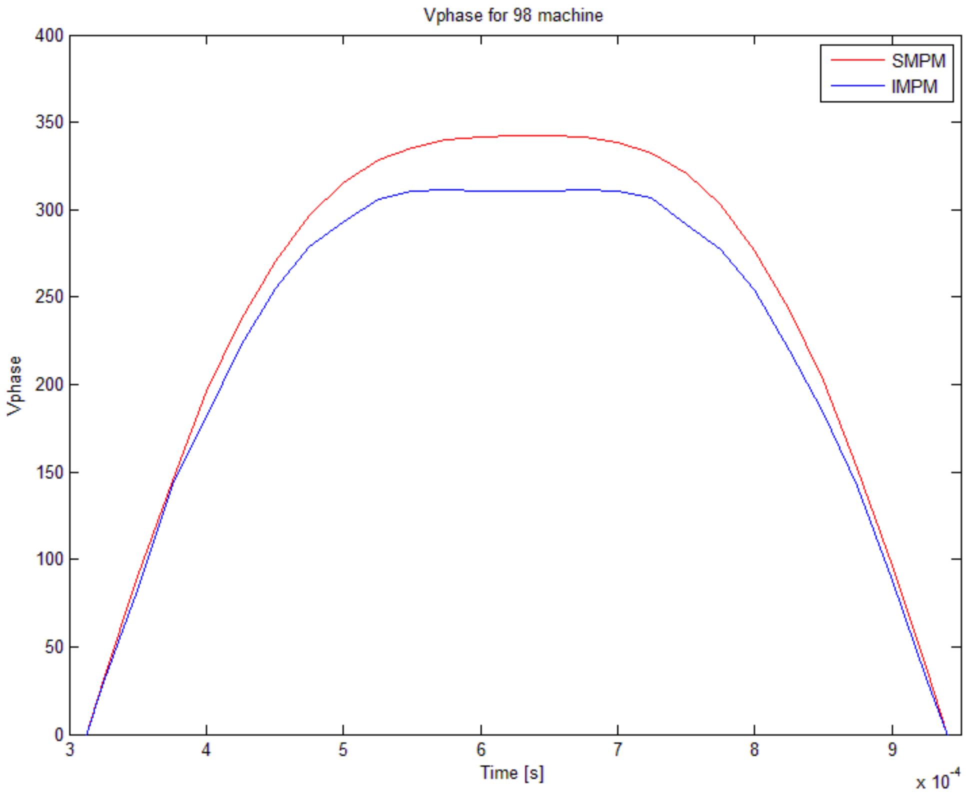

Fig. 17 Induced voltage comparison for 9/8 slot-pole combination machine

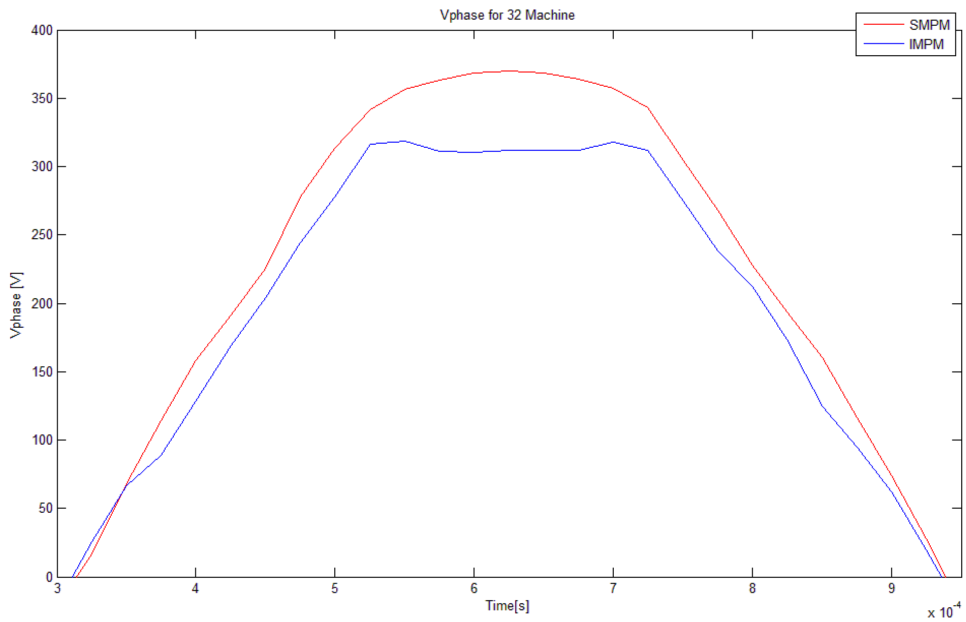

Fig. 18 Induced voltage comparison for 3/2 slot-pole combination machine

Combination Type	$\widehat{V}_{ph}(V)$
SMPM	
98 Combination	343
32 Combination	354
IPM	
98 Var A	311
98 Var B	308
98 Var C	315
32 Var A	320
32 Var B	316
32 Var C	320

Table 2 Induced voltage amplitude of FEM models

As can be seen from table 2 above, the induced voltage amplitude for the IPM generator is lower compared to the SMPM generator. It happens because the magnets in the IPM are buried in the rotor steel. This construction creates a short circuited reluctance in rotor so that some of the flux from magnets leak in the rotor steel. Finally, this additional leakage contributes to the reduction of the induced voltage in the stator windings. The three IPM construction variations don`t show any difference between each other. The induced voltages of the three IPM variations are almost the same.

4.3.2 Inductance calculation

The method to calculate the inductance is by calculating the flux density distribution in the machine model and then calculating the magnetic energy stored in the system. In Comsol, the energy stored can be calculated by the following equation:

$$W_{m,2D} = \iiint v_m dV \qquad (4.3)$$

Where $W_{m,2D}$[J] is the magnetic energy within a certain sub domain in the 2D model, v_m (J/m^3), is magnetic energy density in the sub domain and dV (m^3) is the volume of the sub domain object. On the other hand, the energy stored in the system can also be calculated by the inductance L[H] and a constant current I[A] as follow:

$$W_{m,2D} = \frac{1}{2} \cdot L \cdot I^2 \qquad (4.4)$$

Where I[A] is the current that flows in the coil which produces the flux density in the system. Finally the inductance L[H] is derived from equation 4.4 and multiplying with the number of sector symmetry n_{symm}:

$$\mathrm{L} = \mathrm{n_{symm}} \cdot \mathrm{l_{stk}} \frac{2 \cdot \mathrm{W_{m,2D}}}{I^2} \qquad (4.5)$$

By using equation 4.5, the inductances of prototype generators are presented in table 3 below.

Parameter	Units	9/8 slot-pole combination machine	3/2 slot-pole combination machine
		SMPM	
L_s	µH	548	266
M_{ab}	µH	-42	-132
		IPM	
L_s	µH	1000	550

M_{ab}	µH	-186	-227

Table 3 Inductance calculation from 2D FEM

Table 3 above shows that the inductances for 9/8 slot-pole combination machine are higher compared to 3/2 slot-pole combination machine. It happens because the 9/8 slot-pole combination machine has more coil turns. In addition, the winding configuration in the 9/8 slot-pole combination machine produces more armature flux density in the machine. Therefore, the inductances will be higher compared to the 3/2 slot-pole combination machine. The inductances calculation in table 3 above also shows that the IPM machines have a higher inductance compared to SMPM. The IPM rotor back iron is closer to the stator iron compared to the SMPM machine. It makes the reluctance in the air gap lower so that more armature fluxes cross the air gap. It makes the IPM machine inductance is higher.

4.3.3 Eddy current losses calculation

The eddy current losses calculation was done by injecting a balanced three phase current into the stator windings sub domain. After that, a static simulation at time t=0[s] was done to get an initial value for flux density distribution in the machine. This result is used in the transient time dependant simulation as the initial condition. These two simulations were done to simulate the induced current in the rotor due to a relative changing of armature flux density with the rotor. This induced current flows in the magnet and rotor back iron material. Since these two materials have certain resistivity, the induced current produced heat as the eddy current loss.

In Comsol, the eddy current losses can be calculated by integrating the resistive heating density $W_{loss}(Wm^{-3})$ of the sub domain. The eddy current losses calculation is shown in the following equation:

$$W_{ec} = \iiint W_{loss} dV \quad (4.6)$$

$$= \mathrm{n_{symm}} \cdot \mathrm{l_{stk}} \cdot \iint W_{loss} dA_{draw}$$

Where $W_{ec}[\mathrm{W}]$ is the eddy current losses in the object-material, $\mathrm{V}[\mathrm{m}^3]$ is the volume of the material and A_{draw} is the drawn sub domain surface area.

Figure 19(a) below shows an example of flux density distribution for machine with 3 teeth and 2 magnets pole combination machine. Figure 19 (b) and 19(c) show the induced current and resistive heating respectively in the machine. As can be seen from the result, the induced current and resistive heating only appear in the permanent magnet and rotor back iron since it was assumed that the stator iron has zero conductivity.

Another point that can be seen from the result is that the induced current in the rotor back iron only appears in a small distance to the rotor back iron thickness. It happens due to a small skin depth in the rotor back iron.

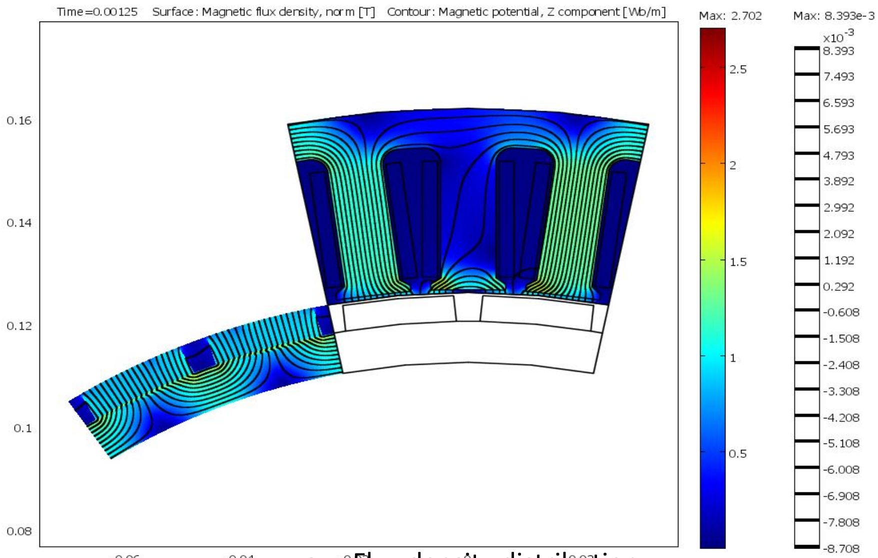

a. Flux density distribution

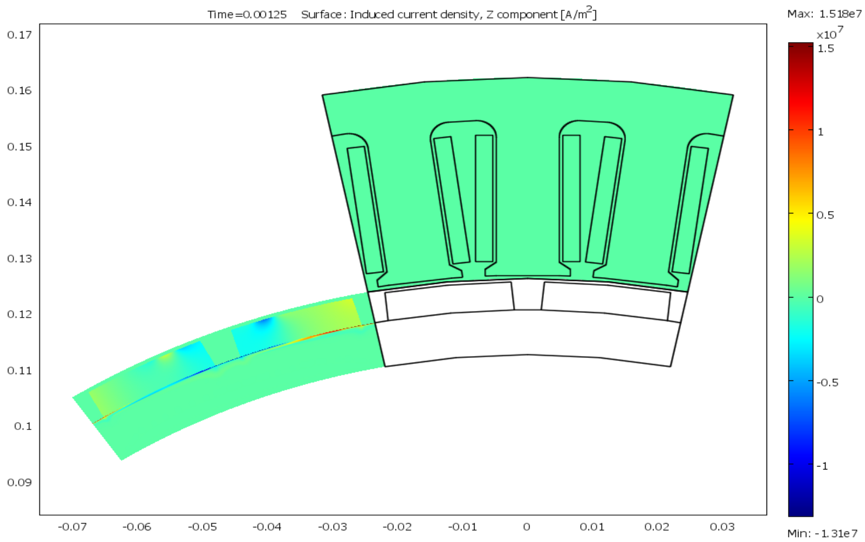

b. Induced current density

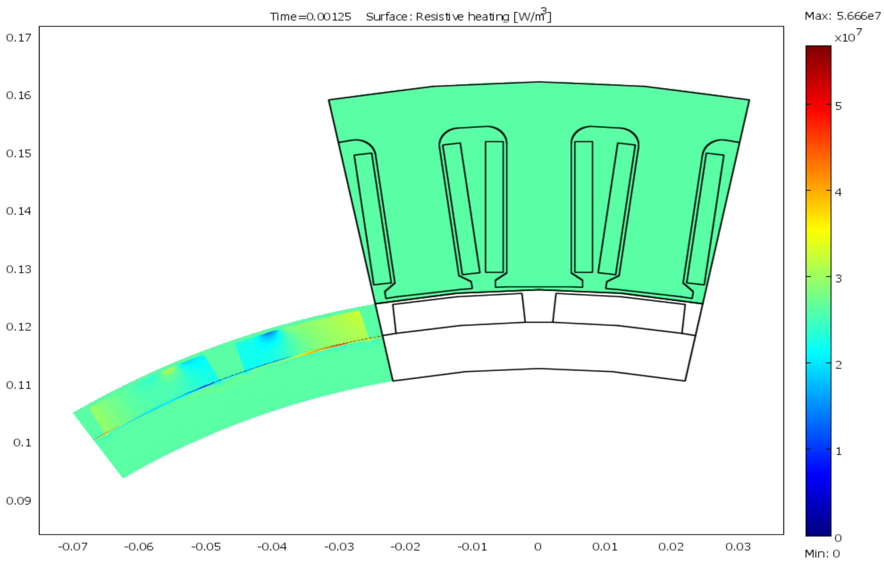

c. Resistive heating

Fig. 19 Simulation result of 3/2 slot-pole combination machine for t=T

Table 4 below shows the eddy current losses in the solid rotor back iron and solid permanent magnet for the SMPM and the IPM machine. As can be seen from table 4 below, the eddy current in solid rotor back iron for IPM machine is too large. A solid construction for rotor back iron cannot be implemented in the IPM machine. Table 5 below shows the eddy current losses in solid magnet for IPM machine. The rotor back iron conductivity is set to zero for laminated back iron.

Combination type	Solid Back Iron Losses (W)	Solid Magnet Losses (W)
SMPM		
98 combination	289	720
32 combination	23.3	150
IPM		
32 combination	4443	27.42

Table 4 Eddy current losses for solid construction

Combination type (IPM)	Solid Magnet Losses (W)
32 Comb. Var A	3.68
32 Comb. Var B	16.4
32 Comb. Var C	20.0
98 Comb. Var A	206
98 Comb. Var B	192
98 Comb. Var C	201

Table 5 Eddy current losses for laminated rotor back iron and solid magnet construction

Table 5 above shows that the solid magnet loss of the IPM machine is lower compared to SMPM machine. It can be understood since the magnet is buried in the rotor steel. Most of the armature flux flows in the rotor back iron and goes back to the stator tooth. The eddy current loss in IPM variation A for 3/2 slot-pole combination is rather smaller. While the variation C is the highest. The construction of the rotor back iron in the IPM variation A leads to less armature flux flows in the magnet sub-domain for a lower armature flux density. In 9/8 slot-pole combination, the armature flux density is higher. Therefore the flux density in a narrow rotor back iron gets higher and creates a region which is highly saturated. The relative permeability of this area becomes closer to the air relative permeability. Thus the construction of the rotor back iron will be the same seen by the flux density. Finally the armature flux density creates almost the same eddy current losses in the magnets.

Table 4 above shows that the eddy current losses in the magnets are quite high for SMPM rotor. An investigation of eddy current losses in the magnet with lamination in circumferential direction is investigated by using 2D FEM model. Figure 20 and table 6 below shows the reduction in eddy current losses in the magnets for SMPM rotor construction. As can be seen from figure 20 and table 6 below, the laminations of the magnet in axial direction significantly reduce the eddy current losses in the magnet. The other advantage to laminate the magnet in axial direction for SMPM is that the possibility to use a block shape magnet compared to an arch magnet. This means a cheaper magnet production can be achieved. To be noted that there will be more flux leakages due to this laminations.

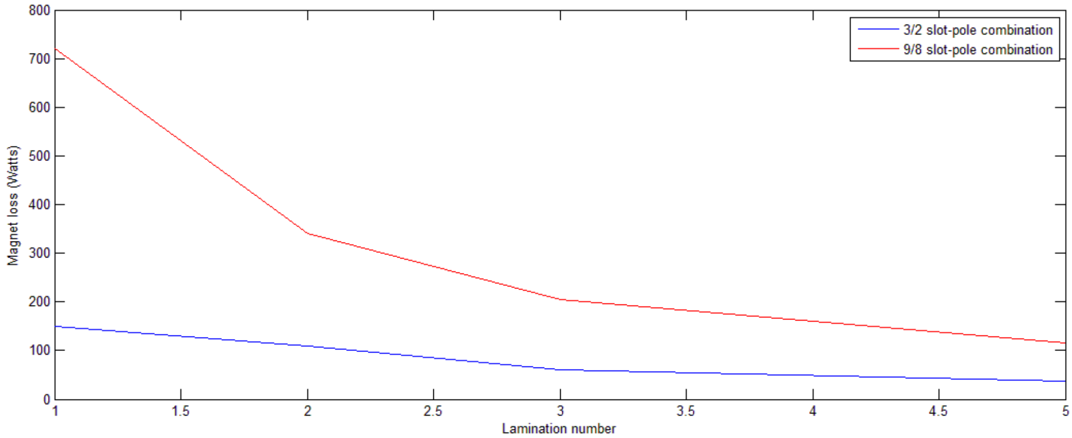

Fig. 20 Eddy current losses as a function of lamination number

Machine type	Lamination number			
	1	2	3	5
SMPM	Magnet losses (Watts)			
3/2 slot-pole combination	150	109	60	37
9/8 slot-pole combination	720	340	204	116

Table 6 Eddy current losses for various axial magnet lamination on SMPM machine

From the eddy current losses calculation of the prototype machine, the following conclusions can be extracted:

- The eddy current loss of solid magnet construction in 9/8 slot-pole combination of SMPM generator is too high. The solid magnet construction cannot be implemented. A lamination in the magnet can be used to reduce the losses. The circumferential laminations as have been shown in table 6 above can be used as a reference. The other lamination is in the axial direction. The lamination in axial direction will be discussed in chapter 5.
- The eddy current loss of solid rotor back iron in 9/8 slot-pole combination of SMPM generator is too high. The solid rotor construction cannot be implemented. A lamination of rotor back iron can be used to reduce the losses.
- The eddy current loss of solid magnet construction in 3/2 slot-pole combination of SMPM generator is still higher than 100 Watts. The using of solid magnet construction still needs to be investigated for this machine construction. The magnet loss calculation in 3D in chapter 5 could be used to get a better conclusion.
- The eddy current loss of solid rotor back iron in 3/2 slot-pole combination of SMPM generator is less than 100 Watts. It is possible to use a solid back iron construction in this generator type.
- The eddy current losses in solid rotor back iron of all types of IPM generators are too high. The solid rotor construction cannot be implemented. A thin lamination of the rotor back iron can be used to reduce the losses.
- The eddy current losses in solid magnet of 3/2 slot-pole combination of the IPM generator are less than 50 Watts. It is possible to use a solid magnet construction in this generator type. The lamination of the magnets in the IPM machine will be discussed in chapter 5.
- The eddy current losses in solid magnet of 9/8 slot-pole combination of the IPM generator are too high. The solid magnet construction cannot be implemented. A lamination in the magnet can be used to reduce the losses.

5. 3D modeling of prototype generator

This chapter presents the 3D modeling of the prototype generator. The purpose of the 3D model is to get more information when the flux density flows in three directions. With this method, the behavior of flux distribution in the axial direction can be investigated. In this thesis, there are four topics that will be investigated: the flux leakage in the axial direction, the flux distribution in the end section, the investigation the end leakage inductance, the investigation of eddy current losses due to the end windings and the lamination effect on the magnet loss. Since the 3D model is a large model and takes much computer sources, only the 3/2 slot-pole combination machine will be investigated. On the other hand, some of the results also can be applied to the other machines. An example is the calculation results in the magnet lamination effect to the flux leakage or to the eddy current losses in the magnet.

The first model which will be presented in this chapter is the static 3D model. With this static 3D model, the flux density distribution in the machine and also in machine end can be obtained. With this information we can know the other sources of flux leakage in the machine. This leakage corresponds to the reduction of the number of fluxes that cross the air gap which produce the induced voltage. The result from this chapter will be validated with the 2D result and with the measurement results in chapter six.

The second model is built to calculate the end leakage inductance. With a short axial length of the prototype generator, the end leakage inductance could be quite significant in the total inductance. A more accurate inductance calculation will lead to a more accurate machine performance prediction. The result of the end leakage inductance together with the inductance from analytic model and the 2D model will be validated with inductance from the measurement in chapter six.

The third model is built to investigate the eddy current losses in the end stator region due to the end windings. In this model, the eddy current losses will be calculated for different number of turns of each slot and also for different operating frequency.

The last model is built to investigate the magnet lamination effect on the magnet loss. A 3D FEM model will be built for this purpose. First, the investigation of the finite length effect in magnet loss is investigated with this model. The purpose to investigate the finite length effect is to verify the magnet loss calculation in 2D analytic or 2D FEM model from chapter 2 and 4. In 2D model, the axial length of the generator is assumed to be infinitely long. The prototype generator is only 5cm long. Therefore, the magnet loss calculation from 2D model should be further investigated. After that, the magnet lamination effect in magnet loss is investigated.

5.1 Static 3D model

The no load induced voltage in the stator windings of the machine is explained by Faraday`s law as stated in equation 2.58. From this equation we can see that the induced voltage is proportional to the changing flux density which crosses certain surface area with boundary of certain contour C. In this case, the contour C is the stator windings and the flux density linking with the stator coils is called flux linkage. The flux linkage is lower compared to the flux that is produced by the magnets in the rotor due to various leakages that happen in the machine.

The investigation of the flux leakage will be carried out for a few topics as follow:

- The investigation of lamination effect
- The investigation of end region of rotor without balancing rim
- The investigation of end region of rotor with a balancing rim

The flux leakages in the machine are calculated by comparing the 2D model from chapter four with the 3D model in this chapter. As already mentioned in chapter four, the flux density in axial direction is neglected, thus the end leakage is neglected as well. The method for comparison is by calculating the flux linkage for certain area in the model. For the first investigation, the area of the flux linkage is the surface of the permanent magnet. For the second and the third investigation, the surface area will be the tooth of the stator iron. The calculation of the flux linkage uses the following equation.

$$\lambda = N_c \cdot \sum \bar{B} \cdot \Delta A \tag{5.1}$$

Where $\lambda[Wb - turns]$ is the flux linkage, $N[turns]$is the number of turns per coil in the winding, B$[T]$ is the flux density and $A[m^2]$ is a discretization of the surface area crossed by the flux. The flux density from the FEM model was imported to the FEM structure and the flux linkage in equation 5.1 was calculated by using matlab script.

Equation 5.1 will be used to show different values of the flux linkage in various places in the machine. Figure 21 and figure 22 below show the surface area to measure the flux linkage on top of the laminated magnet and on stator tooth.

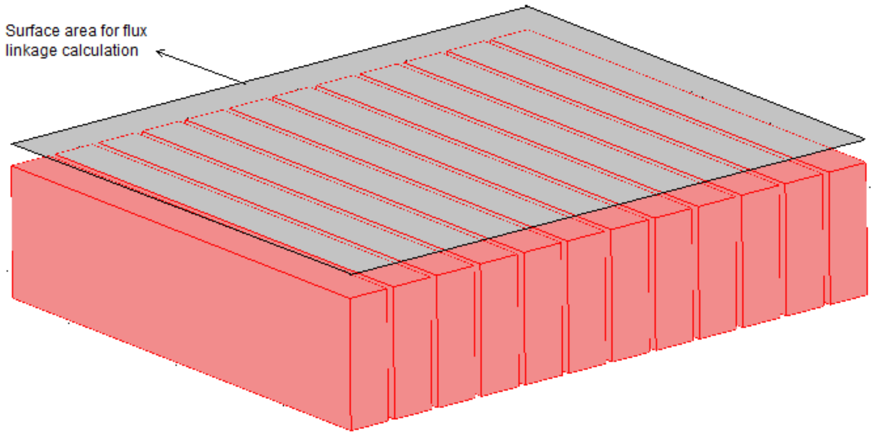

Fig. 21 Surface area on permanent magnet

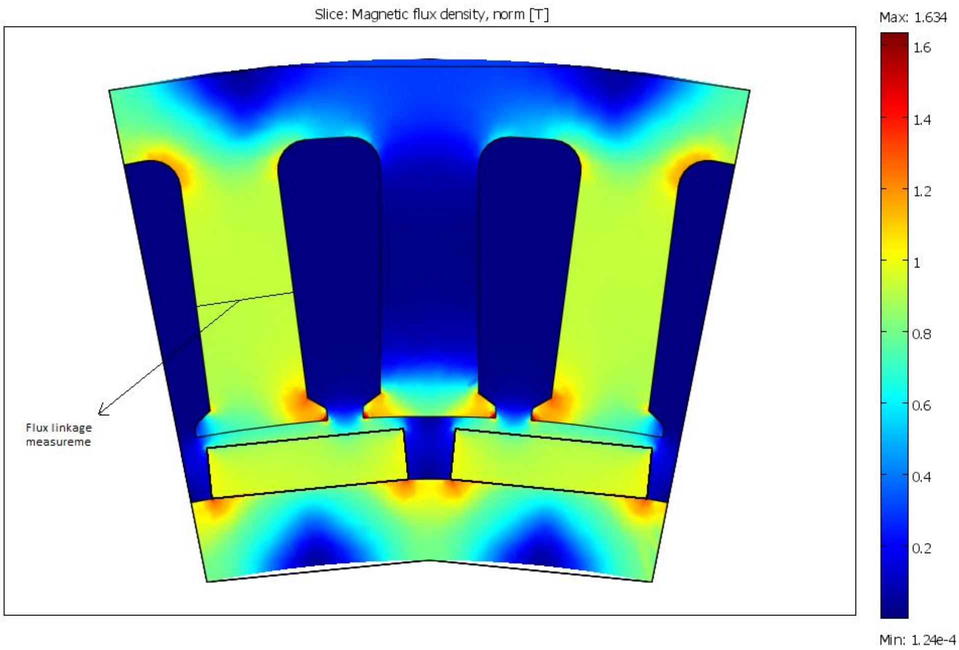

Fig. 22 Surface area for flux linkage on stator tooth

To calculate various flux leakages, a 3D model is built with the following assumptions:

- The machine is in no load condition, thus the current flow in the windings is zero
- The material for stator and rotor back iron is an isotropic material and non linear.
- The space between the magnet laminations is filled with air

5.1.1 System definition

Based on the assumption used above, the application mode for this model is *magnetostatic with no current*. From the first assumption, the stator coil windings can be removed because it gives the possibility to remove sharp edges from the coil sub domain which prevent the creation of more meshes to be solved. With the disappearance of current in the system, the right side of the equation 3.1 is zero.

$$\nabla \times \vec{H} = 0 \qquad (5.2)$$

Therefore, we can define the flux intensity as a gradient of scalar field. Equation 3.13 introduced the magnetic scalar potential which defines the magnetic field intensity. From the general constitutive relation in 3.7 and 3.13, the equation 3.4 can be written as follow:

$$-\nabla \cdot \left(\mu_0 \mu_r \nabla V_m - \vec{B}_r\right) = 0 \qquad (5.3)$$

5.1.2 Simulation setup

This model represents a more complete construction of the prototype generator, especially in the end section. The prototype generator has some materials to support its construction. In the end section, a balancing rim of a steel material is inserted in the rotor to improve the balance of the rotor. There is also an aluminum rim at the end of stator windings which is part of the housing of the machine. All these material could influence to the machines performance. The steel balancing steel is assumed to be of a linear material with relative permeability, $\mu_{r,br}$ of 100. This assumption can be used since most of the flux from the permanent magnet flows in the radial direction to the stator iron. Thus the flux density in the balancing rim is not expected to be high. The aluminum rim in this simulation is assumed to be air since it has the relative permeability, $\mu_{r,Al}$ is 1. Due to symmetry in its axial direction, the model was built only for half of its axial length. The permanent magnet is laminated into 24 parts.

There are three different boundary conditions used in these models:

- Magnetic insulation boundary: this boundary is applied in the outer stator iron and inner rotor back iron faces. The magnetic flux density which crosses in this area is set to zero, $n \cdot \vec{B} = 0$.
- Continuity boundary: in this boundary, the normal flux density crosses this boundary is expressed by $n \cdot \left(\vec{B}_1 - \vec{B}_2\right) = 0$.
- Periodic boundary condition: The periodic boundary condition between two sections of the model is set to continuity which means that the magnetic scalar potential source is equal to magnetic scalar destination, $V_{m,dst} = V_{m,source}$.

The meshing process of this model didn`t take a special meshing in certain points. Since the distance between the permanent magnet laminations is small, 0.1 mm, the meshing in this region and in the air gap area is automatically fine enough. With this meshing method, a vast number of mesh elements are created. The tetrahedral mesh element is 310686 while the triangular element is 52092 elements. The model was solved by using *Conjugate Gradient* solver.

5.1.3 Simulation results

In this section, the simulations were conducted for SMPM and IPM rotor of 32-combination machine. This machine combination has a lower eddy current loss as has been shown in previous chapter. On the other hand, a 3D model for 3/2 slot-pole combination machine only one sixteenth of the full machine model compared to the 9/8 slot-pole combination machine. With this model, a finer mesh can be used to calculate the eddy current losses in stator iron end due to end windings. This calculation is conducted in sub-chapter 5.3. Figure 23 below shows the static simulation result for SMPM machines.

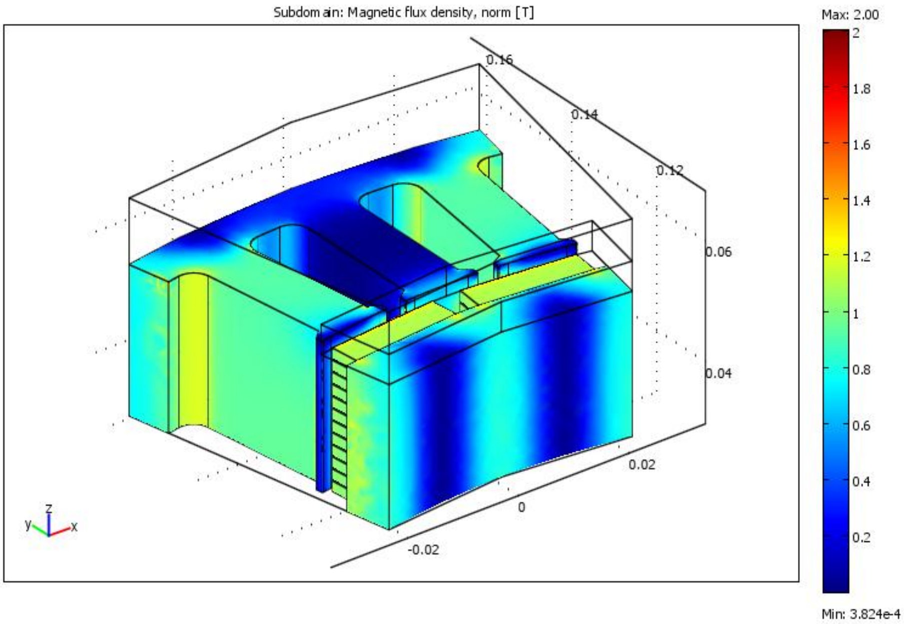

Fig. 23 Flux density distribution

Figure 24 shows the comparison of flux linkage on a solid magnet and laminated magnet. The figure shows the flux linkage as a function of axial length position. As can be seen, there is additional flux leakage due to the lamination. The flux will leak in the space between the magnets segmentation so that less flux links the surface area which crosses the air gap.

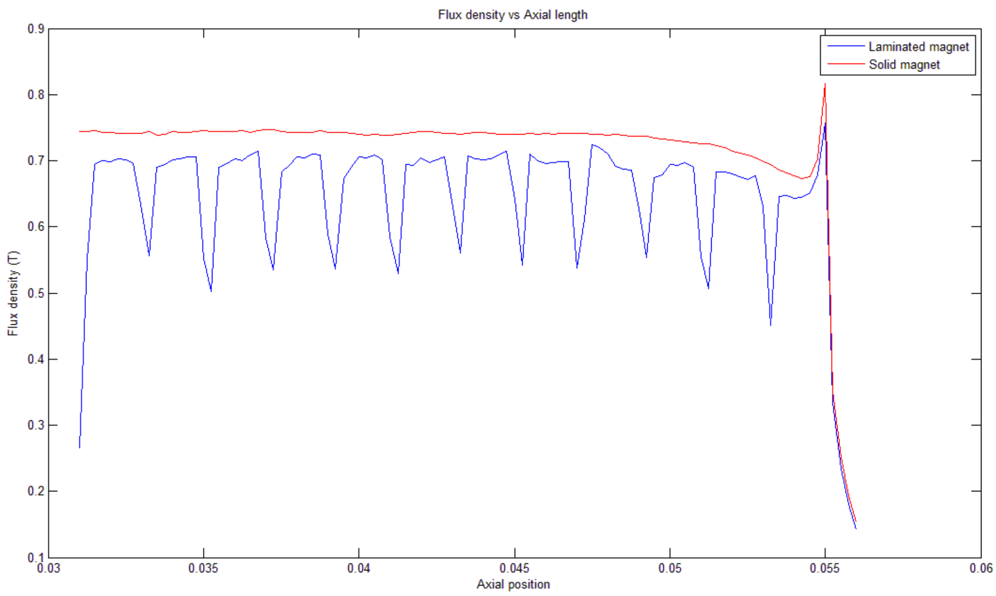

Fig. 24 Flux density distribution vs Axial length

Figure 25 below shows the flux linkage in the stator tooth for 2D model, 3D model without balancing rim (air), and with balancing rim. The 3D model below uses laminated magnet construction.

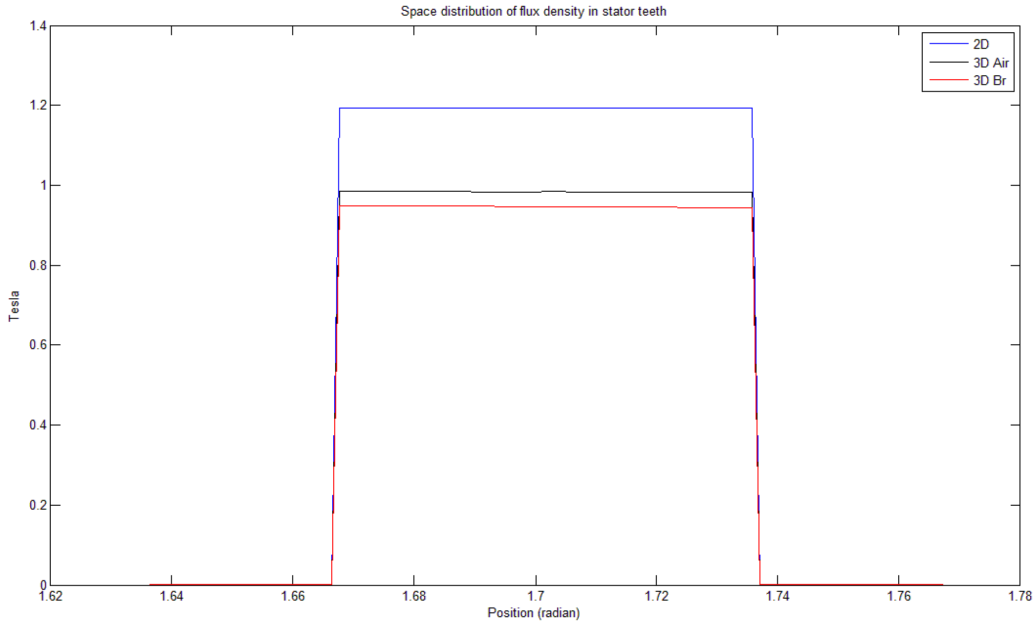

Fig. 25 Flux density distribution in stator tooth for 3 different model

It shows that the flux linkage for the machine with laminated magnet and with balancing ring installed have the smallest value. It means that the induced voltage will be lowered with this configuration compared to the 2D simulation result.

Figure 26 shows the flux linkage distribution with axial length position for the machine with and without a balancing rim in laminated magnets.

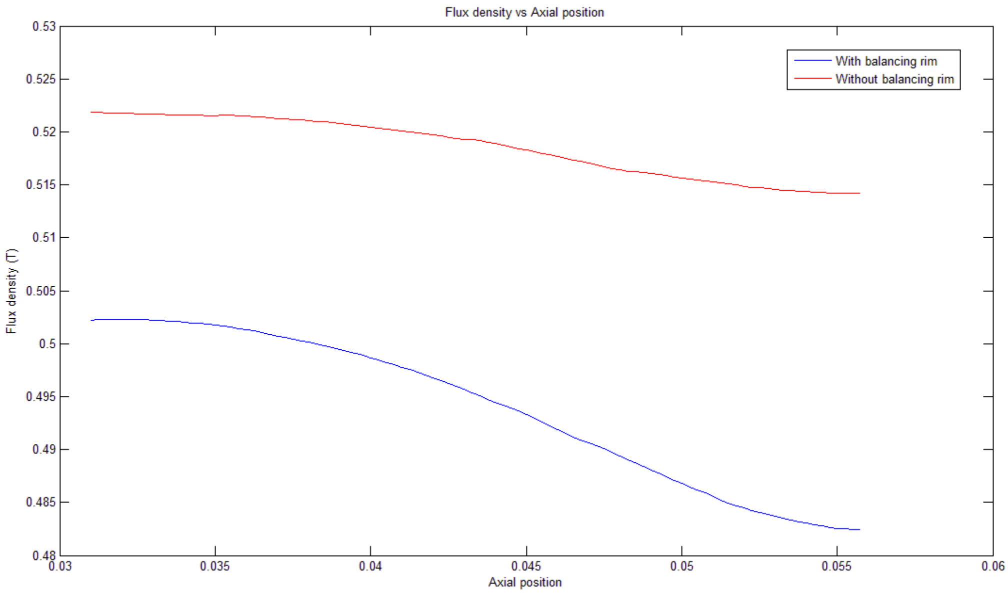

Fig. 26 Flux density as a function of axial length position in laminated magnet

A balancing rim which is installed in the end of the rotor increase the end flux leakage. It happens because the relative permeability of the steel is 100 times higher compared to air so that the reduction of the flux linkage in the end region is higher than without balancing rim.

Table 7 below shows the summary of the total flux linkage which already observed.

Index	Models	Total flux linkage (Wb-turns)	Reduction (%)
	2D Model		
1	Magnet surface	0.0233	-
2	Tooth area	0.0146	-
	Magnet surface (3D)		
3	Solid magnet	0.0226	3
4	Laminated magnet	0.0207	11.16
	Tooth area (3D with laminated magnet)		
5	Without balancing rim	0.0119	18.5
6	With balancing rim	0.0113	22.6

Table 7 Total flux linkage for various surface area

From table above, the following conclusions can be drawn.

- From comparison index 1 and 3 we can see that the difference is 3%. It means that this is the flux leakage in the end region of the magnets without balancing rim. It will be called the magnets end leakage
- From index 3 and 4 the difference is 8.2% which correspondence to the flux leakage due to lamination of the permanent magnet. It will be called the magnets lamination flux leakage
- From the leakage due to lamination and index 5 the difference is 7.34% which means that it is the flux leakage in the air of end region. It will be called the end air flux leakage
- From the leakage of the end region and index 6 the different is 4.1% which correspondence to the addition flux leakage in the end region due to balancing rim installed at one side of the rotor. It will be called the end balancing rim flux leakage.

5.1.3.1 Lamination effect to induced voltage

In this part, the lamination effect on the induced voltage will be investigated. The same method as for the previous section will be applied here. The flux linkage on top of the magnet surface is measured for various magnet laminations. The different measurements of flux linkage show the different flux reduction due to magnet laminations.

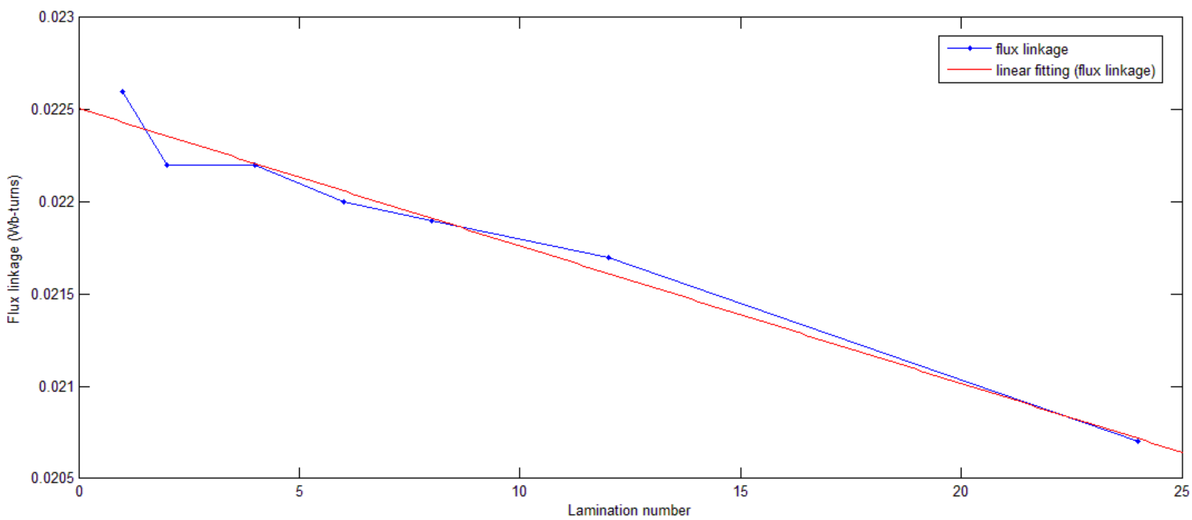

Fig. 27 Flux linkage as a function of magnet laminations

	Laminations number						
	1	2	4	6	8	12	24
Flux linkage (Wb-turns)	0.0226	0.0222	0.0222	0.0220	0.0219	0.0217	0.0207

Table 8 Flux linkage as a function of magnet laminations

Figure 27 and table 8 above shows the flux linkage measurements on top of magnet surface for various magnet laminations. In figure 27, there is also a linear curve fitting added. This regression gives us a picture that the flux leakages due to laminations in the magnet seem to be linearly proportional to the number of magnet segments. The measurement difference in some point could be due to different meshing in each model. With the increasing of magnet laminations, the meshes on top of the magnet become finer. From this result, we can conclude that the no load induced voltage in stator windings reduce linearly with the increase of magnet segments.

5.2 End leakage inductance calculation

Stator end-windings leakage inductance ($L_{end}[H]$) is the inductance due to the armature magnetic flux due to current in the end windings. Most of this flux flows in the end region of the machine.

The armature flux that flows in the end region originates from two sources. The first source is due to a current flow in the stator coil in the active region. It lies in the stator slot. Some of the armature flux from this source can leak in the machine end. The second one is due to the current flows in the end windings. To determine the L_{end}, the separation of the flux fringing and the flux from the end turn is importance in the calculation.

In 1951 E.C. Barnes [Bar 51] conducted an experimental study to measure the machine end-windings leakage reactance. In his experiment, he measured the voltage, current and power and then from the available data he calculated the reactance of the machine. The machines in the measurement had 4 different axial lengths and they were built with more attention to create as identical machine as possible. The measurements were conducted with two different conditions, with rotor and without rotor inserted in the stator bore. The reactances of the measurement were the total reactance which consists of the active region and the end region. After that the results were plotted and an extrapolation was made to a zero axial length of the machine. The reactance when the axial length zero will be the end reactance and the conclusion can be drawn is that the end reactance is the same with or without the rotor inserted in the machine.

The advantage of Barnes work is used by Brahimi [Brh 92] and Ranran Lin [Lin 09] to calculate the end inductance numerically by building the 3D model without the rotary part. The advantage is that the saturation in the steel due to the flux density from permanent magnet is avoided. With this condition, it needs less time to simulate the model. In Lin`s work, she built a 3D model of the stator iron. Due to symmetry, she built only half of the stator iron and made 40 slices in the stator iron model. The magnetic energy of each slice was calculated and the magnetic energy due to current in the end region is arithmetically separated from the total energy. The magnetic energy due to current in the stator slot is the multiplication the number of segments with the magnetic energy in the first slices which expected has no influence with the flux from end windings.

In this thesis, the $L_{end}[H]$ was calculated by comparing the magnetic energy from 3D model with the 2D model. With this method, the segmentation of stator iron, which produced much more meshes can be avoided so that the computation time is faster. Furthermore, a thinner stator iron can be used to reduce the machine size.

In the first part, the definition of the model system is provided to give information about the application mode that will be used. After that the simulation setup presents the simulation preparation and the last part, the simulation result is presented. The end inductance $L_{end}[H]$ calculation result along with the 2D FEM result will be compared with the inductance from measurement in chapter six.

To build this model, the following assumptions are used:

- The stator steel operates in linear region. Since the rotor is removed, the flux density flows in stator steel is expected to be low. With this assumption, the saturation is not considered in the steel.
- The flux density doesn`t flow in the other model section. As has been done in 2D model, there is only one phase conducting current. This means that, there is only a small part of the flux flows to the other section model.

5.2.1 System definition

The end windings inductance $L_{end}[H]$ calculation is done as in chapter 4.3.2 when calculating the inductance with the 2D model. The flux density in the system is produced by the current that flows in the stator coil. In this model a peak phase current $\hat{\imath}_a[A]$ is injected in the stator coil. Since the current is constant, a magnetostatic application mode can be used in this model.

In the 3D model, the spatial current definition is rather difficult to be determined, especially in the round section of the end windings. In this model, the current definition can be determined by injecting current as inward current in one of the coil legs boundary and set a ground boundary in the other leg. After that, with the conductivity in the coil, an electric potential is built in the coil and the current is distributed in the system due to the electric field in the system. The geometry model of the system will be further explained in chapter 5.2.2. Since the electric field and magnetic field need to be solved, the application mode used in this model is *magnetostatic* with both electric and magnetic potential activated.

With the definition of electric field as the gradient of electric field as stated in equation 3.9 and also the definition of current density in 3.8, equation 3.5 becomes:

$$-\nabla \cdot \left(\sigma \nabla V - \vec{J}^{e}\right) = 0 \tag{5.4}$$

By using equation 3.7, 3.8, and 3.9 in the Ampere`s law equation we get:

$$\nabla \times \left({\mu_0}^{-1}{\mu_r}^{-1} \nabla \times \vec{A} - \vec{B}_r\right) + \sigma \nabla V = \vec{J}^{e} \tag{5.5}$$

5.2.2 Simulation setup

Based on [Bar 51] we can build the model without the rotor to calculate the end inductance. On the other hand, due to symmetry, the machine model is only built for half of its axial length. This simplification reduced the model size quite significant. The model is shown in figure 28 below.

There are four boundary conditions used in this model:

- Magnetic insulation and electric insulation: This boundary is used in the outermost of the model. The magnetic vector potential and the current density in this boundary are expressed by $\mathrm{n} \times \vec{A} = 0$ and $n \cdot \vec{J} = 0$.
- Continuity: in this boundary, the magnetic intensity and the current density are expressed by $\mathrm{n} \times \left(\vec{\mathrm{H}}_1 - \vec{\mathrm{H}}_2\right) = 0$ and $n \cdot \left(\vec{J}_1 - \vec{J}_2\right) = 0$.
- Magnetic insulation and inward current flow: The inward current flow is set in one of the coil legs. The magnetic vector potential and the current density for this boundary are expressed by $\mathrm{n} \times \vec{A} = 0$ and $-n \cdot \vec{J} = J_n$.
- Magnetic insulation and ground: The ground setting is set on the other coils leg. The magnetic vector potential and the electric scalar potential are expressed by $\mathrm{n} \times \vec{A} = 0$ and $V = 0$.

From the second assumption above, the periodic boundary condition is not used here. The reluctance in the air gap is much higher compared to the reluctance in stator iron, therefore, the assumption above can be used.

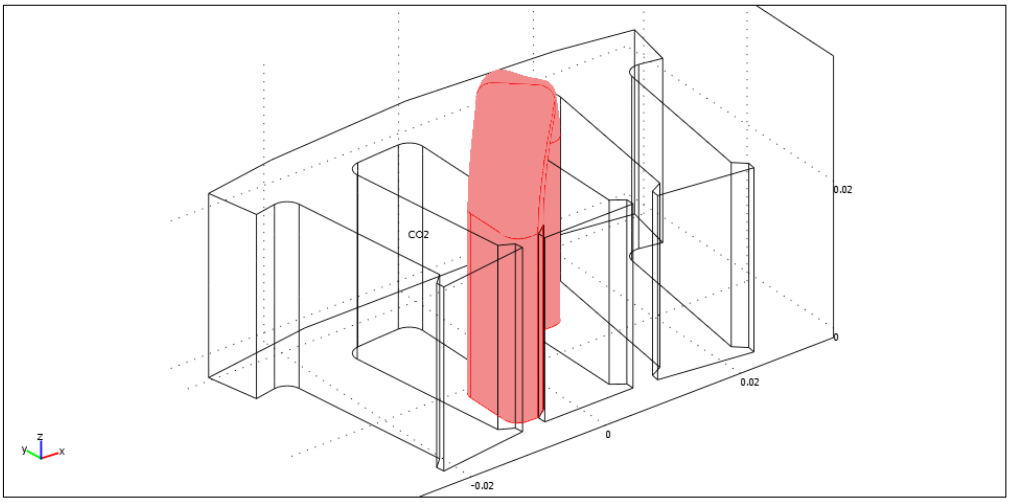

Fig. 28 3D model of SMPM rotor and 3/2 slot-pole combination machine

After setting the material characteristic and the boundary setting in the machine model, the model mesh is initialized. The number of tetrahedral meshes is 100297 while the triangular meshes is 18028.

5.2.3 Simulation result

This section shows the simulation result for SMPM rotor and 32-combination machine. Figure 29 below shows the flux density distribution in the machine due to current in the coils.

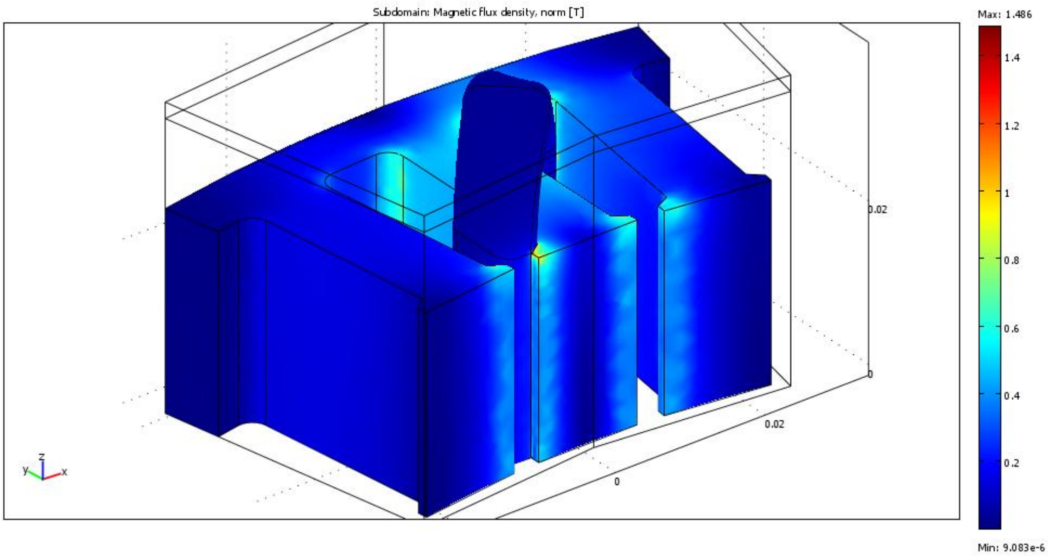

Fig. 29 Flux density distribution

Figure 30 below shows the total current density that flows in the machine. As can be seen, the current only flows in stator coil sub-domain. The flux density distribution in figure 29 is produced by this current.

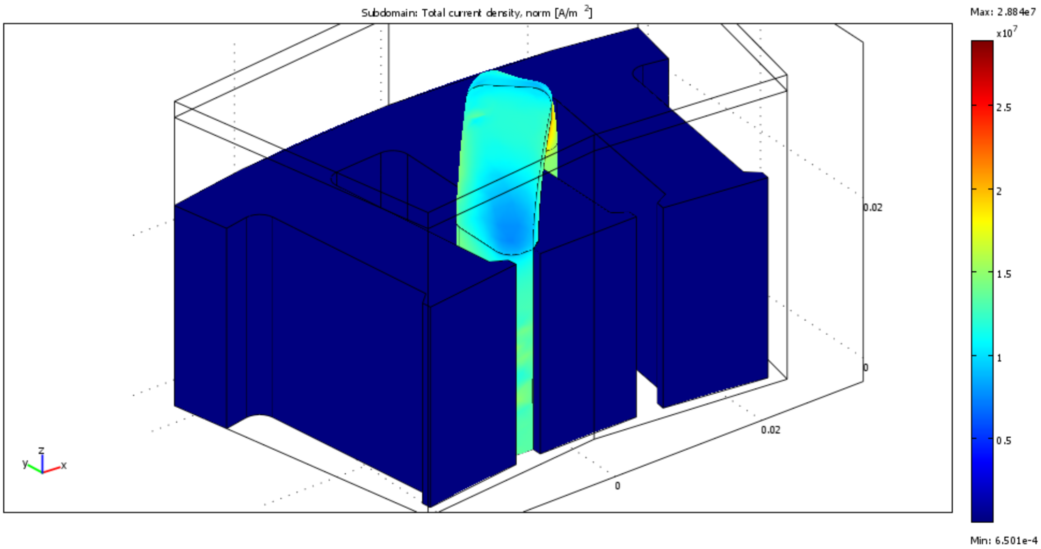

a. Total current density distribution in subdomain

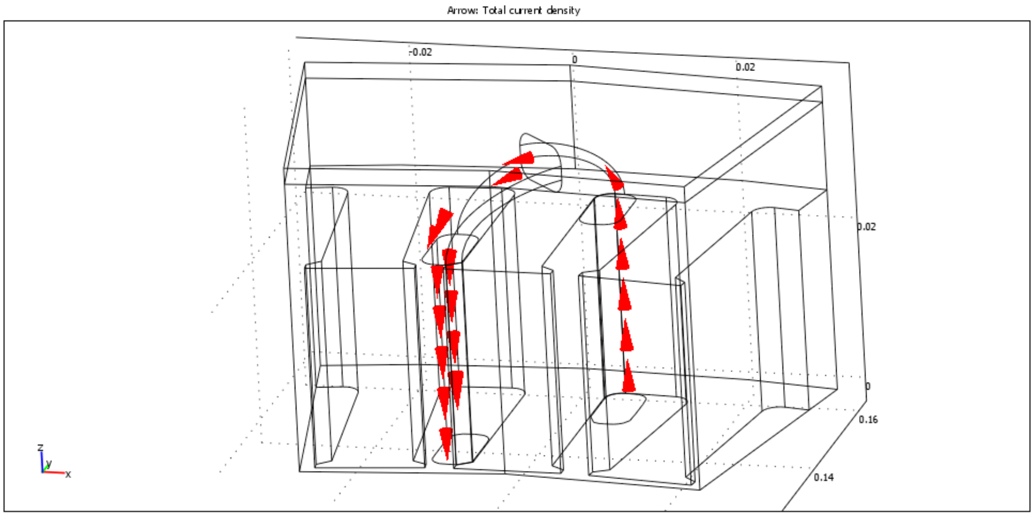

b. Total current density direction

Fig. 30 Total current density distribution

The end inductance L_{end} is calculated from the magnetic energy stored in the machine model. In Comsol, the energy stored can be calculated by the following equation:

$$W_{m,3D} = \iiint v_m dV \quad (5.6)$$

With $W_{m,3D}$[J] is magnetic energy within certain sub domain, v_m (J/m^3), is magnetic energy density in the sub domain and dV (m^3) is the volume of the subdomain. This method is the same as for calculating the inductance by using the 2D model of chapter 4.3.2. The magnetic energy which is calculated from equation 5.6 is the total magnetic energy due to the current in the stator coil in the slot including the end winding. To separate the magnetic energy from the end windings and the windings in stator slot, the magnetic energy from 3D model is compared with the magnetic energy from 2D model. The magnetic energy in 2D model is not influenced by the end windings so that it represents the flux density distribution due to only the windings in the slot. The magnetic energy due to the end windings $W_{m,end}$[J] is calculated as follow:

$$W_{m,end} = W_{m,3D} - W_{m,2D} \quad (5.7)$$

Figure 31 below shows the 2D model to calculate the magnetic energy from 2D model $W_{m,2D}$[J]. This calculation is presented in chapter 4.3.2. With the number of model symmetry section, n_{symm}, and the amplitude of current that flows in the coil, I[A], the end inductance can be calculated as in equation 4.5 with the following equation:

$$L_{end} = n_{symm} \cdot 2 \cdot \frac{2 \cdot W_{m,end}}{I^2} \tag{5.8}$$

The multiplication factor 2 is used since the 3D model in this section only half of the total axial length.

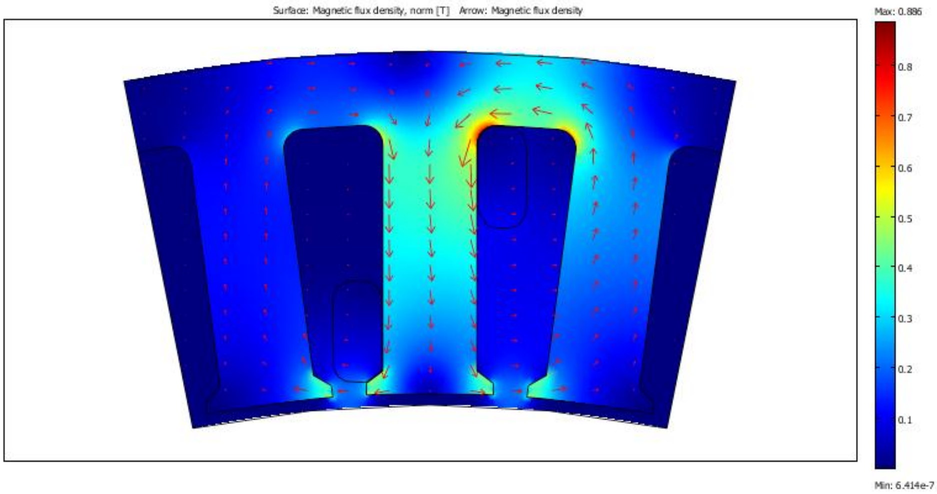

Fig. 31 2D model for end inductance calculation

The amplitude current that flows in the stator coil is set to be 65 A. From this model, the end inductance of prototype generator with 32 combination type is **43.22 µH.** To explore the possibility to create a shorter axial length generator, the end inductances for several axial lengths are calculated. The axial length of the generator is set to 50mm, 35mm and 25 mm. The other generator dimensions are kept constant. To keep the induced voltage in the same level, the number of coil turns should be increased to compensate a shorter axial length. Therefore, the number of turns is set to 7, 10 and 14 for the respective axial length. To be noted is that since the slot area is the same, the cable cross section area will be reduced which can create more copper losses in the machine. Table 9 below shows L_{end} for various axial lengths.

Axial length (mm)	n_c (turns)	L_{end} (µH) (FEM)	Factor Increment
50	7	43.22	-
35	10	88.16	2.04
25	14	172.29	4

Table 9 End inductance calculation result

As can be seen from table above, L_{end} is quadratic proportional to the number of coil turns.

5.3 End section stator iron losses

A lamination in the prototype generator is used to reduce the eddy current loss in the machine. The stator steel of prototype generator is laminated in radial direction to reduce the surface area which is exposed to the flux from the permanent magnets. Therefore, it reduces the eddy current loss. This lamination also reduces the eddy current loss due to armature reaction flux. With this lamination, the eddy current losses can be reduced significantly.

In the end region, the flux density from the current in end windings enters the stator iron perpendicularly. The stator iron is laminated in the radial direction. Therefore, the stator iron is not laminated seen from the end flux. Thus, the eddy current could be high in the stator end region. With this reason, the eddy current in this region need to be investigated.

The induced current that flows in the stator end flows in a small depth due to a high frequency of the induced current. This skin depth can be calculated from equation 2.57 in chapter two. This phenomena also appears in the eddy current losses calculation for rotor back iron calculation. With this knowledge, we don`t need to build a full model. In this thesis, a model with 1 mm stator iron thickness was built. In 3D model, this is an advantage since it greatly reduces the computing time.

The following are some assumptions that are used in 3D modeling to calculate eddy current losses:

- Flux density`s influence on to the next coil is considered small. It means that most of the losses are assumed to be accumulated in the stator end just below the coil of each tooth.
- Flux density flows to the next model segment is small so that most of the flux flows in only one segment (consist of 3 teeth).
- Linear stator iron is assumed. With this assumption, the stator iron saturation is not considered.

To explore the eddy current loss in the stator iron, some models with various axial lengths and various operating frequencies are built. The changes in axial length lead to a change in the number of coil turns. These changing give the eddy current loss as a function of the number of turns and a function of frequencies.

5.3.1 Application mode definition

When a current is induced in the stator steel, it takes place in a small volume of the stator iron due to the skin depth. A finer mesh should be made in this region so that the calculation of losses has small error. Since the flux density enters the end stator iron perpendicularly, the induced current is expected to appear in the stator surface area. Therefore, a fine mesh will be made in the surface of the end stator iron.

To simulate the eddy current due to current in stator iron, a spatial current distribution must be defined in the model. This current distribution is different from the current in section 5.2 when calculating end inductance. The current must be changing in time. There are two ways to determine a current in the coils for eddy current losses calculation:

1. By injecting current in coil`s sub domain for transient analysis type in perpendicular induction current. This application mode is used in the eddy current losses calculation in section 4.3.3.
2. By employing two application modes: *time harmonics, electric current* to calculate spatial current density and *time harmonics for magnetic* to calculate the flux density distribution.

The first mode is difficult to implement because we should determine the current direction in the coil by using spatial equations. For an arbitrary coils shape like in the model, the current distribution in end turns of the coil is difficult to determine.

The second modes basically employ the same method as in the L_{end} calculation. The current distribution is calculated by injecting current density in one of the leg of the coils and ground in the other leg. In this method, the current will flow through a high conductivity sub domain of the copper coils. After that, the current distribution result from this application mode is coupled to the time harmonics, magnetic application mode by using the *extrusion coupling variable* for sub domain of the coil. This extrusion is showed in figure 32:

The *extrusion coupling variable* maps the current distribution from the first application mode to the second application mode by using linear transformation of space position of a sub-domain in one model to the second model. Since the extrusion uses a space position of the sub-domains, the two sub-domains should be identical.

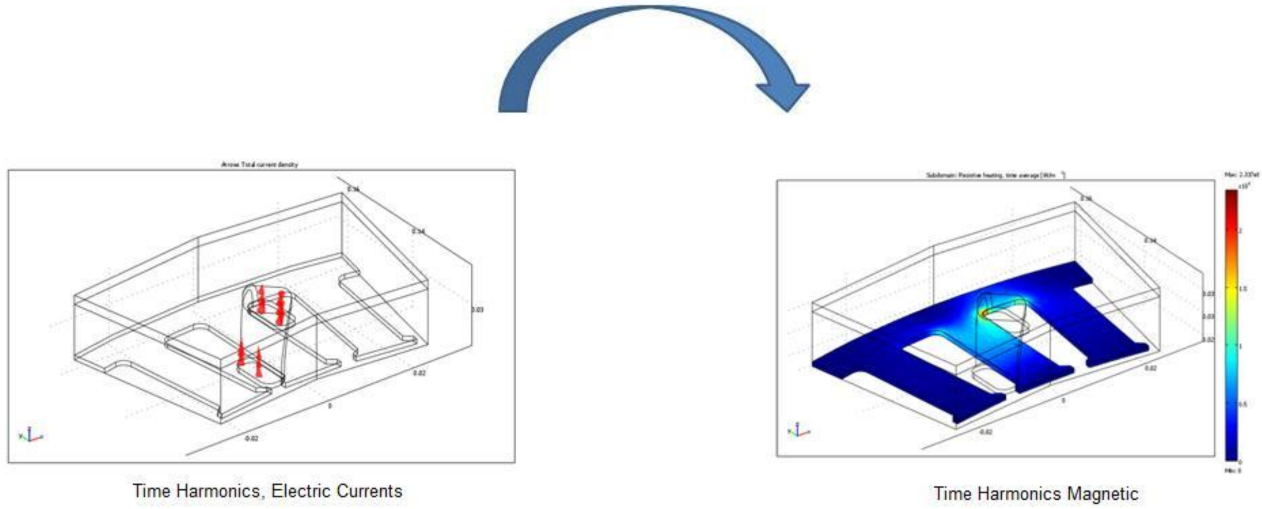

Fig. 32 Extrusion coupling variables method

5.3.2 System definition

The *time harmonics, electric current* is used to determine spatial current density in the stator coils. Thus there is no flux density distribution in the system. In this case, the right hand part of equation 3.2 become zero and the electric field can be expressed as the electric scalar potential as in equation 3.9. In time harmonics mode, equation 3.5 can be expressed as:

$$\nabla \cdot \vec{J} = -j\omega\rho \tag{5.9}$$

With the constitutive relation in 3.8, the electric scalar potential in 3.9 and equation 5.9 above, we can write:

$$-\nabla \cdot \left(\sigma\nabla V - \vec{J}^{e}\right) = -j\omega\rho \tag{5.10}$$

With equation in 3.3 and constitutive relation in 3.6 we get the following equation which is used in the system of *time harmonics, electric current* application mode:

$$-\nabla \cdot \left((\sigma + j\omega\varepsilon_0\varepsilon_r)\nabla V - \left(\vec{J}^{e} + j\omega\vec{D}_r\right)\right) = 0 \tag{5.11}$$

As has been described in chapter 5.3.1, the spatial current distribution from *time harmonics, electric current* application mode is mapped into the coil in the *time harmonics, magnetic* application mode. This changing current produces a changing magnetic flux density in the system and finally the induced current appears in the stator iron which has a finite resistivity. The eddy current losses in stator iron sub-domain are calculated by integrating the resistive heating as in chapter 4.3.3 about calculating eddy current in 2D FEM model.

Ampere`s equation in 3.1 can be written in phasor representation as follow:

$$\nabla \times \vec{H} = \vec{J} + j\omega\vec{D} \tag{5.12}$$

With D is the electric field density which is described in 3.6. From the definition of magnetic flux density and electric flux strength with the magnetic vector potential and electric scalar potential in equations 3.10 and 3.12 respectively, Ampere`s law can be expressed as follow:

$$(j\omega\sigma - \omega^2\varepsilon_0\varepsilon_r)\vec{A} + \nabla \times \left(\mu_0{}^{-1}\mu_r{}^{-1}\nabla \times \vec{A}\right) + (\sigma + j\omega\varepsilon_0\varepsilon_r)\nabla V = \vec{J}^e \quad (5.13)$$

For the *time harmonics, magnetic* application mode, the electric potential in equation 5.13 doesn`t need to be solved so that it reduces to:

$$(j\omega\sigma - \omega^2\varepsilon_0\varepsilon_r)\vec{A} + \nabla \times \left(\mu_0{}^{-1}\mu_r{}^{-1}\nabla \times \vec{A}\right) = \vec{J}^e \quad (5.14)$$

5.3.3 Simulation setup

In this simulation, the stator iron is only one millimeter thick due to the skin effect. From the first assumption used in this model, only one coil is drawn in each model. The boundary conditions for this model are divided into two parts since there are two models needed to calculate the eddy current loss.

The boundary conditions for *time harmonics, electric current* application mode are:

- Electric insulation: This boundary is used in the outermost of the model. The current density in this boundary is expressed by $n \cdot \vec{J} = 0$.
- Continuity: in this boundary, the current density is expressed by $n \cdot \left(\vec{J}_1 - \vec{J}_2\right) = 0$.
- Inward current flow: The inward current flow is set in one of the coil legs. The current density for this boundary is expressed by $-n \cdot \vec{J} = \vec{J}_n$.
- Ground: The ground setting is set on the other coils leg. The electric scalar potential is expressed by $V = 0$.

The boundary conditions for *time harmonics, magnetic* application mode are:

- Magnetic insulation: This boundary is used in the outermost of the model. The magnetic vector potential in this boundary is expressed by $\mathrm{n} \times \vec{A} = 0$.
- Continuity: in this boundary, the magnetic intensity is expressed by $\mathrm{n} \times \left(\vec{H}_1 - \vec{H}_2\right) = 0$.

From the second assumption above, the periodic boundary condition is not used here. The reluctance in the air gap is much higher compared to the reluctance in the stator iron, therefore, the assumption above can be used.

The meshes between the first application-mode to the other should be made identical to give a better and faster calculation time since the result from one model is mapped to the other model. If the meshing is not identical, sometimes the simulation does not converge. The number of meshes for one model is 127145 elements for tetrahedral mesh and 35987 elements for triangular mesh.

5.3.4 Simulation results

In this model, there are two flux sources that create eddy current loss in the stator end. These two fluxes are produced by the current that flows in the coil in the stator slot and by the current that flows in the end windings. Therefore, the eddy current losses in this model appear not only due to the current in the end winding, but also from the current in the stator winding in the stator slot. Figure 33a shows the spatial current distribution in the model with the time harmonics, electric current application mode and figure 33b and 33c gives the simulation result in the model with the time harmonics, magnetic application mode.

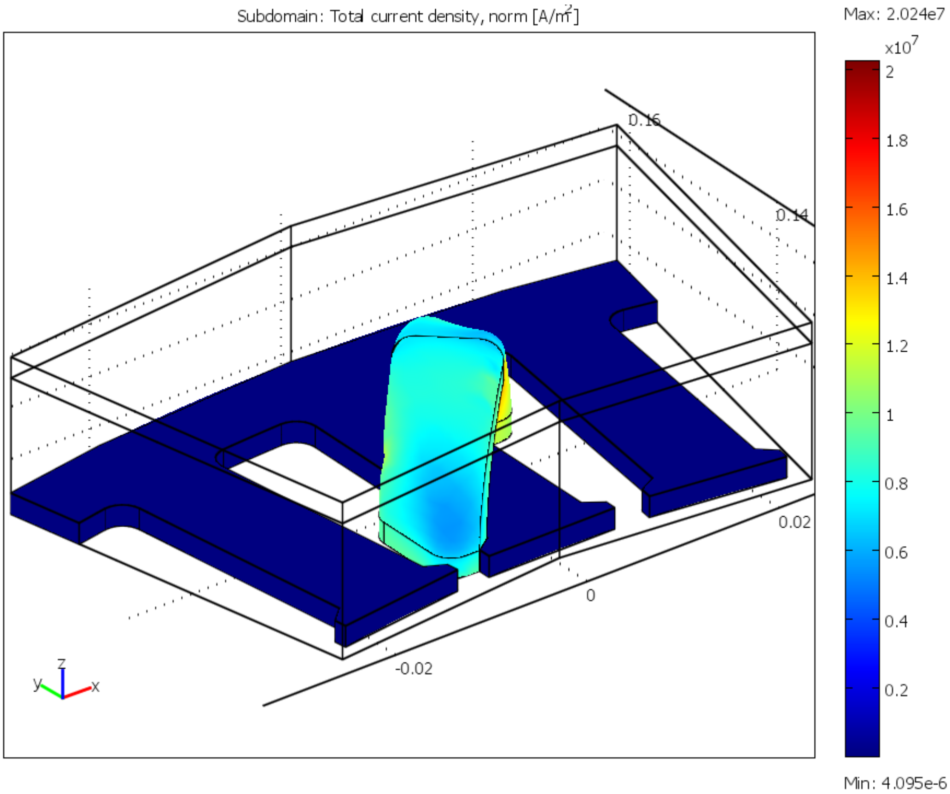

a. Total current density distribution

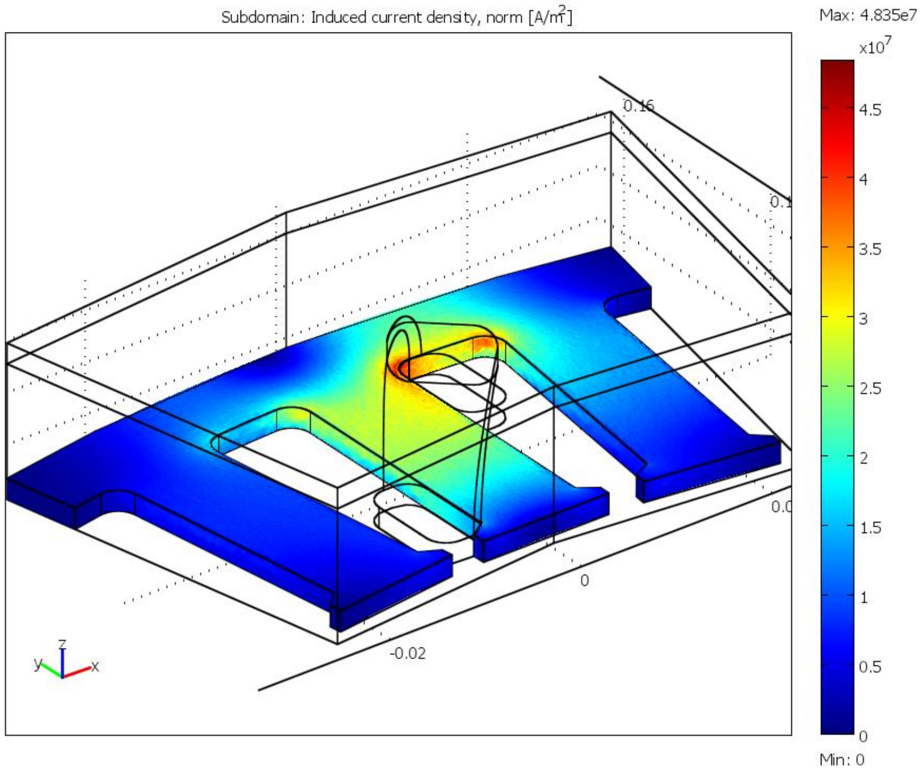

b. Induced current density

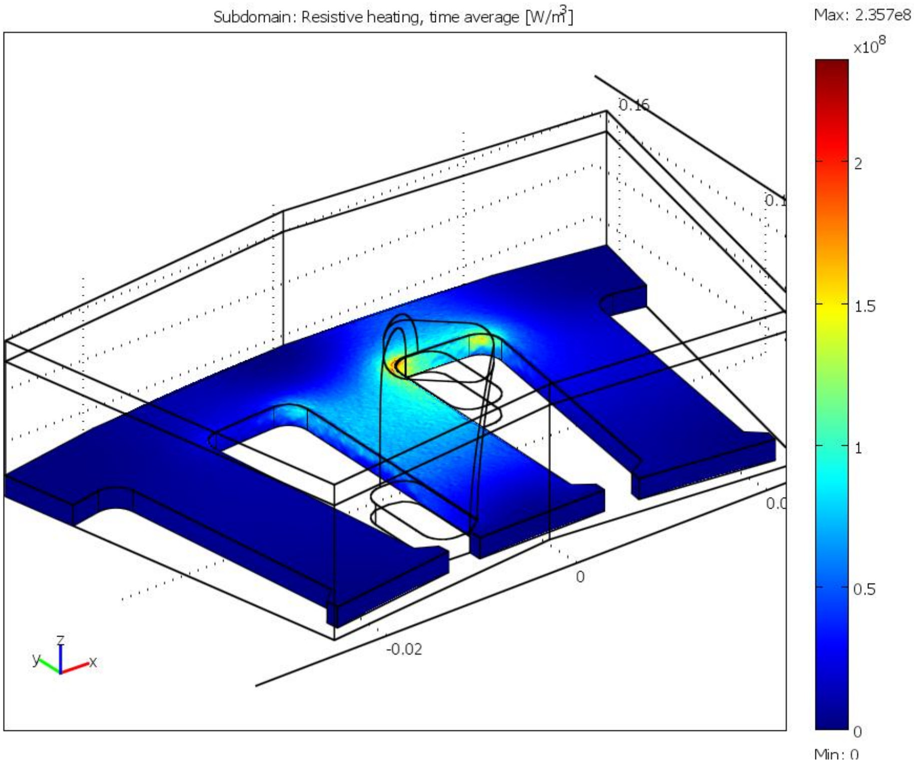

c. Resistivity heating

Fig. 33 3D simulation result

First, the investigation of eddy current losses for different stator thickness model is presented. A thicker stator iron in the model produced much more meshes. This model needs a more powerful computer to solve the problem. The thicknesses of stator iron for this investigation are 1 mm, 2 mm and 4 mm. The same mesh setting is applied in each model. The eddy current loss can be calculated by integrating the average resistive heating in a sub-domain. Total eddy current loss in the machine is calculated with the following equation:

$$W_{ec,end} = 2 \cdot \mathrm{N_s} \cdot \iiint W_{av} dV \qquad (5.15)$$

Where $W_{ec,end}[W]$ is the eddy current losses in stator end, $\mathrm{N_s}$ is the number of slots, $W_{av}[W/m^3]$ is the average loss per unit volume. With this equation, the eddy current losses in stator end are presented in figure 34 and table 10 below.

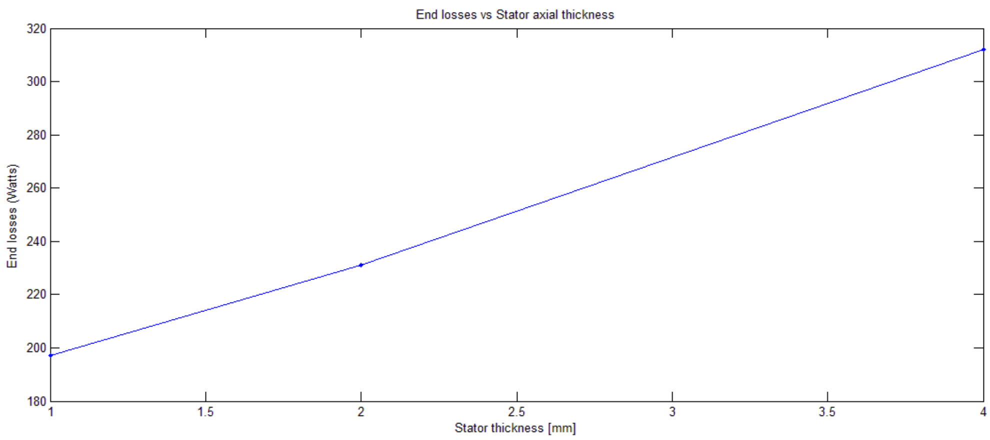

Fig. 34 End losses for various axial length

Machine type	Stator iron axial length (mm)	Eddy current losses (W)
3/2 slot-pole combination machine	1	197
	2	231
	4	312

Table 10 End losses for various axial length

As can be seen from figure 34 and table 10 above, the eddy current losses in stator end region increase with the increment of stator thickness. These losses consist of two sources. The first source is due to a current that flows in the stator end winding. The second source is due to a current that flows in the stator winding in the stator slot. With a thicker stator, the end losses due to the windings in the slot become larger. Therefore, the stator thickness of 1mm will be used to explore the eddy current losses in the stator iron end when the number of coil turns and operating frequencies are changed. The other eddy current losses appear in the aluminum rim in the end of stator windings. The eddy current in the aluminum rim is **12.09** Watts. This loss is low so that it will not be calculated in the next eddy current calculation.

Figure 35 and table 11 below show the end eddy current losses for various number of coil turns with fixed operating frequency at 800 Hz.

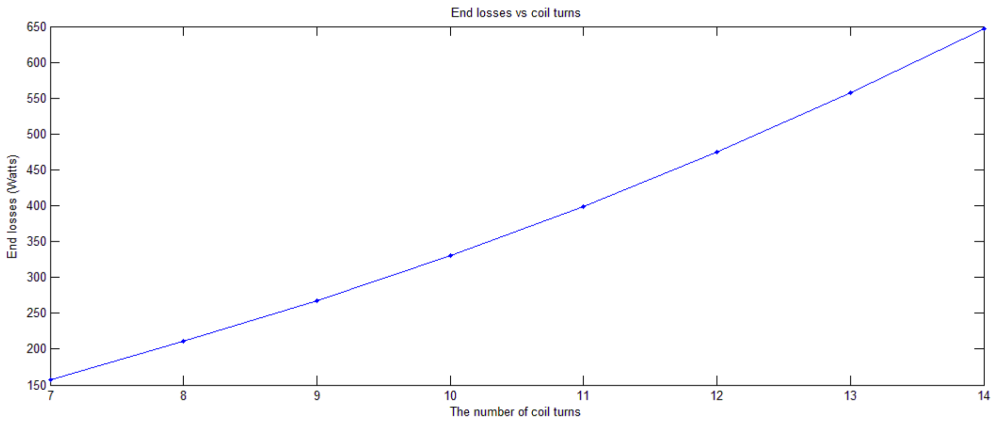

Fig. 35 End losses vs coil turns

	Number of turns							
	7	8	9	10	11	12	13	14
Losses (W)	156.79	211.10	267.17	329.84	399.10	474.97	557.43	646.48
Increment factor	-	1.35	1.37	2.10	2.54	3.03	3.56	4.12

Table 11 End losses for various number of turns

As can be seen from figure 35 and table 11 above, the eddy current losses increase quadratically when the number of turns is increased. The increment factor in table 11 shows the increase of loss relative to the base loss. The base loss is the loss when the number of coil turns is 7. These results are as expected since the eddy current loss is proportional to flux density square. Figure 36 and table 12 below shows the eddy current loss in end region for various operating frequencies with fixed 7 number of coil turns.

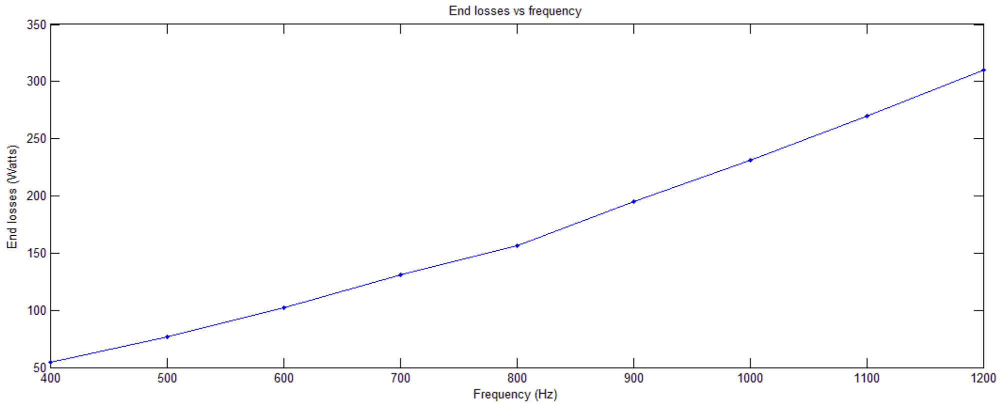

Fig. 36 End losses vs operating frequencies

	Operating Frequencies (Hz)								
	400	**500**	**600**	**700**	**800**	**900**	**1000**	**1100**	**1200**
Losses (W)	54.27	76.79	102.29	130.61	156.79	195.20	231.22	269.56	310.12
Increament factor	0.35	0.49	0.65	0.83	-	1.24	1.47	1.72	1.98

Table 12 End losses for various operating frequencies

Based on Faraday`s law in equation 2.58, the induced current is proportional to the changing rate of the flux density and its amplitude. Since, the eddy current losses are proportional to the square of induced current, therefore the eddy current losses are proportional to the square of the changing rate of the flux density, $\left(\frac{dB}{dt}\right)^2$. It means that the eddy current losses are proportional to the square of frequency (f^2). However, the losses in table 12 above doesn`t give the result as expected. The eddy current loss in stator iron end is the same as the eddy current loss in rotor back iron. If we see equation 2.55 in chapter 2.3.2, the losses is also proportional to the skin depth. Therefore, we will expect a lower value in higher frequency due to a thinner skin depth and a higher value in lower frequency due to a thicker skin depth.

5.4 Eddy current losses in a laminated magnet

In this section, the investigation of a finite length of permanent magnet to the magnet loss is presented. The analytic derivation in chapter 2.4 assumed that the magnet length in axial length is infinite so that the magnet resistivity in width direction can be neglected. In the prototype generator, the axial length of the magnet is 48 mm while the width is 19.5 mm. With this dimension, the used of equation 2.68 from chapter 2.4 can lead to a wide deviation.

The analytic equation of eddy current losses in finite length magnet can be derived by using Faraday`s law as in chapter 2.4. This method was also used in [Ruo 09]. Figure 37 shows the geometry that is used to derive the 3D magnet losses. The flux density flows perpendicular to the drawing plane in the y-direction

From the Faraday`s law in equation 2.58, we get:

$$\begin{aligned}
&-2\cdot z\cdot E_z(x)+2\cdot z\cdot E_z(-x)-2\cdot x\cdot E_x(z)+2\cdot x\cdot E_z(-z) \qquad (5.16)\\
&= -2\cdot z\cdot \frac{d}{dt}\int_{-x}^{x}\bar{B}(t)\cdot dA\\
&= -2\cdot z\cdot 2\cdot x\cdot \frac{d\bar{B}(t)}{dt}\\
&= -4\cdot x\cdot z\cdot \omega_r\cdot \hat{B}\cdot \cos(\omega_r\cdot t)
\end{aligned}$$

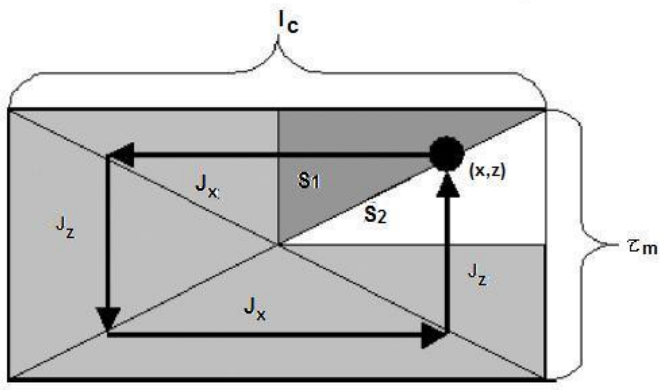

Fig. 37 Geometry that is used in 3D magnet loss calculation

The position of the x=0 and z=0 so that it will be in the middle of the magnet. Thus the electric field will be an odd function:

$-E_z(x) = E_z(-x)$ and $-E_x(z) = E_x(-z)$

The electric field can be expressed with the current density with the same direction of electric field J_z[A.m^{-2}] and the magnet resistivity ρ_m[Ωm].

$$E_z(x) = \rho_m \cdot J_z(x) \text{ and } E_x(z) = \rho_m \cdot J_x(z) \quad (5.17)$$

With the electric field expression and equation 5.17, equation 5.16 can be written as follow:

$$z \cdot J_z(x) + x \cdot J_x(z) = \frac{1}{\rho_m} \cdot x \cdot z \cdot \omega_r \cdot \hat{B} \cdot \cos(\omega_r \cdot t) \quad (5.18)$$

With the geometry property in figure 37, variable x, z, $J_z(x)$ and $J_x(z)$ are related as follows:

$$z = \frac{\tau_m}{l_c} x, \qquad J_z(x) = \frac{\tau_m}{l_c} J_x(z) \quad (5.19)$$

The eddy current losses can be calculated as follow:

$$P = \rho_m \cdot l_m \cdot 4 \cdot \left(\iint_{S1} J_x{}^2(z) dS + \iint_{S2} J_y{}^2(x) dS \right) \quad (5.20)$$

With equation 5.18, 5.19 and 5.20, the magnet loss average for one period of time is calculated as follow:

$$P = \frac{1}{32} \cdot \frac{1}{\rho_m} \cdot \frac{x^3 \cdot l_c{}^3 \cdot l_m}{(l_c{}^2 + x^2)} \cdot (\omega_r \cdot \hat{B})^2$$

The equation above can be rewritten in the form of magnet loss per unit volume of 3D analytic calculation as follow:

$$p_{m,spec,3D} = \frac{1}{32 \cdot \rho_m} \cdot \left(\frac{l_c{}^2}{(l_c{}^2 + x^2)} \right) \left(x \cdot \omega_r \cdot \hat{B} \right)^2 \quad (5.21)$$

If x is set to the magnet width $\tau_m[m]$, and the equation 5.21 is compared to equation 2.66, we obtain a correction factor C as follow:

$$C = \frac{p_{m,spec,3D}}{p_{m,spec}} = \frac{3}{4} \cdot \frac{l_c{}^2}{l_c{}^2 + \tau_m{}^2} \quad (5.22)$$

Correction factor also can be determined qualitatively. In 2D magnet loss derivation the neglect of the magnet width creates a higher induced current because the resistivity of the magnet is reduced. Resistivity is proportional to the length of the induced current contour. Therefore, the induced current is inversely proportional to the length of induced current contour. On the other hand, the magnet loss is proportional to the induced current square. From these considerations, the following expressions can be obtained as the correction factor C.

$$C = \frac{p_{m,3D}}{p_{m,2D}} \sim \frac{{I_{3D}}^2}{{I_{2D}}^2} \sim \left(\frac{l_{2D}}{l_{3D}}\right)^2$$

Where $p_{m,3D}$ is the magnet loss when the end effect is not neglected, $p_{m,2D}$ is the magnet loss when the end effect is neglected, I_{3D} is the induced current when the end effect is not neglected, I_{2D} is the induced current when the end effect is neglected, l_{2D} is the contour length when the end effect is neglected, l_{3D} is the contour length when the end effect is not neglected. With: $l_{2D} = 2l_c$ and $l_{3D} = 2(l_c + \tau_m)$, the correction factor can be calculated as follow:

$$C_2 = \frac{p_{m,spec,3D}}{p_{m,spec}} = \left(\frac{l_c}{(l_c+\tau_m)}\right)^2 \quad (5.23)$$

The eddy current losses for finite magnet length can also be calculated by using 3D FEM model. With this model, a lamination effect in the eddy current losses can be determined. As have been mentioned in previous section, the three dimensional model need much more time and a powerful computer to be solved. Equation 5.22 and 5.23 above suggests that the eddy current losses can be calculated only using 2D model with a correction factor. Therefore it saves much computation time.

In this section, the eddy current losses will be calculated for various lamination segments. A 3D FEM model will be built for this purpose. After that, the calculation results from this model are compared with the 2D FEM model. The 2D FEM model calculation which is presented in chapter 4.3.3 will be corrected by the correction factor in equation 5.22 and 5.23.

5.4.1 System definition

To model the eddy current losses in 3D, the following assumptions are used:

- The end effect is neglected. It means that the armature flux leakage to the end section is assumed to be small. Therefore, the magnetic potential in axial direction $A_z[Wb/m]$ is uniform throughout the machine axial length. In reality, the armature flux density is lower near to the end of the machine so that the eddy current in the end section is lowered. By neglecting this effect, the loss calculation is overestimated.
- The eddy current loss in the magnet due to the end turn windings is neglected. Most of the flux from the end windings is assumed appear in the end stator region. Therefore, the eddy current due to the flux from the end windings can be expected to be small.

To simulate the eddy current in this section, the following procedures are used:

1. Build a 2D FEM model. The static simulation of this model is used to get the armature flux density distribution in the system. After that extract the magnetic vector potential $A_z[Wb/m]$ distribution in the air gap. The transient simulation of this model is used as the comparison to the time harmonics application mode. The method of transient simulation is explained in chapter 4.3.3.
2. Calculate the space harmonics of magnetic vector potential in air gap from previous step. The harmonics can be calculated by using Fast Fourier transform of Matlab toolbox.
3. Build a 3D FEM model which consist only the rotor part. The thickness of the model in axial direction is the segmentation length.
4. The magnitude of major harmonics of the magnetic potential is used as the boundary condition in the 3D time harmonics application mode. The 2nd, 4th, and 5th harmonics will be considered since these three harmonics produced most of the eddy current losses in the rotor.
5. Execute the time harmonics simulation to solve the magnetic vector potential.

5.4.2 Simulation setup

In this section, the eddy current losses will be calculated for 3/2 slot-pole combination machine. After building the model, the following boundary conditions are used:

- Magnetic insulation: This boundary is used at bottom of the rotor back iron. The magnetic vector potential in this boundary is expressed by $\mathrm{n} \times \vec{A} = 0$.
- Continuity: in this boundary, the magnetic intensity is expressed by $\mathrm{n} \times (\vec{\mathrm{H}}_1 - \vec{\mathrm{H}}_2) = 0$.
- Periodic boundary condition: The periodic boundary condition between two sections of the model is set to continuity which means that the magnetic vector potential source is equal to magnetic vector destination, $\mathrm{A_{dst}} = \mathrm{A_{src}}$.
- Magnetic potential: this boundary is set in the outmost rotor model. In this boundary, the harmonics of magnetic potential from the 2D model is specified. The magnetic potential in this boundary is expressed by: $\mathrm{n} \times \vec{A} = \mathrm{A_0}$. The magnetic potential $\mathrm{A_0}[\mathrm{Wb/m}]$ distribution is set as the following:

$$\mathrm{A_0} = \mathrm{c} \cdot \mathrm{e}^{\mathrm{j} \cdot 2 \cdot \theta} \tag{5.26}$$

Where c is the harmonics amplitude from step two above, $\theta[\mathrm{rad}]$ is the angle in the rotational direction of the plane around the z-axis.

5.4.3 Simulation result

The magnet eddy current loss calculation is done for various magnet laminations. There are two types of segmentation: the segmentation in the rotational direction and the segmentation in the axial direction. First, the time harmonic calculation method will be validated with the eddy current losses with transient simulation mode with the following steps.

Step 1. Transient 2D FEM model.

The magnet eddy current loss for 32 combination SMPM machine in the transient simulation is **150.65 Watts**. This is the same result as presented in chapter 4. The magnetic vector potential in the air gap is extracted from static simulation. Az distribution in the air gap is shown in figure 38.

Step 2. Calculation of the space harmonics of Az

The space harmonics for Az is calculated from the Az distribution from previous step. The result is shown in the right side of figure 38. It shows that the third harmonics and its multiplication is zero because of a balanced three phase current in the stator. The amplitude of the harmonics are 0.68 mWb/m, 0.22 mWb/m, 0.067 mWb/m and 0.051 mWb/m for 1st, 2nd, 4th and 5th harmonics respectively. From equation 2.49 in chapter 2.3.1, the 1st harmonic is the fundamental harmonic and rotates with the same speed of the rotor. The 2nd, 4th and 5th harmonics rotate in the opposite direction of the rotor at 1200 Hz, 600 Hz and 960 Hz at rotor frame.

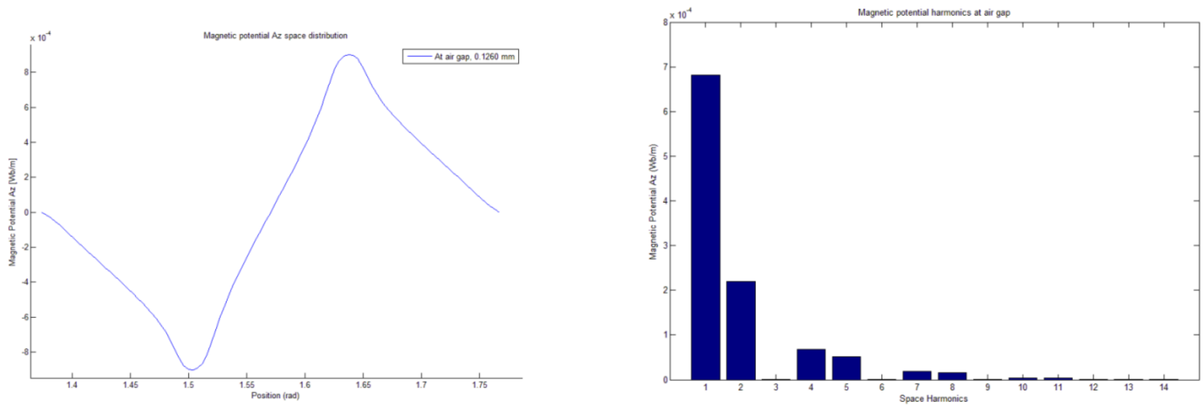

Fig. 38 Magnetic potential distribution and its harmonics

Step 3 Time harmonics 2D FEM model.

The model for time harmonics calculation consist only the rotor part. The boundary conditions are set as explained in chapter 5.4.2. The magnetic potential boundary condition uses the harmonics amplitude calculated from step two above in equation 5.26. The calculation is repeated for each harmonics in step 2. There are three harmonics which is considered in this calculation: 2^{nd}, 4^{th} and 5^{th} harmonics. The eddy current loss in permanent magnet is **132.8 Watts**. The result is lower compared to the transient simulation because of the neglecting of higher harmonics.

5.4.3.1 Eddy current losses for lamination in axial direction

In this section, the magnet was cut into several laminations. The eddy current loss was calculated for each lamination by using the method described above. For a comparison, the correction factor in equation 5.22 is used in combination with the 2D FEM model to predict the eddy current losses.

Figure 39 below shows the resistive heating and the induced current direction in the magnet lamination.

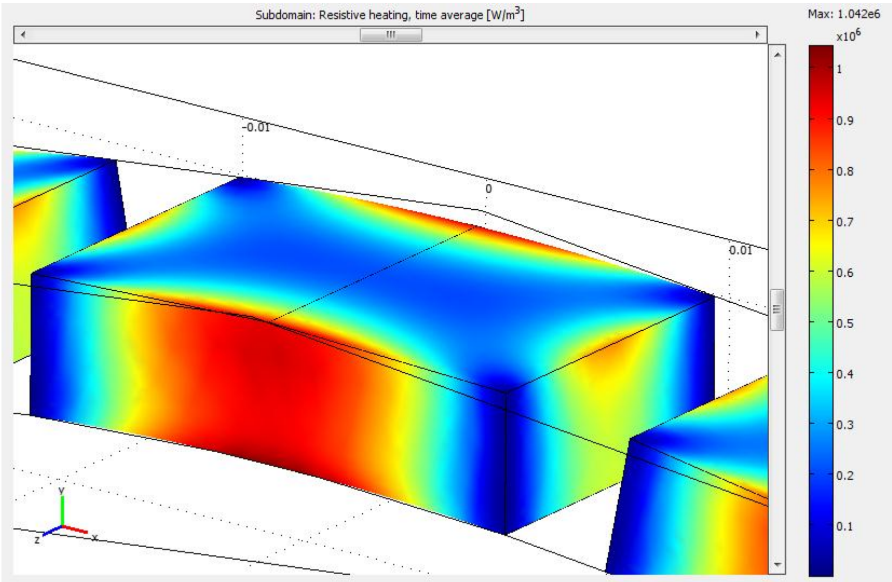

a. Resistive heating in magnet sub-domain

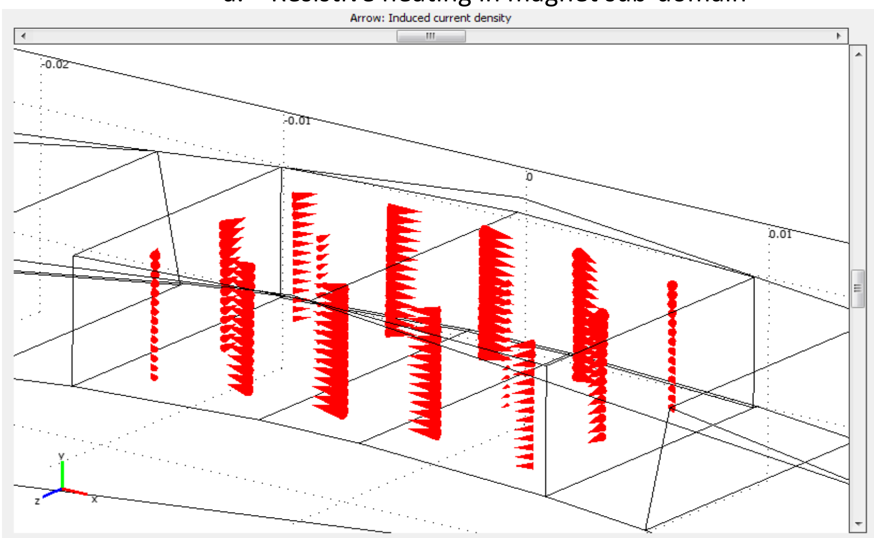

b. Induced current flow in magnet sub-domain

Fig. 39 Simulation result for time harmonic application mode

As can be seen from figure 39 above, the induced current is circulating in the magnet sub domain. It doesn`t happen in the 2D model since the magnet length is assumed to be infinitely long. Figure 40 and table 13 below shows the eddy current losses from the 3D model and from 2D model with correction factor in equation 5.22 and 5.23.

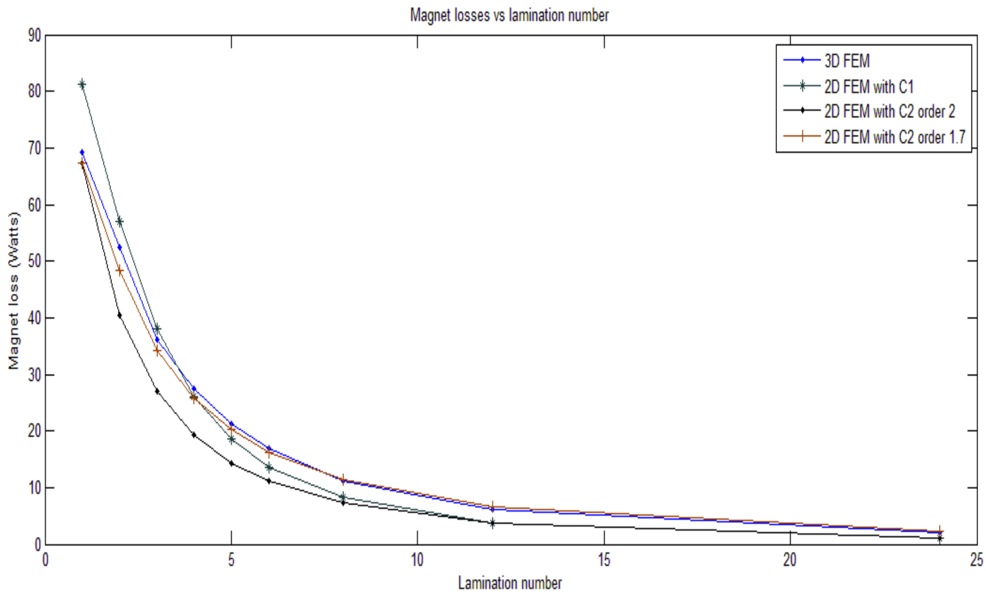

Fig. 40 Magnet loss for various magnet segmentation

Calculation type	Lamination number								
	1	2	3	4	5	6	8	12	24
	Magnet losses (Watts)								
3D FEM	69.3	52.4	36.1	27.6	21.2	17.0	11.2	6.1	2.1
2D FEM with C1	81.3	57.0	38.1	26.0	18.5	13.6	8.2	3.8	1.0
2D FEM with C order 2	67.2	40.4	27.0	19.3	14.4	11.2	7.4	3.8	1.1
2D FEM with C order 1.7	-	48.3	34.3	25.8	20.2	16.3	11.4	6.5	2.3

Table 13 Magnet losses for various magnet segmentation

As can be seen, the eddy current losses calculation for solid magnet gives almost the same result from both 3D FEM and 2D FEM with correction factor in equation 5.23. For higher magnet segmentation, the 2D FEM losses with correction factor order 2 have more errors. One of the reason is due to the fact that the induced current doesn`t flow following the magnet edge as can be seen in figure 39.b. Since equation 5.23 includes the magnet corner, the resistance in the equation 5.23 is overestimated which reduces the induced current in the magnet. In a longer magnet length, this phenomena is not too obvious because the resistance of magnet length is more dominant. When a magnet is laminated into two or more segments, the ratio of the magnet length and magnet width $\frac{l_c}{\tau_m}$ becomes smaller. This effect is more dominant which results in a lower magnet loss as can be seen in figure 40. To overcome this problem, the order of correction factor C of equation 5.23 is changed to 1.7 for magnet with laminations. With this new correction factor order, the result in figure 40 shows a better agreement with 3D model.

The magnet losses calculation with a correction factor in equation 5.22 is not too accurate. When the magnet length l_c is longer than the magnet width τ_m, the losses are overestimated. On the other hand, when the magnet length is shorter than the magnet width, the magnet losses are underestimated. It happens because the angle of diagonal line in figure 37 always changes when the variation is made in the magnet length. From here we can conclude that the assumption of the induced current flow in the derivation of equation 5.22 is not too accurate.

With this result, the magnet losses for the other machine type are calculated from 2D FEM model calculation results in chapter 4 and correction factor in equation 5.23 with the order of 2 and 1.7. Figure 41 and table 14 below show the summary of the magnet losses for all of the machine types.

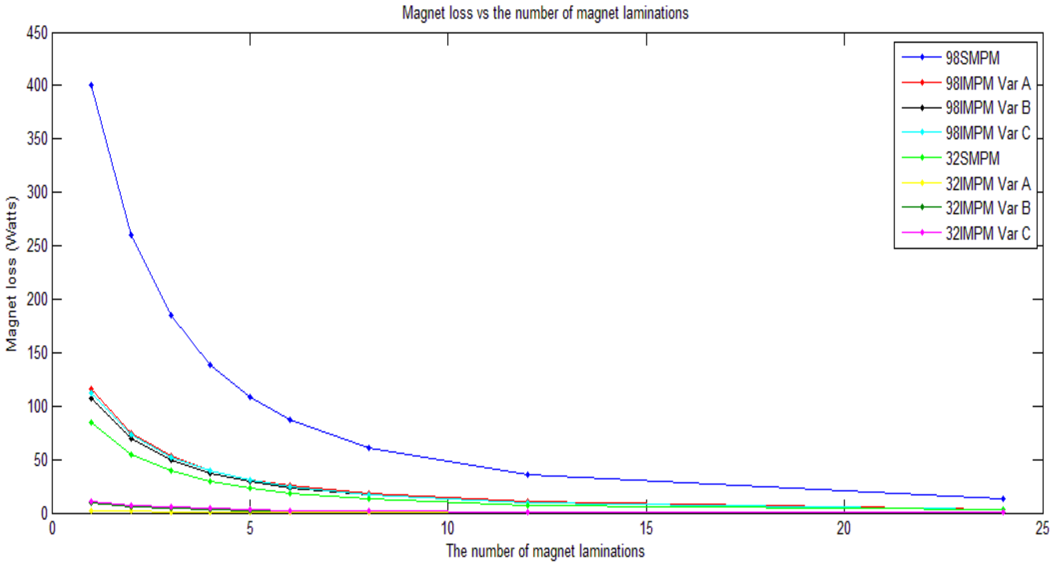

Fig. 41 Magnet loss for various magnet segmentation and machine types

Machine type	Lamination number								
	1	2	3	4	5	6	8	12	24
	Magnet losses (Watts)								
98 SMPM	361	260	184	139	108	87	61	35	13
32 SMPM	75.8	54.6	38.7	29.1	22.8	18.4	12.8	7.4	2.6
98 IPM Variation A	104	75	53	40	31	25	18	10	4
98 IPM Variation B	97	70	50	37	29	24	16	9	3
98 IPM Variation C	102	73	52	39	31	25	17	10	4
32 IPM Variation A	1.9	1.4	0.95	0.71	0.56	0.45	0.31	0.18	0.06
32 IPM Variation B	8.3	6.0	4.2	3.2	2.5	2.0	1.4	0.9	0.3
32 IPM Variation C	10	7.3	5.2	3.9	3.0	2.4	1.7	01.0	0.4

Table 14 Magnet losses for various magnet segmentation and machine types

5.4.3.2 Eddy current losses for lamination in circumferential direction

The eddy current in the magnets when it is laminated in axial direction has been shown in chapter 4. The result didn`t include the finite length magnet effect. In this section, the same method as in chapter 5.4.3.1 is implemented. The eddy current losses of laminated magnets in chapter 4 are recalculated with the correction factor C of order 2. Figure 42 and table 15 below show the eddy current losses in the magnet with laminations in axial direction for SMPM machine.

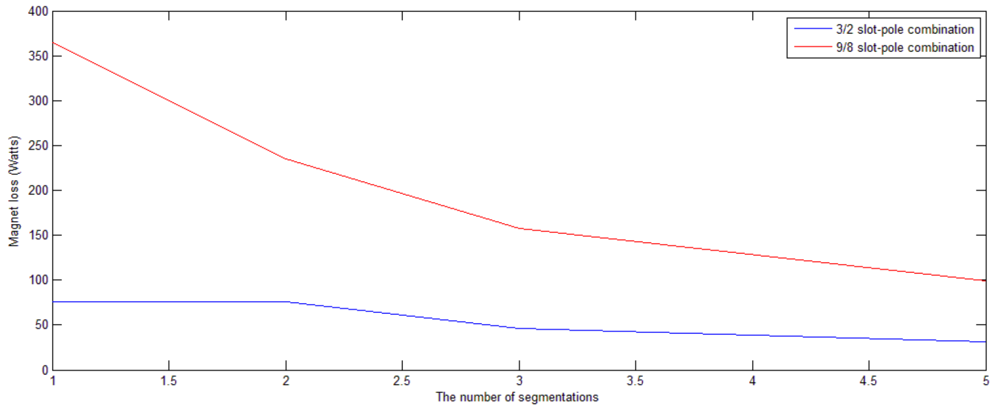

Fig. 42 Eddy current losses as a function of segmentations number

Machine type	Segmentations number			
	1	2	3	5
2D FEM and correction factor	**Magnet losses (Watts)**			
3/2 slot-pole combination	75.8	75.8	46.6	31.4
9/8 slot-pole combination	364	234	158	99
2D FEM	**Magnet losses (Watts)**			
3/2 slot-pole combination	150	109	60	37
9/8 slot-pole combination	720	340	204	116

Table 15 Eddy current losses as a function of segmentations number for SMPM machine

The eddy current losses in solid and 2 segmentations magnet in 3/2 slot-pole combination has the same results. It happens due to a higher correction factor compared to the solid construction. As can be predicted, the correction factor becomes closer to 1 since the ratio of magnet axial length to magnet width getting higher. It is clearer in magnet with 5 segmentations. The eddy current in the magnet in 2D FEM calculation and the 3D FEM calculation in table 15 almost the same.

6. Result and discussion

This chapter summarizes the calculation result from the analytic, 2D and 3D FEM model. The results are compared for various methods that have been explained in previous chapter. Some of the results are validated from the measurement of the prototype generator in the laboratory [PP 11]. The following are overview of results that are presented in this chapter:

- The armature reaction from analytic and 2D FEM model
- The eddy current losses in the rotor from analytic, 2D and 3D FEM model
- Machine inductance from analytic, 2D, 3D FEM model, and lab measurement result.
- Eddy current losses in stator end.
- The flux leakages in the machine and induced voltage from 2D, 3D FEM model and lab measurement result.

6.1 The armature reaction modeling result

In this section, the analytic modeling of armature reaction flux density in chapter 2.2 is presented. The result is validated with the 2D FEM model. Table 16 below shows the summary of maximum flux density distribution for SMPM machine for both 98-combination machine and 32-combination machine. This flux density is measured when the magnet and the stator tooth is aligned.

Parameter	36 teeth stator 32 poles		48 teeth stator 32 poles	
	Analytic	FEM	Analytic	FEM
$\hat{B}_{ar,magnet}$	0.14	0.13	0.09	0.08
$\hat{B}_{ar,ry}$	0.19	0.16	0.11	0.08
$\hat{B}_{ar,sy}$	0.55	0.63	0.32	0.40
$\hat{B}_{ar,tooth}$	0.62	0.63	0.50	0.55

Table 16 Armature flux density distribution

Table 16 shows that the reluctance network model gives quite a good agreement with the 2D FEM model for the prediction armature flux density distribution in the generator, especially for the maximum armature reaction flux density in the magnet. The flux density in the magnet will be used to calculate the magnet loss which will be discussed in chapter 6.2. From this result, we can conclude that the reluctance model can be used to calculate the maximum armature flux density distribution in the generator.

6.2 Eddy current losses calculation

The analytic calculations of eddy current losses for rotor back iron and permanent magnet are presented in chapter 2.3 and 2.4 respectively. The first step to calculate the eddy current losses in the rotor is to determine the flux density distribution in the air gap. The amplitude of flux density is presented in table 16 above. The second step is to determine the flux density space distribution and its space harmonics as described in chapter 2.3.1. The assumption of air gap armature flux density distributions were shown in figure 11 for 98-combination machine and figure 12 for 32-combination machine. Figure 44below shows the comparison of the air gap armature flux density space distribution from analytic and 2D FEM model. This figure shows the space flux density distribution when one phase conducting. There are two positions to measure the flux density in FEM. First in the magnet near air gap and the second one is in the magnet near the rotor back iron. These measurement positions are shown in figure 43.

Measurement position 1 in figure 43 corresponds to the flux density that crosses the permanent magnet. On the other hand, measurement position 2 in figure 43 corresponds to the flux density which crosses to the rotor back iron. As can be seen from figure 44, the flux density crosses to the back iron much less and doesn`t have any spike in the tip of the magnet. This spike happens due to the slotting effect in the stator. Although the amplitude of the armature flux density is almost the same as shown in table 16, the space flux distribution from 2D FEM is different from the assumption in figure 11 and figure 12 in analytic model. This different leads to different eddy current losses calculation result

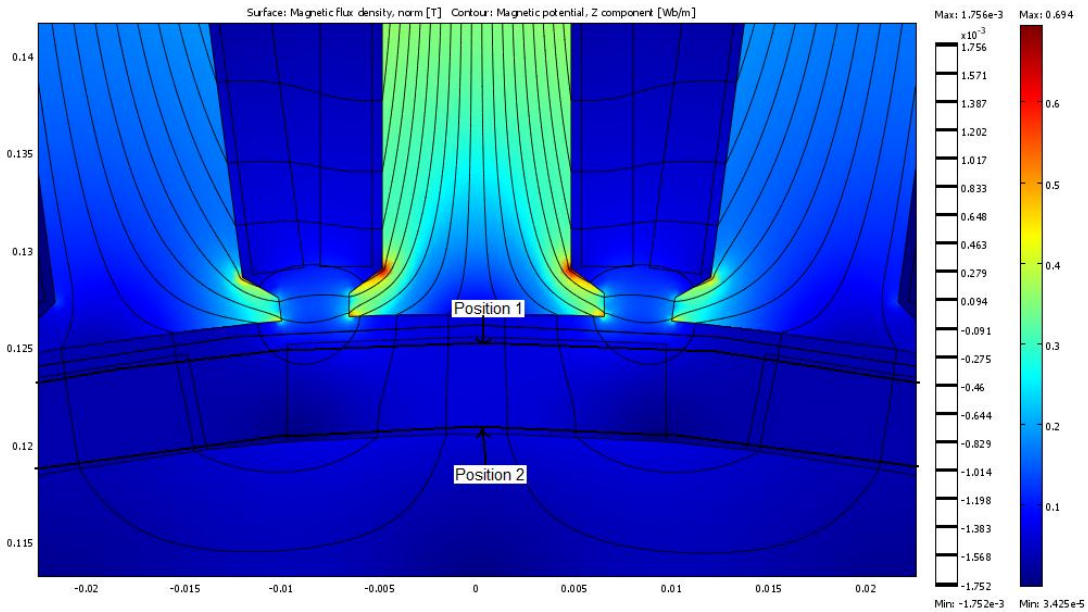

Fig. 43 FEM flux density measurement position

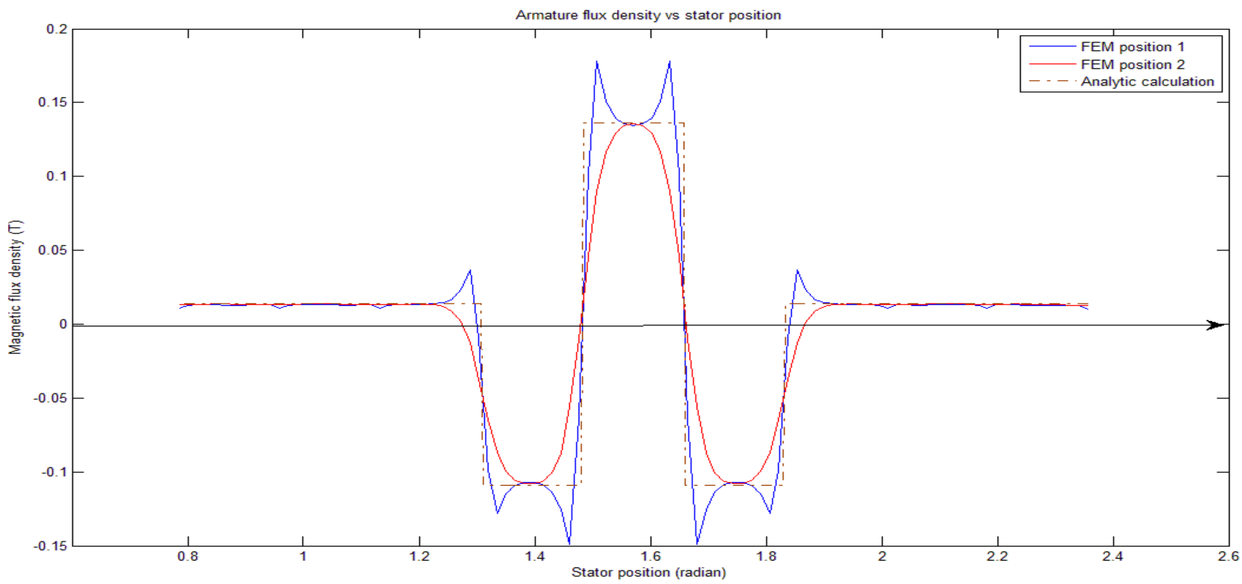

a. 9/8 slot-pole combination machine

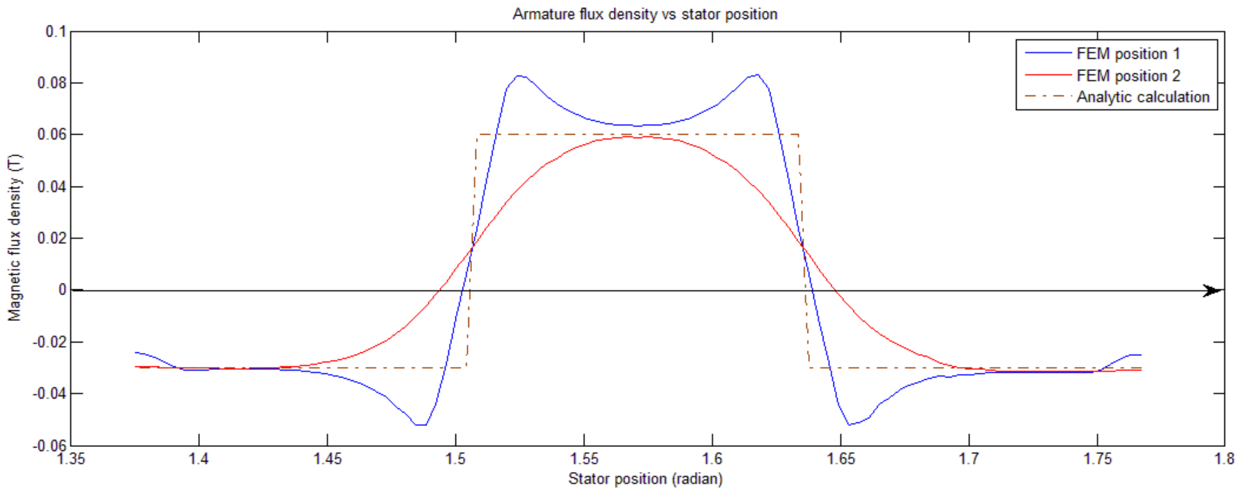

b. 3/2 slot-pole combination machine

Fig. 44 Space armature reaction distribution

6.2.1 Rotor eddy current losses for solid construction

Table 17 below summarizes the eddy current losses calculation for solid magnet and solid rotor back iron.

Combination type	Solid Back Iron Losses (W)		Solid Magnet Losses (W)	
	Analytic	FEM	Analytic	FEM
SMPM construction				
9/8 slot-pole	463	289	872.37	720.2
3/2 slot-pole	132	23.3	198.09	150.65
IPM construction (laminated back iron)				
9/8 slot-pole Variation A	-	0	-	206
9/8 slot-pole Variation B	-	0	-	192
9/8 slot-pole Variation C	-	0	-	201
3/2 slot-pole Variation A	-	0	-	3.68
3/2 slot-pole Variation B	-	0	-	16.4
3/2 slot-pole Variation C	-	0	-	20.0

Table 17 Eddy current losses results for solid back iron (SMPM) and solid magnet

Table 17 above shows that the analytic calculations and FEM results for SMPM construction have large different result. One of the reasons is in the assumption of space armature flux density distribution. Figure 45 below shows the harmonics of air gap flux density from analytic and FEM calculation.

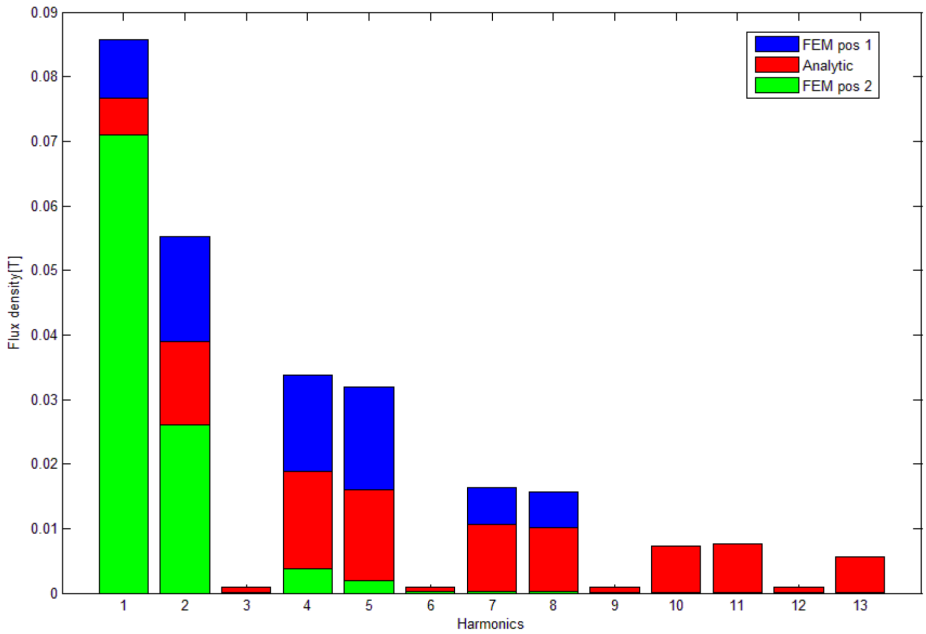

Fig. 45 Harmonics of 3/2 slot-pole combination machine

As can be seen, the space harmonics in position 2 measurement has a significant lower value compared to the harmonics in the air gap from analytic calculation. This measurement corresponds to the flux density which is responsible for the eddy current loss in the rotor back iron. This fact explains a lower eddy current loss in rotor back iron from 2D FEM model. On the other hand, the magnet loss from FEM is expected to be higher compared to analytic calculation. The analytic calculation for magnet loss is not too accurate. The reason of this result could be:

- The assumption of a homogenous flux density distribution throughout the magnet width is not completely correct for a higher space harmonics. With this assumption, the flux crosses the magnet surface area is larger from a sinusoidal distribution flux density.
- The eddy current effect to the armature flux density is neglected in analytic calculation. The induced eddy current in the magnet flows in such a direction so that the flux density produced by the induced current opposes the changing armature flux. With neglecting the eddy current effect, the flux crosses magnet surface area can be higher.

From the results in this chapter, we can conclude that the assumption of armature flux density distribution should be improved. Although the amplitude of armature flux density in the air gap is fairly the same as has been shown in chapter 6.1 and figure 44, the different of flux density distribution in the air gap can lead to a different rotor eddy current losses calculation compared with the 2D FEM model results.

6.2.2 Comparison of magnet loss from 2D and 3D model

The effect of a finite axial length effect to the eddy current losses in the magnet is presented in chapter 5.4. This effect was investigated with 3D FEM model. The 3D model was built for 3/2 slot-pole combination machine.

Equation 5.23 in chapter 5.4 suggests that with the lamination length $l_m[m]$ equal to the axial length $l_{stk}[m]$, the magnet loss should be around half of the 2D FEM simulation for solid magnet construction. The simulation was conducted with time harmonics application mode for both 2D and 3D model. In these simulations, only 2nd, 4th and 5th harmonics are used. The 2D FEM magnet loss calculation gives **132.8 Watts.** The 3D FEM magnet loss calculation gives **69.3 Watts.** This result shows that the prediction from equation 5.23 give a quite good agreement with 3D model. However, for higher magnet segmentation, the correction factor in equation 5.23 should be corrected with order of 1.7. Figure 46 below shows the correction factor C as a function of lamination length and magnet width ratio. Another conclusion can be extracted from figure 46 for the correction factor in equation 5.22. The correction factor doesn`t give a result as expected for an infinitely long axial length machine. It appears due to the ¾ factor in equation 5.22.

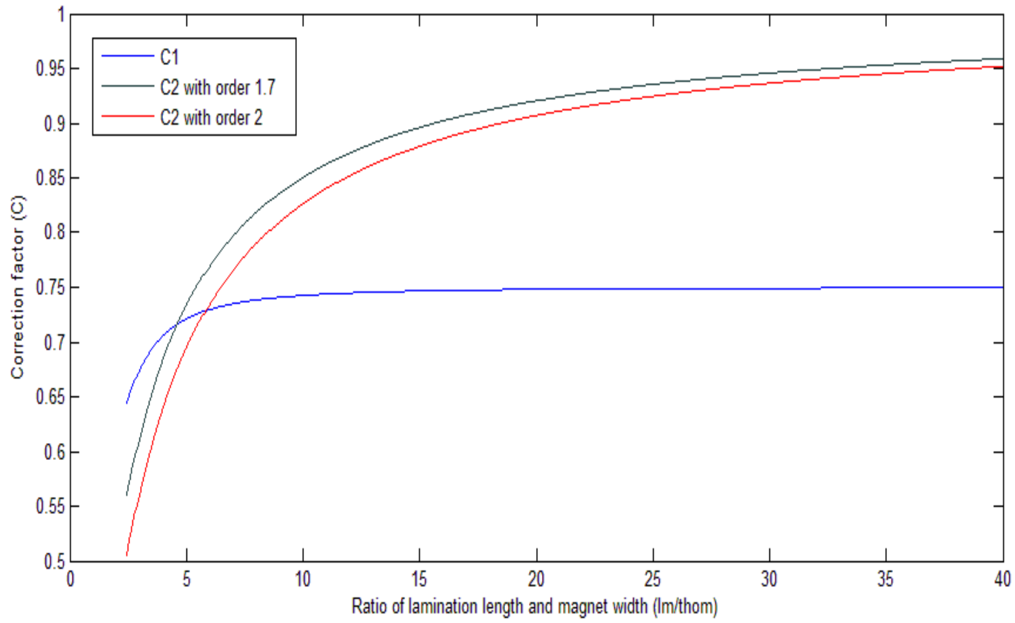

Fig. 46 Correction factor as a function of lamination length and magnet width ratio

However, from all of the correction factors in figure 46 we can conclude that for a low ratio of magnet axial length over magnet width, $\left(\frac{l_m}{\tau_m}\right)$, the magnets losses calculation in the 2D FEM model have a large error compared to the 3D FEM model. With correction factor in equation 5.23, an error of 5% is acquired in 2D Fem magnet loss calculation when the ratio of magnet axial length over magnet width is around 38. Therefore, for a short machine axial length, the end effect could not be neglected from the magnet loss calculations.

Figure 47 and table 18 below summarizes the magnet loss calculations when finite magnet length effect is included.

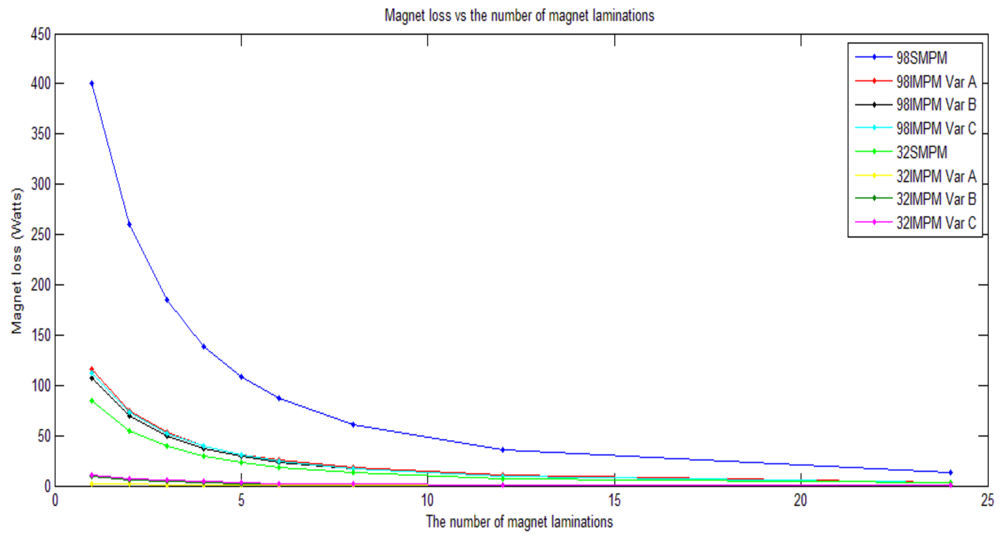

Fig. 47 Magnet loss for various magnet segmentation and machine types

Machine type	Lamination number								
	1	2	3	4	5	6	8	12	24
	Magnet losses (Watts)								
98 SMPM	361	260	184	139	108	87	61	35	13
32 SMPM	67.2	48.3	34.3	25.8	20.2	16.3	11.4	6.5	2.3
98 IPM Variation A	104	75	53	40	31	25	18	10	4
98 IPM Variation B	97	70	50	37	29	24	16	9	3
98 IPM Variation C	102	73	52	39	31	25	17	10	4
32 IPM Variation A	1.9	1.4	0.95	0.71	0.56	0.45	0.31	0.18	0.06
32 IPM Variation B	8.3	6.0	4.2	3.2	2.5	2.0	1.4	0.9	0.3
32 IPM Variation C	10	7.3	5.2	3.9	3.0	2.4	1.7	01.0	0.4

Table 18 Magnet losses for various magnet segmentation and machine types

6.3 Inductance calculation result

In this section the summary of inductance calculation for analytic and FEM model are provided. Table 19 below shows the inductance calculation results.

Parameter	Units	9/8 slot-pole combination machine			3/2 slot-pole combination machine		
		Analytic	2D FEM	3D FEM	Analytic	2D FEM	3D FEM
		SMPM					
$L_{s,2D}$	µH	554	548	-	263	266	-
L_{sm}	µH	257	-	-	89	-	-
$L_{s\sigma}$	µH	297	-	-	174	-	-
L_{end}	µH	-	-	66	-	-	43
M_{ab}	µH	-59	-42	-	-132	-132	-
$L_{s,total}= L_{s,2D}+L_{end}$	µH	614			309		
Measurement		L_s		M_{ab}	L_s		M_{ab}
	µH	590		-37	300		-108
		IPM					
L_s	µH	-	1005	-	-	550	-
L_{end}	µH	-	-	66	-	-	43
M_{ab}	µH	-	300	-181	-	200	-227
$L_{s,total}= L_{s,2D}+L_{end}$	µH	1066			593		
Measurement		L_s		M_{ab}	L_s		M_{ab}
	µH	950		-54	460		-174

Table 19 Inductance calculation results from analytic, 2D, 3D FEM and measurement

As can be seen in table 19, the self inductance, L_s[H], calculation between analytic and FEM model gives a good agreement. But, the comparison of these two results with total inductance measurement in the lab gives error around 7% in 9/8 slot-pole combination machine and 11.3% in

3/2 slot-pole combination machine. This different is quite high and can influence in the other machine performance calculation such as in torque or power output calculation.

With the addition of end leakage inductance L_{end}[H] from 3D FEM model, the error becomes around 4% in 9/8 slot-pole combination machine and 3% in 3/2 slot-pole combination machine. It shows that the L_{end} takes around 11-14% of total inductance for the prototype machine. This value is quite significant and should not be neglected.

As already discussed in chapter 5.2, the L_{end}[H] is quadratic proportional to the number of turns. The increment of the coil turns correspond to the reduction of the machine axial length. This relation is to maintain the same induced voltage when the machine axial length is reduced. This result is shown in table 9 in chapter 5.2. In addition, the self inductance L_s[H], also calculated for various number of turns. The L_s and L_{end} calculation results are shown in figure 48 below. This figure shows various inductances as a function of the number of coil turns. This figure is obtained by using basic fitting of L_s and L_{end} from 2D and 3D FEM model. The L_s changes linearly with the increment of coil turns while L_{end} changes quadratically with the increase of coil turns.

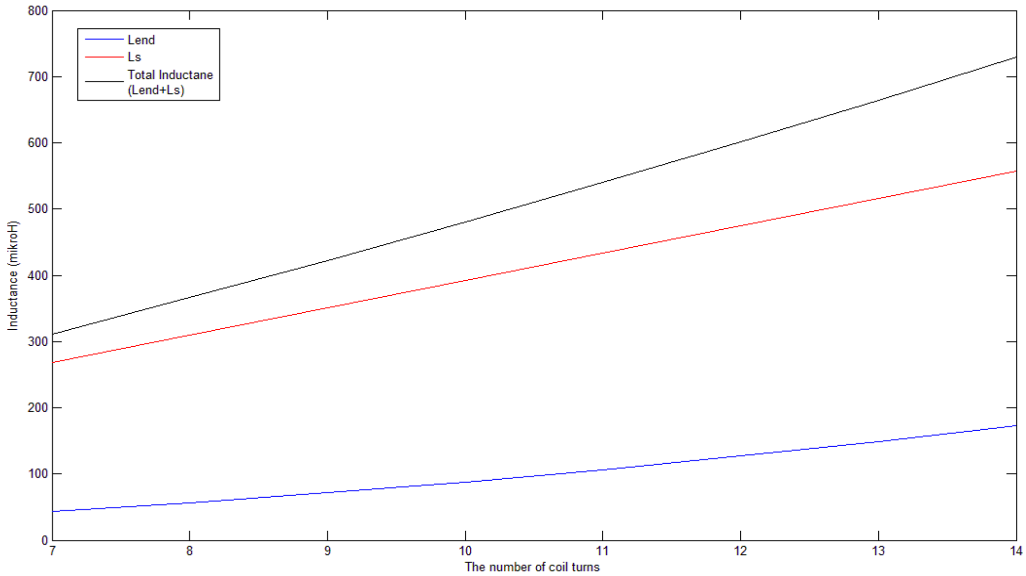

Fig. 48 Inductance as a function of the number of coil turns for 3/2 slot-pole combination machine

Figure 49 below shows the percentage of L_{end} as a function of the number of coil turns. As can be seen from this figure, the percentage of L_{end} increases quadratically with the increment of the number of coil turns. From this result, we can conclude that the end inductance becomes more important with the reduction of machine axial length. Therefore, the end inductance L_{end} cannot be neglected.

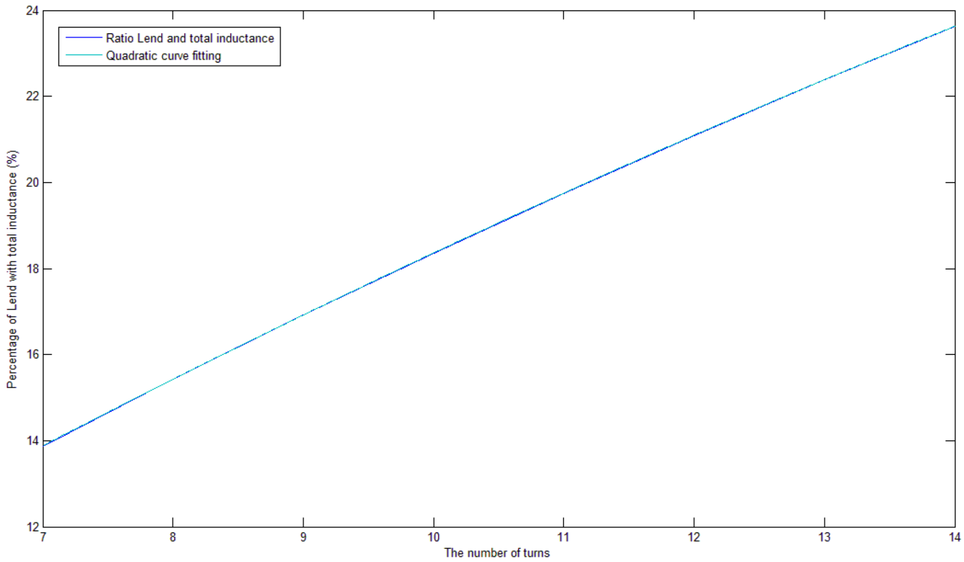

Fig. 49 L_{end} percentage from total inductance as a function of the number of coil turns for 3/2 slot-pole combination machine

The inductance for IPM machine is larger compared to the SMPM machine. It happens because the rotor back iron is closer to the stator tooth in the IPM machine. This condition creates a lower system reluctance. It makes the inductance for this machine also more sensitive to the changing of air gap length. A small change in air gap creates quite large inductance different. Figure 50 below shows the self inductance of the machine when the air gap length is changed in 2D FEM model. As can be seen from figure 50, the inductance change in the IPM is around 100 μH while in SMPM is hardly change. It also could be one of the reasons of a larger different in inductance calculation in the IPM machine. The air gap distance in the prototype machine could be different with the FEM model. The other reason could be from the characteristic of rotor back iron. In the prototype machine, there is a flux contribution from the magnet while in the FEM model the magnet flux is set to zero. With the contribution of flux from the magnet, some parts of the rotor back iron are in saturation region. Therefore, the overall system reluctance is increased which reduces the armature flux density in the system.

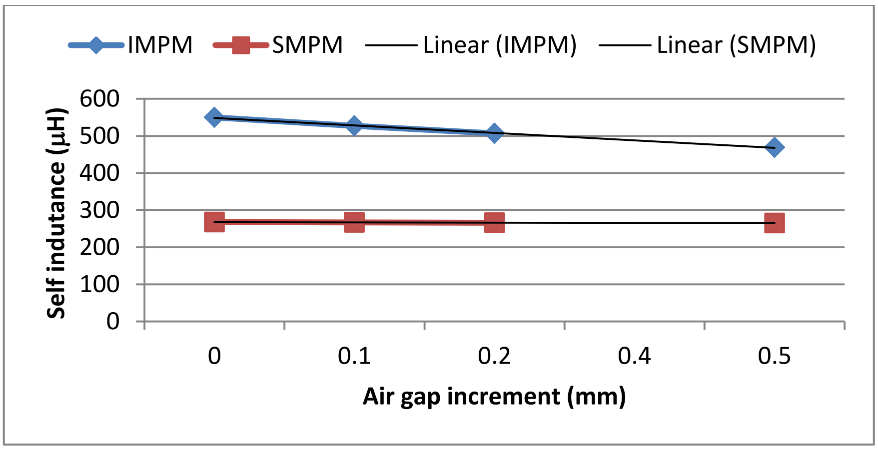

Fig. 50 Self inductance vs the increment of air gap length for 3/2 slot-pole combination machine

From these results, we can make some conclusions as follow:

- The end leakage inductance in the machine can be investigated by using a static 3D FEM model and with comparison from 2D model. Furthermore, it is possible to calculate the end leakage inductance with a thin stator axial length, such as 1mm thickness. With this fact, the end leakage inductance can be investigated with a much smaller 3D FEM model.

– The end inductance of both 9/8 and 3/2 slot-pole combination machine with SMPM construction is quite high. The end inductance takes 11%-14% of total self inductance of the machine. This end inductance should not be neglected. The end inductances are higher with the reduction of axial length or with the increasing the number of coil turns.
– The self inductance for IPM machine is higher because the rotor back iron is closer to the stator tooth. The inductance is more sensitive in air gap changes.

6.4 End section stator iron losses

The flux density from end windings crosses the stator iron perpendicularly. Since the stator iron is not laminated parallel to the flux from the end windings, the eddy current in this section is expected higher. The eddy current in end region appears in the surface of the stator with a small penetration due to the skin depth. As already shown in chapter 5.3, the end stator loss is **197 Watts** for 3/2 slot-pole combination machine with 1 mm stator thickness. This loss is part of the total losses produced in the stator region. To be noted that this loss also including the eddy current loss due to a current in stator coil in stator slot. Therefore, the eddy current losses in the end region due to only the end winding could be smaller than this value.

The stator iron is laminated in radial direction. This lamination could be thinner than 1 mm. Therefore, to see the effect of stator lamination thickness, an additional simulation to calculate the eddy current losses in the end region were conducted for a few stator thicknesses. The stator thicknesses are set to 0.2 mm, 0.25 mm and 0.3 mm. The simulation results for these models are shown in figure 51 and table 20 below.

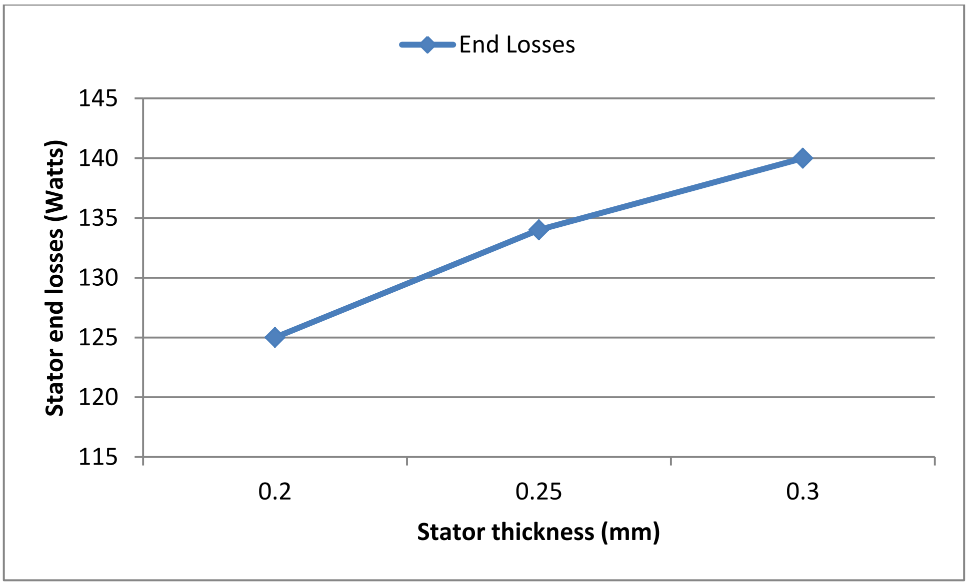

Fig. 51 Stator end losses as a function of stator thickness

Machine type	Stator axial length (mm)	Eddy current losses (W)	Skin depth ratio (stator thickness/δ)	End losses prediction (W)
3/2 slot-pole combination machine	0.2	125	1.78	150.3
	0.25	134	2.22	150.3
	0.3	140	2.67	150.4

Table 20 Stator end losses as a function of stator thickness

The eddy current losses in stator end in table 20 shows a decreasing loss when the stator thickness is reduced. This reduction corresponds to the skin depth in the stator iron. The skin depth of the induced current from simulation result is **0.1125 mm**. The ratio of the stator thickness and skin depth is presented in the table 20 above. From this skin depth ratio, the end losses prediction in the last column of table 20 is presented. It shows that the end loss prediction is almost the same which is **150 Watts**. This is the end losses when the stator thickness is much larger than skin depth. This is the end loss due to the current in end winding.

Another conclusion which can be obtained from this simulation is that the stator end losses are limited by the stator iron lamination thickness. The relationship of the loss reduction is the same with the skin depth relation. For example, with lamination thickness equal to skin depth, the eddy current losses will be around 63% lower compared to when the lamination thickness is much larger than the skin depth.

The simulation results also show that the end loss increases quadratically with the increases of the number of coil turns. It means that with a shorter axial length, the end windings produce more loss which can lead to thermal problem in the stator. To reduce the end losses, a thin material with high resistivity can be placed in the end of stator iron laminations. With a higher resistivity, the induced current will be limited and finally reduce the total stator iron loss. The simulation results for stator end loss are presented in chapter 5.3.4.

6.5 Flux leakages and no load induced voltage

The static simulation in chapter 5.1 determines the contribution of leakage flux of the permanent magnets. These leakages are the leakage due to lamination of the magnet, the magnet leakage in the end region, the leakage to the air end region without balancing rim and the leakage to the balancing rim. The calculated flux leakages are for the machine with 3/2 slot-pole combination.

The different of stator tooth flux linkage of 2D FEM model and 3D FEM model is around **18.5%** for the machine without balancing rim and **22.6**% for the machine with the balancing rim. Since the balancing rim is installed only in one side of the rotor, the average of flux linkage reduction is around **20.5%**. This different leads to the different of induced voltage in the stator of both models. The measurement result shows that the difference for 3/2 slot-pole combination machine with the IPM rotor is **18%**.

From these results, the following conclusions can be drawn:

- The flux leakage due to magnet laminations is quite high. This leakage reduces the flux linkage in stator coil around 8.2%. This leakage changes linearly with the number of magnet laminations. This leakage can be reduced by reducing the number of magnet laminations.
- The addition of balancing rim can add the flux leakages in the end region. It happens because the balancing rim has higher permeability compared to the air. The permeability of the steel is around 100 while the air is 1. Using a balancing rim with a non magnetic material reduces this leakage.
- The end leakage to the end region is quite high. This leakage reduces the flux linkage in stator coil around 8.2%. This leakage should be included in the analytic model to get a better result.

7. Conclusion and future work

7.1 Contributions and Conclusions

There are two major topics that have been investigated in this thesis. The first topic is the investigation of the eddy current losses in the rotor back iron and in the permanent magnets of the prototype generators. The second topic is the investigation of the influence of the machine ends and end windings on the flux distribution and inductivity of the prototype generators. These topics were investigated either by using analytic, 2D FEM or 3D FEM model. These two topics are investigated to see the possibilities for further development of the prototype generators for range extender application.

The investigation of the eddy current losses in the rotor of the prototype generator is done to see the possibilities of using a non laminated structure in the rotor. With a non laminated structure, the production cost of the lamination processes can be reduced, especially for the magnet lamination process. From the investigation of the rotor losses in this thesis, the following conclusions can be drawn.

- A solid magnet construction in SMPM generator cannot be implemented. The magnets losses are too high, in 9/8 slot-pole combination machine. This high loss could increase the magnet temperature. Thus, the magnets are exposed to the dangerous of the magnet demagnetization. It happens because the magnet is closer to the stator iron. Therefore the magnet eddy current losses are higher in this construction. To reduce the magnet loss, a lamination process can be done in the machine. However, the number of magnet laminations is not necessarily too many. The number of laminations can be chosen based on the magnet loss calculation in this thesis. The determination of the number of magnets lamination depends on the maximum allowed magnet loss which is still safe for the magnet. With this less lamination, the production cost for magnet laminations can be reduced.
- The eddy current losses in the solid magnets in the IPM rotor are much less compared to the SMPM rotor. It happens because the magnets are buried deep down in the rotor steel. Therefore, the eddy current losses are lower. From the simulation results, a solid magnet construction can be implemented in the IPM rotor, especially for 3/2 slot-pole combination. On the other hand, the 9/8 slot-pole combination machine still produces a high solid magnet loss. Therefore, a lamination process is still necessary for this machine construction. The number of magnet laminations can be determined from the results in this thesis. With these results, a cheaper production cost of prototype generators can be obtained.
- The eddy current losses of solid rotor back iron in 9/8 slot-pole combination of SMPM generator are too high. The solid rotor construction cannot be implemented. A lamination of rotor back iron can be used to reduce the losses.
- The eddy current losses of solid rotor back iron in 3/2 slot-pole combination of SMPM generator are less than 100 Watts. It is possible to use a solid back iron construction in this generator type.
- The eddy current losses in solid rotor back iron of all types of the IPM generators are too high. The solid rotor construction cannot be implemented. A thin lamination of the rotor back iron can be used to reduce the losses.

3D FEM models have been used to investigate the influences of machine end and end winding in the prototype generators. A better insight into the flux density behavior, especially in the axial direction, leads to various flux leakages information that cannot be observed from the 2D model. Furthermore, the neglect of end effect, including the end winding, could lead to a larger deviation compared to 3D simulation results. This information gives various topics that should be taken into account when exploring the possibility in designing the machine for a shorter axial length.

With a shorter axial length, the generator could be cheaper and less weight. The following conclusions could be made regarding the end effect of the machine:

- The additional flux leakages in the 3D FEM model explain a lower induced voltage in the performance measurement of the prototype generators. These flux leakages should be further parameterized so that the flux leakages could be included in the analytic calculation. In addition, a solid construction or a fewer magnet laminations also reduces the flux leakages due to magnet laminations. It means that a solid or a fewer magnet laminations not only reduces the magnet loss but also reduces the leakage flux due to magnet laminations. The flux leakages in the balancing rim also can be reduced by using a more non magnetic material for the balancing rim.
- The end inductance composition in the total prototype generator self inductance is quite high. Furthermore, this composition becomes higher for a shorter generator axial length. This end inductance cannot be neglected in these prototype generators.
- The eddy current losses in the stator end region are quite high. This loss is part of the total stator losses which can increase the stator temperature. The stator end losses increase quadratically with the increase of the number of coil turns. A thin stator iron lamination in the end region could reduce this loss. For a stator lamination thickness equal to the skin depth of the induced current (0.1125 mm), the end loss reduction is around 63%. Another method to reduce the end loss is by using a material with high resistivity in the end stator region.

7.2 Future works

- Developing an analytical model to obtain a better accuracy results. The investigation of the prototype generators in this thesis can be used to develop the analytic model. With this model, the best construction variations for range extender generator can be investigated faster and with a better accuracy.
- Investigating the magnet loss limit. This loss limit is the maximum loss which increases the temperature that is undangerous to the permanent magnet demagnetization. This limit corresponds to the determination of the number of magnet laminations.
- Investigating the thermal distribution within the machine. With this thermal model, an optimization of the cooling system of the machine could be done to remove the heat from the generator effectively.

References

[BAR 51] E.C. Barnes, *"An experimental study of induction machine end-turn leakage reactance",* AIEE Transactions, 1951

[BRH 92] A.T. Brahimi, A. Foggia, G. Meunier, "*End winding reactance computation using a 3D finite element program*", IEEE Transactions on magnetic, 1993

[CM08a] Comsol Multiphysics AC/DC Module Model Library, Comsol AB, 2008

[CM08b] Comsol Multiphysics Matlab Interface Guide, Comsol AB, 2008

[Eia 10] http://www.eia.gov/oiaf/ieo/transportation.html

[Fey 64] R. P. Feynman, R.B. Leighton, M. Sands, "The Feynman Lectures on Physics Vol 2", Addison-Wesley: California 1964.

[Fir 08] M. Firmansyah, "*Eddy current losses calculation in the rotor back iron and magnets for concentrated winding PM generator*", Msc. Thesis: Delft, 2008

[Gie 02] J.F. Gieras, M.Wing,"*Permanent magnet motor technology*", Marcel Dekker: New York, 2002

[Han 94] D.C. Hanselman, "Brushless *permanent-magnet motor design*", McGraw-Hill: Maine 1994.

[LIN 09] R. Lin, A. Arkkio, "*Calculation and analysis of stator end-winding leakage inductance of an induction machine*", IEEE transactions on magnetics, 2009

[Oecd 11] http://www.oecd.org, 2011

[PP 10] http://www.peec-power.com, s`Gravendeel, 2010

[PP 11] T.D. Strous, *"Test report on the prototype generator for the Peec-Power range extender",* Delft:2011

[Pol 98] H. Polinder, "On the losses in a high speed PM generator with rectifier", Ph.D. dissertation: Delft, 1998

[Pol 07] H. Polinder, J.G.Slootweg, M.J. Hoeijmakers, J.C.Compter,"*Eddy current losses in the solid back iron of PM machines for different concentrated fractional pitch windings",* IEEE machine and drives conference, 2007

[Ron 02] Q. Ronghai, A. L. Thomas, "*Analysis and Modeling of Airgap and Zigzag Leakage Fluxes in a Surface Mounted-PM Machine*", Industry Applications conference: IEEE, 2002

[Ruo 09] S. Ruoho, *"Modeling Magnet Length in 2-D Finite-Element Analysis of Electric Machines"*, IEEE transactions on magnetic, 2009

[Sen 97] P.C. Sen, "Principles of Electric Machines and Power Electronics", J.Willey: Canada: 1997

[Str 10] T. D. Strous, "*Design of a permanent magnet radial flux concentrated oil generator for a range extender application*",Msc. Thesis: Delft, 2010

Appendix 1: Sheet steel characteristics

The stator and rotor back iron in the prototype generators use M270-35A electrical steel. The steel characteristic and material properties are presented in this appendix.

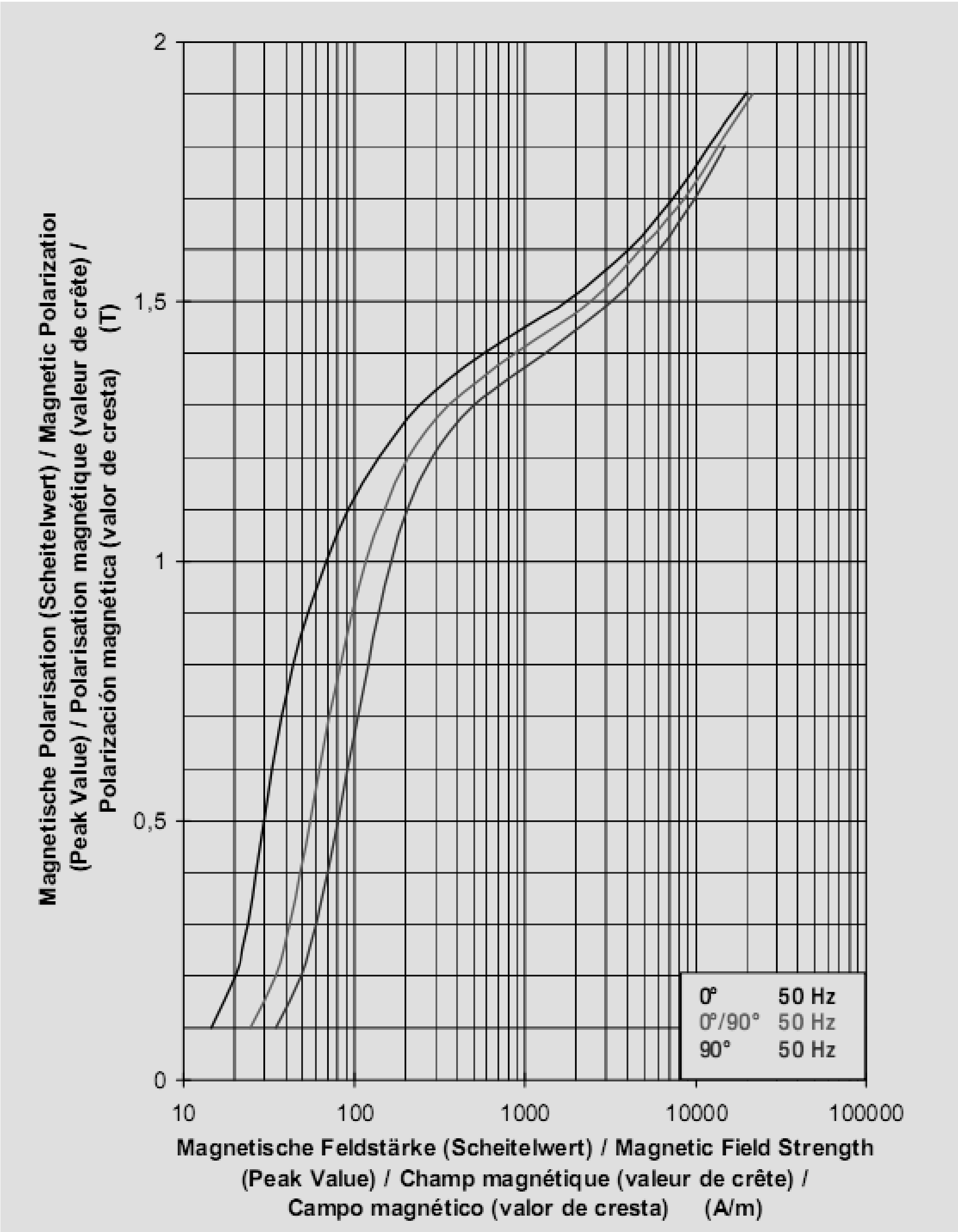

Fig. 52 B-H characteristic

The specific losses $p_{Fe,Spec}[W/kg]$ are presented below.

f= 50Hz								
J T	H A/m			μ_s	P_s W/kg			S_s VA/kg
	0°	90°	0°/90°	0°/90°	0°	90°	0°/90°	0°/90°
0,5	30	81	55	7185	0,24	0,39	0,31	0,57
0,6	33	92	63	7590	0,33	0,52	0,43	0,77
0,7	38	105	72	7760	0,43	0,67	0,55	1,00
0,8	44	121	83	7679	0,55	0,83	0,69	1,27
0,9	54	140	98	7342	0,68	1,00	0,84	1,62
1,0	**69**	**167**	**118**	**6728**	**0,83**	**1,19**	**1,01**	**2,06**
1,1	94	207	151	5806	1,01	1,39	1,21	2,70
1,2	140	285	210	4552	1,22	1,64	1,43	3,72
1,3	241	506	359	2885	1,48	1,96	1,71	5,98
1,4	577	1324	889	1254	1,79	2,36	2,02	13,80
1,5	**1767**	**3214**	**2437**	**491**	**2,11**	**2,69**	**2,34**	**40,95**
1,6	4045	6069	4717	271	2,42	2,93	2,67	88,43
1,7	7340	9880	8614	158	2,65	3,17	2,95	184,92
1,8	12026	15036	13557	107			3,21	317,86
1,9	19614	23058	21713	71				

f= 400Hz				
J T	H A/m 0°/90°	μ_s 0°/90°	P_s W/kg 0°/90°	S_s VA/kg 0°/90°
0,2	44	3652	0,91	1,50
0,3	56	4284	1,93	2,85
0,4	66	4800	3,25	4,53
0,5	76	5210	4,83	6,52
0,6	87	5520	6,70	8,84
0,7	97	5739	8,84	11,54
0,8	108	5870	11,28	14,70
0,9	121	5915	14,06	18,43
1,0	**138**	**5785**	**17,49**	**23,30**
1,1	161	5437	21,16	29,30
1,2	214	4466	25,37	38,27
1,3	354	2923	30,40	56,79
1,4				
1,5				
1,6				

f= 500Hz				
J T	H A/m 0°/90°	μ_s 0°/90°	P_s W/kg 0°/90°	S_s VA/kg 0°/90°
0,2	46	3456	1,25	1,95
0,3	59	4024	2,67	3,79
0,4	71	4482	4,49	6,05
0,5	82	4842	6,73	8,77
0,6	93	5108	9,29	11,90
0,7	105	5284	12,30	15,60
0,8	118	5378	15,75	19,92
0,9	132	5410	20,02	25,35
1,0	**150**	**5296**	**24,66**	**31,65**
1,1	174	5030	30,02	39,78
1,2	218	4385	36,06	51,32
1,3	359	2883	43,35	74,95
1,4				
1,5				
1,6				

f = 1000Hz				
J T	*H* A/m 0°/90°	μ_a 0°/90°	P_s W/kg 0°/90°	S_s VA/kg 0°/90°
0,2	58	2761	3,56	4,84
0,3	76	3150	7,56	9,65
0,4	92	3446	12,72	15,65
0,5	109	3652	19,07	22,98
0,6	129	3716	27,05	32,14
0,7	148	3754	36,39	42,97
0,8	170	3736	47,22	55,66
0,9	195	3673	60,30	71,16
1,0	**222**	**3581**	**75,51**	**89,58**
1,1	253	3465	93,14	111,89
1,2	287	3331	113,99	141,68
1,3				
1,4				
1,5				
1,6				

f = 2000Hz				
J T	*H* A/m 0°/90°	μ_a 0°/90°	P_s W/kg 0°/90°	S_s VA/kg 0°/90°
0,2	78	1027	10,46	12,96
0,3	103	1544	21,77	25,96
0,4	130	1837	37,45	43,50
0,5	158	2021	56,95	65,49
0,6	189	2104	81,22	92,84
0,7				
0,8				
0,9				
1,0				
1,1				
1,2				
1,3				
1,4				
1,5				
1,6				

Table 21 Specific losses $p_{Fe,Spec}[W/kg]$ for M270-35A

Appendix 2: Magnet materials characteristic

Magnet material properties:

NEODYMIUM SINTERED									
Grade	corrosion stable *1 specify as: grade+"/S"	Remanence Br mT min	typ	Normal coercivity Hcb kA/m min	typ	Intrinsic coercivity Hcj kA/m min	Max. energy product BH(max) kJ/m3 min	typ	Max. operating temp.
N38 UH	38 UH/S	1220	1260	900	950	1989	279	303	180
N44 SH	44 SH/S	1330	1360	970	1020	1592	334	350	150

B-H Characteristic of N38UH for SMPM machine:

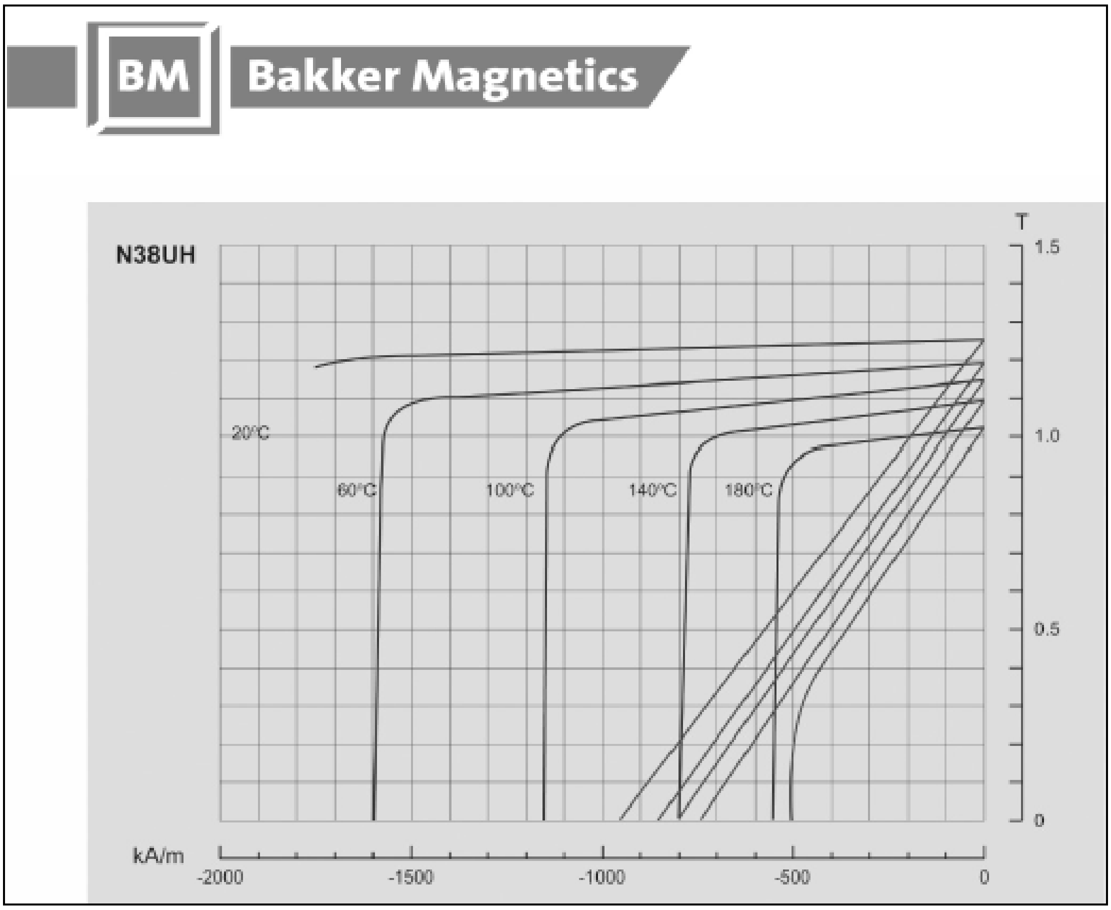

B-H Characteristic of N44SH for the IPM machine: